SOIL LANDSCAPE CHARACTERIZATION OF CROP STUBBLE COVERED FIELDS USING IKONOS HIGH RESOLUTION PANCHROMATIC IMAGES

BY

YANN S. PELCAT

A Thesis
Submitted to the Faculty of Graduate Studies
in Partial Fulfillment of the Requirements
for the Degree of

MASTER OF SCIENCE

Department of Soil Science
University of Manitoba
Winnipeg, Manitoba

THE UNIVERSITY OF MANITOBA

FACULTY OF GRADUATE STUDIES

*****

COPYRIGHT PERMISSION

Soil Landscape Characterization of Crop Stubble Covered Fields using IKONOS High Resolution Panchromatic Images

By

Yann S. Pelcat

A Thesis/Practicum submitted to the Faculty of Graduate Studies of The University of

Manitoba in partial fulfillment of the requirement of the degree

of

Master of Science

ABSTRACT

Pelcat, Yann Stephane. Msc., The University of Manitoba, May, 2006. Soil Landscape Characterization of Crop Stubble Covered Fields Using IKONOS High Resolution Panchromatic images. Major Professor; Paul Bullock.

Soil landscape characterization into landform elements for precision agriculture has become an important issue. As soil properties and crop yields change over the landscape, delineating landform elements as a basis for site-specific application of crop inputs has become a reality.

Two different methods of delineating landform elements from agricultural fields were tested and compared. The first method delineated landform elements from digital elevation maps with the use of the LandMapR^{tm} software, the second method delineated classes from IKONOS high resolution panchromatic images using an unsupervised classification algorithm. The LandMapR^{tm} model delineated landform elements from true elevation data collected in the field and was considered the reference dataset to which the image classification maps were compared to.

The IKONOS imagery was processed using a combination of one filtering algorithm and one unsupervised classification method prior to being compared to the classified DEM. A total of 20 filtering algorithms and two unsupervised methods were used for each of the five study sites. The study sites consisted of four agricultural fields covered with crop stubble and one field in summer fallow. Image classification accuracy assessment was reported as overall, producer's and user's accuracy as well as Kappa statistic.

Results showed that filtering algorithms and classification methods had no effects on image classification accuracies. Highest classification accuracy of image map to landform element map comparison achieved for all study sites was 17.9 %. Classification accuracy was affected by the heterogeneity of the ground surface cover found in each field. However, the classification accuracy of the fallow field was not superior to the stubble fields.

ACKNOWLEDGEMENTS

I wish to acknowledge the Indian Head Agricultural Research Foundation (IHARF) and the Canadian Adaptation and Rural Development Saskatchewan (CARDS) for giving me the opportunity to undertake this research project and in the process learn new skills.

I wish to sincerely thank my committee members, Dr. Guy Lafond, Dr. David Lobb, Dr Rene Van Acker and my supervisor, Dr. Paul Bullock, for their continuous technical and moral support over the years; Dr. Prakash Basnyat, GIS and remote sensing expert who taught me so much over the years; and my current employer, Alberta Agriculture Food and Rural Development (AAFRD) including John Hermans and Arva Traynor for their wonderful support over the past year.

I also wish to thank my parents: Liette and Maurice Pelcat, my grandma: Mamie, all my friends as well as the rest of my family for their tremendous moral support over the past few years.

TABLE OF CONTENTS

LIST OF TABLES

LIST OF FIGURES

LIST OF ABBREVIATIONS

BV	Brightness value
DEM	Digital elevation map
DEP	Depression
DGPS	Differential global positioning system
GCP	Ground control point
GIS	Geographic information system
GPS	Global positioning system
IDW	Inverse distance weighting
IFOV	Instant field of view
LE	Landform element
NAD 27	North American Datum 1927
NAD 83	North American Datum 1983
NIR	Near Infrared
PA	Precision agriculture
RTK	Real time kinematic
SSCM	Site specific crop management
TIN	Triangulated irregular network
USDA	United States department of Agriculture
WGS 84	World Geodetic System 1984

1 INTRODUCTION

As Whelan and McBratney (2000) described it: “Precision Agriculture (PA) should be considered as a philosophical shift in the management of variability within agricultural industries. It must be aimed at improving profitability and/or environmental impact (both short and long term)”. The management of variability in agronomy is expressed, in one form, as site-specific application of crop inputs within a field. This philosophy is based on improving field profitability by matching crop inputs to soil variability and crop requirements across the landscape.

The first step to site-specific crop management (SSCM) is to delineate management zones of relatively homogeneous soil characteristics and/or crop response in a field. The most common practice of creating management zones is based on soil nutrient analysis from georeferenced soil sampling site taken over the entire field using a grid base approach. Using a geographical information system (GIS), a soil fertility map is created and separated into nutrient zones. As this method is very expensive and labor intensive, there is a need for a more robust and effective method to delineate management zones. Although widely used, this approach to management zones delineation does not usually take into account the effect of landscape position on soil properties.

Soil pedogenesis is affected by landscape characteristics such as slope gradient, curvature and profile due to soil movement from water erosion (Hall and Olson, 1991), wind and tillage erosion (Lobb, 1999). Soil redistribution across the landscape directly

affects soil properties such as organic matter, depth to carbonate (Pennock et al., 1987), nutrient levels (N, P, K, S), pH and soil moisture holding capacity (Manning et al., 2001a), which in turn affects crop yields (Manning et al., 2001b; Moore et al., 1999; Walley et al., 2001). Therefore a management zone approach based on landform characterization maybe most effective.

Historically, delineation of landform elements required years of expertise from soil scientists and remained a tedious and subjective exercise that could not have been feasible on a commercial basis. However, with the availability of digital data model (DEM), Pennock et al. (1987) developed a landform element classification that identified seven landform elements based on slope gradient, slope length, plan and profile curvature. In 2000, MacMillan et al. developed a more sophisticated landform element model, to delineate 15 landform elements from a DEM and further summarize the classes into four major classes with significantly different topographic properties. However, as DEM data collection and processing remains expensive, a different methodology of creating landform element (LE) maps for agricultural fields is required.

Classifying and mapping soils using aerial photographs has been a common practice in the United States of America (USDA 1966). When combined with photogrammetry and expert knowledge, soil scientists were able to map soil groups based on topography and differences in color tones of black and white aerial photographs. Given that soil properties such as color and moisture content affected the tonal gradient of aerial photographs, where moist dark soils had a low tonal value and drier light soils had higher tonal values, it was possible to map soils for entire counties. Although this soil mapping technique was successful on a regional scale, it still remained too coarse for

the purpose of precision farming.

Other studies on image interpretation have been conducted on the solonetzic soils of Saskatchewan. McCaan (1995) developed a method for delineating solonetzic soils in hummocky landscapes based on the computerized image classification of digital aerial photographs. The method consisted of scanning black and white aerial photographs into a computer to acquire digital images composed of 256 gray tones from black (0) to white (255). Training classes of gray tones, based on specific soil properties acquired from an extensive soil survey done on a small part of the field, were used to classify the entire landscape into soil zones using image analysis software called ERDAS^{tm}. His method showed accuracies of up to 86 % in delineating solonetzic soils in hummocky terrain, thus delineating Landform Elements (LE) such as shoulder/crest, back-slope, toe-slope and depression areas. Although this technique was successful, a large amount of ground truth data was needed to validate the image classification, information that would not be available on a commercial basis.

With the availability of digital, geo-referenced high-resolution IKONOS panchromatic satellite images and advanced image analysis software, it may be possible to delineate LE using the differences in color tones of the imagery as a classification criteria.

The main objective of this research was to evaluate the feasibility and appropriate methods for classifying IKONOS panchromatic images into landform elements.

Other objectives of this research were:

1) To characterise quantitatively and qualitatively landform elements of 5 agricultural fields from digital elevation data using the LandmapR^{tm} software

(MacMillan et al., 2000).

2) To test the relative effectiveness of various image classification and filtering techniques on IKONOS panchromatic images to delineate landform elements.

3) To test the accuracy of the image classification for delineating landform elements.

2 LITERATURE REVIEW

2.1 Soil Erosion and Redistribution within the Landscape

Soils of Saskatchewan have changed considerably in the last 100 years from the native prairie soils to the soils we have today. Decades of cultivation along with wind and water erosion has resulted in soil transformations within the landscape, affecting pedogenesis and soil properties.

Soil erosion processes and water distribution have affected soil-forming processes within the landscape. Walley et al. (2001) demonstrated the association between slope segments and soil distribution within a glacial till landscape in southern Saskatchewan. Their research showed a relationship between soil landform characteristics, water movement and soil forming processes. Typically, drier shoulder complexes were dominated by Orthic Regosols or weakly developed Chernozems with thin A Horizons. Moister foot slopes and level depressional areas were dominated by Gleysolic soils and mid-slope positions showed a transition between the two types of soil series and moisture range. Similar results were found in Manitoba by Manning et al. (2001a) where Gleyed Eluviated Black Chernozems dominated convergent lower parts of the landscape, and well-drained Orthic Black Chernozems dominated the upper convex parts of the landscape. Furthermore, thickness of the A horizon, solum depth, soil organic carbon and soil moisture (Manning et al. 2001b) were all related to lower convergent landform

positions.

Soil pedology within the landscape can also be attributed to soil movement by water, wind and tillage erosion. Soil movement due to water erosion is minimal at the convex shoulder part of the landscape and increases on backslope and upper footslope. Topsoil removal from backslope areas will be deposited in concave mid to lower footslope and toeslope positions (Schumacker et al. 1999). Water erosion processes on hummocky terrain with steeper and longer slopes is more evident in the backslope areas as greater amounts of topsoil is removed, exposing coarse texture, less fertile, more calcareous B and C soil horizons. Soil removed from the backslope area is then deposited in concave and level depressional areas of the landscape, resulting in increased soil organic matter and moisture holding capacity (Troeh et al. 1980).

Soil erosion due to wind also played an important role in the redistribution of soils within the lansdcape. Summer fallowing was a common agricultural practice which left uncovered soils vulnerable to winds for long periods of time. Wind erosion in hummocky terrain has eroded upper parts of the knolls exposed to the prevailing winds, as wind velocity at the top of the knolls was higher than in depression areas, moving silt and very fine sand particles away from the convex shoulder slopes and deposited them in convergent low areas of the field, thus contributing to the removal of topsoil and exposing a less fertile, coarser texture, more calcareous subsoils (Verity and Anderson 1990).

In the last 90 years, tillage erosion has caused a significant translocation of topsoil from convex upper slopes to concave footslope and toeslope areas resulting in a change of soil type in each landscape position (Pennock and Corre 2001). This soil translocation

is more noticeable on hummocky landscape with steep slope gradient (Lobb and Kachanoski 1999).

In a natural environment, soil redistribution within the landscape is caused by a combination of all erosion processes. Schumacher et al. (1999) modeled water and tillage erosion for a typical hummocky landscape catena and found that the combined effect of the two erosion processes better explained the soil redistribution within the landscape than each process considered separately. The interaction between both erosion processes resulted in greater soil loss in the upper shoulder position and greater soil deposition farther upslope. Soil translocation from shoulder complexes to backslope was explained by the changes in hillslope morphology from water erosion. The net movement of soil resulted in a thinning of A horizon on upper parts of the landscape and a thickening of the A horizon in the lower parts of the landscape.

As water and tillage erosion processes affect the distribution of soil chemical and physical properties within the landscape, soil variability within the landscape is somewhat predictable. Well-drained, coarse textured, highly carbonated soils are more likely to be found on divergent higher parts of the landscape. Thicker, higher organic carbon content and wetter soils are more likely to be found in convergent low-lying areas (Pennock et al. 1987).

2.2 Soil Landform Delineation Techniques

2.2.1 Soil Landform Delineation from Elevation Data

The Canadian System of Soil Classification (CSSC, 1976) has developed a soil landform classification system based on general categorical soils information collected at

a regional scale. The landform classification key is based upon two criteria: the genetic material of the soil and the form or surface expression of the landscape. The genetic material criteria was composed of four groups: unconsolidated material, organic material, consolidated material and ice. The surface expression category was defined by 12 groups. Each surface form group was defined by a dominant slope gradient, slope length and a visual description of each landform. The soil landform field classification system was used by pedologists to categorize soil landforms across Canada resulting in a soil landform classification mapping system that was a very good indicator of dominant landforms present at a large geographical area. However, resolution was too coarse and not precise enough for precision farming.

One of the first successful attempts to delineate landforms at a field scale was done by Pennock et al. (1987) on glacial till soils of southern Saskatchewan. Pennock and his colleagues developed an automated landform element delineation process from digital elevation maps created from elevation data collected in the field using conventional survey equipment. Their approach was to create a smooth digital elevation map (DEM) from elevation data collected in the field then delineate seven landform facets using boolean rules based on landform derivatives such as slope gradient, length, aspect plan and profile curvature. The seven calculated landform facets were divergent and convergent shoulders, divergent and convergent backslope, divergent and convergent footslope and level elements. The landform facets were considered to have significant differences in soil and hydrology properties. The original seven landform facets model was modified to nine landform elements where the original level element was split into low catchment and high catchment level elements depending on the relative location of

the landform element in the landscape (Pennock et al. 1994). Although Pennock's approach used strict rules for the delineation of Landform elements, six elements were easily identified but the program had problems classifying the level elements correctly in certain types of landscape (MacMillan et al. 2000)

MacMillan et al. (2000) developed an automated landform element delineation model for Alberta soils based on Pennock's et al. model (1994) but expanded the total number of landform elements to 15. Pennock's original six elements were used as a basis for the model but the original level elements were replaced with six separate units to differentiate level and depressional areas within the upper, mid and lower landform elements. An extra class was also used in the mid and lower slope position to delineate slope planar units and one extra class was added to define divergent shoulders within low lying areas such as foot and toe slope areas. Furthermore, the 15-landform element classes could be generalized to four classes (upper, mid, lower and depression areas) based on their relative position within the landscape. The resulting four class classification showed significant differences in terms of canola yield and soil properties (MacMillan et al., 2000). Their approach used fuzzy logic based on heuristic rules developed by experienced soil pedologists, to delineate landform elements from DEM created from raw elevation data collected in each field. As Macmillan et al. used a set of heuristic rules developed by Canadian pedologists to define LE in a landscape, their method was applicable to various types of landscapes within Canada .

2.2.2 Soil landform Delineation from Remote Sensing Data

Classifying and mapping soils using aerial photographs has been a common practice in the United States of America since the 1950's (USDA 1966). Using photo

interpretation methods and expert knowledge, soil scientists were able to map soil groups based on topography and differences in color tones from black and white aerial photographs. By knowing that soil color and moisture content affected the tonal gradient of aerial photographs, where dark moist soils had a low tonal value and light dry soils had higher tonal values, scientists were able to delineate soils maps for entire counties. Although this method of mapping soils was successful on a regional scale, it remained very expensive, time consuming and required a lot of expert knowledge which varied considerably between image analysts.

Further studies using orthophotos were conducted on solonetzic soils of Saskatchewan. McCaan (1995) developed a method of delineating soil management units in hummocky landscape based on a supervised classification of the imagery using training classes determined from extensive field survey. His method consisted of digitizing black and white aerial photographs of bare soil fields into 8 bit images composed of 256 gray tone values (from black to white, 0 to 255). Training classes of gray tones, created from soil profile and analysis data done on the field, were used to classify the entire landscape into four management units using ERDAS^{tm} image analysis software. The soil management units were correlated to landform elements delineated from elevation data in the field. McCaan's method showed accuracies of up to 86% in delineating soil management in hummocky terrain thus delineating soil landform features. However, for the technique to be successful, the study area needed to be characterized by an extensive soil and topography survey which is too expensive to acquire for large grain farms in Western Canada.

Peng et al. (2003) were able to delineate soil drainage classes (well, moderately

and poorly drained) over a large area with accuracies of 73%. Their method consisted of using a supervised classification of a combination of Landsat-7 multispectral imagery, digital orthophotos of bare soil and elevation and slope metrics calculated from digital elevation maps. The resulting soil drainage classes delineated from remote sensing analyses showed more variability than the classes delineated from past soil surveys, but nevertheless were very accurate. The authors felt that their method would be appropriate to map soil drainage class for glaciated soils and could be improved with the use of higher resolution remote sensing data.

2.2.3 Remote Sensing of Soils

2.2.3.1 Soil Organic Matter

Soil reflectance is influenced by specific soil properties and ground cover. Early research to delineate organic matter from aerial photographs was done by Schreier et al. (1988). Using a supervised classification of color aerial photographs of bare soil fields from British Columbia, they were able to delineate three distinct classes of soils (inorganic soils, degraded organic soils and undisturbed organic soils) with a success rate of 70%. Their technique consisted of developing training classes by correlating organic matter content from soil analysis to image pixel brightness values and running a supervised classification on the entire image.

Major et al. (1992) measured the reflectance of 18 different soils found in Southern Alberta in the visible and near infrared spectrum. Their results showed that soil reflectance decreased with increasing organic carbon content in a quadratic fashion and a positive linear correlation existed between reflectance and soil carbonate content, thus

proving that A horizon reflectance was much lower than a B or C horizon. The same results were found among different soil types where reflectance would increase from a black to dark brown to brown soils. Furthermore, the authors suggested that soil moisture, ground cover and surface texture would affect the reflectance of soils.

McCaan (1995) showed that organic matter affected soil color which in turn affected reflectance. Soils with high organic matter content had the darkest color and hence appeared darker on the image, and soils with high inorganic carbon levels had a brighter color and appeared lighter on the image. He also suggested that delineation of landform elements from remote sensing images should be done using images acquired in the spring after soil thaw and before crop emergence as critical soil properties such as color, organic matter and moisture are more clearly visible.

Agbu et al. (1990) used low-resolution multispectral SPOT satellite images of bare soil fields to determine the spatial variability of soil properties within a county in eastern Illinois. By using multiple-regression analysis between soil properties and image spectral data, they were able to determine that A horizon organic carbon content was significantly correlated to the red (610 - 680 nm) and green (500 - 590 nm) band brightness values.

Chen et al. (2000) used color aerial photographs to classify soil organic matter content of a summer-fallowed field in Georgia into eight different classes. Their approach consisted of building a statistical relationship between soil organic carbon and pixel brightness values in the red, green and blue bands and to classify the aerial photo into classes based on the developed relationship. Their results showed a classification accuracy ranging between 74% to 77% depending on the classification method used. The

authors suggested that using digital images would have increased the classification accuracy as digitizing paper photographs introduced errors into the digital format.

Fox and Sabbagh (2002) used the soil line concept to develop a method for mapping organic matter from aerial photographs of bare soil in agricultural fields based on the reflectance of the red and near-infrared bands. The soil line was first calculated to build a predictive relationship between the amount of organic matter on the soil surface and the reflectance intensity in the red and near infrared band. The soil line Euclidean distance (SLED) technique was then used to predict the organic matter content for pixels representing the sampling sites in the study fields. The success rates were in the range of 68% which is comparable to findings from Chen et al. (2000).

In summary, remote sensing and image analysis methods conducted on bare soils have been successful for delineating and predicting organic matter distribution within a landscape using multispectral imagery. However, little or no research has been done on zero-till fields which have a permanent cover of crop residues.

2.2.3.2 Soil Moisture

Reflectance of the soil is not only affected by soil organic matter content but also moisture content. Earlier studies in Belorussia by Afanas'eva et al. (1983) showed the effects of soil moisture content on aerial black and white images. They noticed that dark, almost black, tones in the photographs corresponded to saturated soils; dark gray tones corresponded to soil containing 30% to 50% moisture; light gray to gray tones corresponded to soils with low moisture levels and whitish tones represented eroded dry soils. McCaan et al. (1996) also noted similar findings.

Muller and Decamps (2000) used SPOT multispectral bands to estimate the

moisture content of bare soil before seeding operations in the Garonne Valley, France. Their results showed that there was a relationship between surface soil moisture and reflectance data in the imagery where soil moisture affected the hue of the soil and therefore could be modeled using an exponential or linear regression analysis of the reflectance data. Furthermore, their results showed that modeling of surface soil moisture content for soils with less than 10% volumetric water content from reflectance data did not work. However, the general trend of their results was that reflectance would increase as surface soil moisture decreased from 30% to 0%.

Lobell and Asner (2002) conducted reflectance measurements of four different soil types at various moisture levels in a laboratory setting. Their findings were similar to Muller et al. (2000) as reflectance differences between soil moisture content were best described using an exponential function. Furthermore, Lobell found that reflectance in the visible and near infrared region saturated at soil moisture content of 20% and that longer wavelength, such as the short wave infrared (SWIR), saturated at soil moisture of 50%. They suggested that SWIR reflectance of bare soils could be used to map soil moisture on a commercial basis.

Weidong et al. (2002) also conducted reflectance measurements of 10 soils collected in France within a laboratory setting. Their method consisted of normalizing the reflectance data to the reflectance of the driest soil in order to eliminate reflectance noise created from soil surface roughness, and sensor-source geometry errors prior to data analysis. Their results showed that at soil moisture content below 0.15 $g.cm^{-3}$, the relative reflectance decreased with increasing soil moisture, and at soil moisture content between 0.15 to 0.40 $g.cm^{-3}$ relative reflectance increased with increasing soil moisture.

The critical soil moisture point at which the reflectance behavior reversed was different for each soil type and always happened before the reflectance was saturated by the water absorption signal (0.4 $g.cm^{-3}$). For that reason, their suggestions were that shorter wavelengths were better suited to estimate high soil moisture content and that longer wavelengths were better suited to estimate low soil moisture content.

2.2.3.3 Crop Residue

Biard and Baret (1997) developed a model to estimate cover residue on agricultural fields. Their method consisted of calculating a soil line and a crop residue line based on laboratory spectroradiometer readings of pure soil and corn residue samples and using a linear mixing model, derive a crop residue coverage from soil-residue mixed samples. Their results showed that the CRIM model was successful for estimating the residue cover from laboratory samples (r square = 0.9) of fresh residue at low moisture levels. The CRIM model estimation accuracy of crop residue dropped considerably with increasing residue moisture level, state of decomposition and soil surface roughness. Therefore their recommendations were to use satellite imagery taken shortly after harvest to estimate percent residue cover existing in the field.

Nagler et al. (2000) measured the spectral reflectance of six different soils and 18 soil cover residues at different moisture levels in a laboratory setting. Their first observation was that reflectance of plant litter and soil had a similar reflectance curve in the visible to near-infrared spectrum, which did not allow the discrimination between the two at that reflectance range. Furthermore, the color of the plant litter was affected by moisture content, age and stage of decomposition, which in turn affected the reflectance properties of the crop residues. As dark plant litter would have low reflectance values

and light colored plant litter would have higher reflectance value they were experiencing difficulties in quantifying plant litter in the visible spectrum of wavelengths. However, Nagler et al.(2000) noticed that an absorption signature existed at 2100 nm for dry plant litter which did not exist in the reflectance of pure bare soil. This reflectance absorption was related to the cellulose and lignin content of the plant litter and therefore was useful for the development of a cellulose absorption index (CAI) to estimate residue cover fraction from mixed soil-residue samples. The CAI provided better estimates of residue cover fraction for dry plant litter than for high moisture content plant residue.

Daughtry (2001) further expanded the research on CAI by measuring reflectance of three crop residues (corn, soybean and wheat) and five different types of soils. Their results confirmed an absorption at the 2100 nm range for all dry crop residues which was not present in bare soil reflectance measurements. They also confirmed that as moisture content of crop residues increased, the absorption signature at 2100 nm decreased until it disappeared at 100% water content. Furthermore, their results showed that from dry to moderately low moisture content (0 to 50% relative water content (RWC)), reflectance of mixed crop residue-soil samples in the 2100 nm range increased as residue fraction cover increased. When moisture content increased past 50% RWC, residue cover fraction estimation accuracies decreased considerably. Thus, their recommendation for best corn, soybean and wheat residue cover estimates at a field scale level was to acquire reflectance measurements shortly after harvest when crop residue cover age is young, crop residue decomposition has not yet occurred and moisture levels are low (Daughtry et al. 2004).

Sullivan et al. (2004) used Airborne Terrestrial Application Sensor (ATLAS)

hyperspectral data to estimate wheat straw residue cover from agricultural fields. Their results show that even though wheat straw residue cover estimates were affected by moisture content and degree of decomposition of the straw residues, a combination of ATLAS data in the visible and near infrared spectrum could usefully measure the difference in straw residue density. Furthermore, they achieved their best results by using thermal infrared bands as heat generated from organic and mineral surfaces are very different.

2.3 Surveying Equipment

All modern surveying equipment uses global positioning systems technology (GPS) to collect elevation data on a field. The global positioning system is a satellite-base navigational system built and controlled by the U.S. Department of Defense. The project started in the 1970's and was completed and available to the public in 1993. The system is composed of a network of 24 satellites revolving around the earth, every 12 hours, at an altitude of over 20,000 km, into six equal orbital planes (one every 60 degrees). Each satellite transmits a low frequency radio signal which contains three types of information: 1) a unique pseudo-random code which contains the identification number of the transmitting satellite, 2) an Ephemeris data string which contains information about the date and time and status of the satellite and 3) an Almanac data signal which tells the GPS receiver the position of each satellite at all times. Five ground stations located in different parts of the world accurately monitor each satellite orbit and continuously update their orbital geometry by sending a signal back to them. By comparing the time that a GPS signal was transmitted from a satellite with the time that

the signal was received, the GPS receiver is able to compute the distance separating the two. By triangulating this type of information received from at least four satellites, the GPS receiver is able to calculate a geographical position, an altitude, course and speed in a 1984 World Geodetic Datum System (WGS84) in less than one second. Positional accuracies of 10 to 20 meters can be achieved 24 hours a day, seven days a week, under every weather condition. Positional errors occur due to the fact that GPS radio signals from satellites are affected by the Ionosphere, Troposphere, Multipath from bouncing off objects, slight errors in receiver clock, orbital/ephemeresis errors and satellite visibility which then affects the ability of the receiver to calculate an accurate position (Trimble, 1993).

For precision farming purposes, positional errors are reduced to sub-meter accuracies in both the vertical and horizontal plane by using differential GPS (DGPS). Differential GPS eliminates significant errors caused by the Ionosphere/Troposphere, satellite clocks synchronization and orbital errors by using a stationary GPS receiver that calculates all the errors and transmits the correction factor to the roving GPS unit via radio wave. This process can take up to 10 seconds depending on the distance separating the roving and stationary GPS units. Accuracies of one to two meters are commonly achieved with a DGPS system.

For high accuracy purposes where real time positioning is needed, a variant of DGPS called Real Time Kinematics (RTK) is used to achieve vertical and horizontal accuracies to sub-centimeters by using a stationary and roving GPS unit set-up. The main difference between regular DGPS and RTK systems is that RTK systems will work with carrier phase frequency modulations of the pseudo random code instead of the bits

(or binary content) of the pseudo random code. By using the carrier phase of the signal, higher frequency of the waves are used to achieve high positional accuracy. One restriction to the RTK system is the distance between the stationary and roving GPS unit which have to be less than 10 km (Trimble 1993).

2.4 Geographic Coordinate Systems

Geographic coordinate systems were developed to define locations on a three dimensional spherical representation of the earth. The earth is divided in parallel lines oriented east-west called latitudes, and vertical lines oriented north-south called longitude. Latitude and longitude are measured as degree angles from a point on the surface of the earth to the center of the earth. Latitude 0 degree is called the equator and longitude of 0 degree is call the prime meridian which passes through the Town of Greenwich, England. Latitudes north of the Equator have positive values and south of the equator have negative values. Longitude east of the prime meridian have positive values, and west of the prime meridian have negative values (Bernhardsen, 1999).

As the earth shape is not a perfect sphere but resemble an ellipse, all geographic coordinate systems are based on predetermined spheroids that estimate the shape of the earth. Each spheroid is described by its semi major and semi minor axis and a flattening value. A datum is composed of a spheroid that best fits the surface of the earth for particular areas, thus the center of each datum will be different than the true geocentric center of the earth (Bernhardsen, 1999).

In North America, two datums are commonly used in geography: North America Datum 1927 (NAD 27) and North America Datum 1983 (NAD 83). NAD 27 uses the

Clarke 1866 spheroid to represent the shape of the earth and NAD 83 uses the GRS 1980 spheroid. The differences between the two datums reside in the center of the spheroid used where GRS 1980 is the earth's center of mass. With GPS satellites orbiting around the earth, more precise calculation of the center of mass of the earth was achieved and thus a new datum was created: the World Geodetic System 1984 (WGS 84). The GRS 80 and WGS 84 spheroids are almost identical and therefore the NAD 83 datum is compatible with the WGS 84 coordinate system. As all GPS data acquired with a GPS receiver are in WGS 84, the data can also be used in a NAD 83 datum without having to be reprojected (Bernhardsen, 1999).

2.5 Surface Interpolation and Representation

To represent a continuous landscape surface, two representation methods are available: one based on vector data (points, lines and polygons) and the other on raster data (a grid of regularly spaced pixels with an elevation measurement associated with each pixel).

Vector based surface representation such as Triangulated Irregular Network (TIN), uses the Delauney triangulation method to connect all elevation points to each other using a network of irregular sized triangles therefore using the true elevation of the area of interest. As no interpolation or smoothing occurs between elevation points, morphometric calculations (slope, aspect, plan profile and curvature) are easily calculated. However as the surface is composed of a network of interconnected triangles, it remains coarse and edges of the TIN can be misrepresented if the area represented has an irregular shape (Burrows et al. 1998).

Surfaces generated as raster datasets produce a continuous smooth surface composed of a grid of pixels each representing a specific elevation point. In order to calculate an elevation value for each pixel, elevation data points have to be interpolated between original elevation points collected with survey instrument. Several interpolation methods have been developed over the years, some based on simple mathematical calculations using values of nearest neighboring elevation points to more sophisticated methods, such as Kriging, which uses a mathematical model to fit the data set and interpolate data points.

One of the simplest and most commonly used interpolation technique to create a DEM is Inverse Distance Weighting (IDW). The predicted elevation value for an unvisited point is a function of distance - weighted average of data points included within a search radius of the unvisited. Search radii and/or number of neighbours to use in the calculations are all defined by the user. The result is a grid of regularly spaced pixels with an interpolated elevation value for each cell. The advantage of using IDW is the speed of computation and the final output DEM which is the true result of the interpolation if elevation data points are abundant over an entire area (Burrows et al., 1998).

When elevation data points are sparse, interpolation techniques based on geostatistical methods such as Kriging are better suited to create DEMs (Schmidt and Persson, 2003). Geostatistical analyses allow the user to determine trends, spatial autocorrelation and noise that exist in the data set by using semivariograms. Semivariograms are a graphic representation of the variance difference of pairs of points based on distance. Semivariance of pairs of sampled points are fitted to existing

mathematical models (linear, spherical, exponential and gaussian) and trends (general mean). Auto-correlation and noise can be extracted and used in the calculation of weights and search radius to interpolate values of unsampled data points (Burrows et al.1998). Kriging was originally developed for the mining industry and now is being used for environmental studies to medical sciences.

2.6 Remote Sensing

2.6.1 Basic Concepts of Remote Sensing

According to Jensen (2000), remote sensing is "the art and science of obtaining information about an object without being in direct physical contact with the object. It is a scientific technology that can be used to measure and monitor important biophysical characteristics and human activities on Earth".

In passive remote sensing for agricultural studies, naturally occurring electromagnetic radiation (EMR) reflected from the terrain surface is captured using air or space-borne sensors and transformed into digital images. The imagery is composed of a raster of pixels with digital numbers illustrating the reflectance captured by the sensor.

Each satellite sensor is described by its spatial, spectral, temporal and radiometric capabilities. Spatial capabilities refer to the sensor's precision, measured in meters, at which the sensor can capture information on the ground. The spatial resolution is the area on the ground represented in each pixel of the imagery. Spectral resolution refers to the number and width of the electromagnetic radiation bandwidths the sensor can measure. The radiometric resolution, measured in bits, refers to the sensitivity of the sensor to capture the EMR. The higher the radiometric resolution the more data, or

digital numbers per pixels, the imagery will contain. The temporal resolution refers to the time period between revisiting dates of the same area on earth. Faster traveling satellites will have a shorter revisiting period than slow moving satellites.

Several types of passive remote sensing images are available for agricultural purposes. One of the most commonly used remote sensing source for agriculture is from Landsat satellites. The latest of the Landsat satellites, Landsat-7 ETM+, can provide users with one panchromatic image (black and white) at a spatial resolution of 15 m by 15 m and seven multispectral bands (blue, green, red, near-infrared (NIR), short wave infrared (SWIR), mid IR, thermal IR) at a spatial resolution of 30 m by 30 m, except for the Thermal IR band which is 60 m by 60 m. The satellite has an instant field of view (IFOV) of 170 km by 185 km and has a revisiting date period of 16 days. This allows the earth to be mapped every 16 days (Jensen, 2000).

Kyoo-Seock et al. (1988) used Landsat TM multispectral imagery, combined with a DEM data, to classify the type of soils present in Dane County, Wisconsin, USA. Their results showed that soil units delineated from remote sensing data have 72% accuracy with the existing soil survey maps.

Other satellite platforms offer higher resolution multispectral images that can be used in soil science. For example, the SPOT satellite can provide the user with one 10 m x 10 m panchromatic image and 3 multispectral bands at 20 m by 20 m resolution (green, red and NIR). However the IFOV is only 60 km by 60 km (Jensen, 2000). As the SPOT satellite has pointable instruments on board, the revisiting time period is 26 days on-nadir and can be as high as one per day with different IFOV acquisition angles.

Agbu et al. (1990) used SPOT multispectral imagery of bare soil to predict soil

surface and subsurface soil properties. Their results showed that soil surface properties, such as organic matter and A horizon color value and chroma, were significantly correlated to the green, red and NIR brightness values of the imagery and that sub-surface soil properties were significantly correlated to ratio indecies created from the NIR/red band.

With advancements in space born satellite sensors, it is now possible to acquire high resolution imagery from a satellite orbiting the earth at 700 km altitude. Satellites such as the IKONOS that has been operational since September 30th, 1999 can provide users with five different bands: one Panchromatic that covers the complete visible spectrum (450 nm - 900 nm), and four multi spectral bands (blue (450 nm - 520 nm), green (520 nm - 600 nm), red (630 nm - 690 nm) and NIR (760 nm - 900 nm)). As the satellite instruments are programmable, the revisiting date is less than three days at different IFOV acquisition angles and the footprint size is determined by the user. The panchromatic band has a spatial resolution of 1m x 1m (equivalent or greater to aerial photos) and a radiometric resolution of 11 bits which characterizes reflectance into 2048 brightness values in the gray scale (black and white, 0 to 2047). All images are digital, orthorectified for topography effects and coarsely georeferenced to the respective datum of the footprint which facilitates image analysis (Jensen , 2000).

2.6.2 Image Pre-processing Techniques

Remote sensing images acquired from space borne platforms necessitate radiometric and geometric correction before being analyzed. Radiometric correction refers to correction of the radiance recorded by the sensor. Radiance capture by the satellite sensors are affected by errors from the sensor itself and atmospheric and

topographic effects. Sensor errors are usually easily quantifiable even before the satellite is launched into orbit. As engineers know the limitations of the sensors, error calculations can be performed. Atmospheric errors occur when the atmosphere affects radiance from the earth's surface. This type of error requires ground truth sample data in order to be corrected. Finally, errors introduced by topography have to be corrected, especially in high relief terrain, where shadows can mask the reflectance of the surface of the earth (Jensen, 1996). In dealing with IKONOS imagery, Space Imaging Inc. supplies radiometrically corrected images to their customers, therefore no calculations are required.

Satellite imagery has to be geometrically corrected to compare several images of the same area accurately. Two methodologies can be used to "rubbersheet" images to a common projection system; Image to map rectification and image-to-image registration. Image to map rectification requires a set of ground control points (GCPs) that are easily identifiable on the imagery and the earth surface and the use of an algorithm to calculate the new position of each pixel in the imagery and its new brightness value. Ground control points are selected for their clarity on the image and their geographic location previously georeferenced using a GPS or other survey equipment (Jensen, 1996). Image-to-Image registration is similar, however GCPs are extracted from a second image instead of a GPS survey.

The image rectification process consists of two steps: first, a spatial interpolation where the coordinate of each pixel changes to the new projection and second, an intensity interpolation where the brightness value of each pixel is re-calculated according to its new locations. Spatial interpolation of each pixel is executed by fitting a polynomial

equation to the GCP using the least-squares criteria. In general, a minimum of six GCPs are required and a first order polynomial equation is used for a small area with gentle local surface relief. For an entire footprint of an image with variable landscape surfaces quadratic or cubic transformations are necessary. Before calculating the new position of each pixel, a distortion calculation is calculated for each GCP by using the root mean square algorithm as described below:

$$RMS_{error} = \sqrt{(x' - x_{orig})^2} + (y' - y_{orig})^2$$

where x' and y' are the estimated coordinates in the new image and x_{orig} and y_{orig} are the original coordinates. The image analyst chooses a combination of GCPs to use in the rectification process by minimizing as much as possible the RMS error. Once GCPs are chosen, intensity interpolation for pixel brightness value can proceed (Jensen, 1996).

The intensity interpolation process consists of assigning a new brightness value to the rectified pixels. Three interpolation methods are commonly used: nearest-neighbour, bilinear and cubic convolution interpolation. Nearest neighbour is the favoured method as pixel values are not changed in the resampling process as the value of the nearest pixel is assigned to the new location. Bilinear interpolation method will assign the weighted average of the nearest 4 pixels to the output pixel and cubic convolution will assign the weighted average of the nearest 16 cells to the output cell (Jensen, 1996).

2.6.3 Image Enhancement Techniques

In remote sensing, spatial frequency refers to the number of changes in brightness values (BV) per unit area of the imagery. Areas of multiple changes in BV per unit area are considered as high frequency detailed areas such as mixed vegetation areas, and areas

with little or no changes in number of BV per unit area are considered as low frequency areas such as water bodies. Spatial frequency of imagery can be altered to enhance certain features in the imagery by applying a spatial filter. Two types of spatial filtering techniques exist; first, spatial convolution filters, which are simple to use and can enhance the high or low frequency of an image, and second, a Fourier analysis technique which explodes the image into spatial frequencies, then frequencies are filtered and the frequencies converted back to an image. The Fast Fourier method is complex and is used frequently to remove stripping effects caused by sensor errors (Jensen, 1996).

Spatial convolution filtering technique consists of changing the value of the center pixel of a convolution mask by computing the mean, median or mode of the BV included in the mask. Mask sizes vary from 3 by 3 pixels to 21 by 21. This process is repeated for all the pixels in the image thus altering the imagery. Average or mean filters are usually used to remove noise caused by sensor errors. Median and mode filters are used to remove pixels with corrupted or missing values, thus smoothing the image without blurring sharp edges (Jensen, 1996).

The Fourier theorem states that "any function f(x) can be represented by a summation of a series of sinusoidal terms of varying spatial frequencies". This theorem is applicable to remote sensing data as brightness values of an image are a function of the reflectance captured by the sensor. Fourier transform filtering is done in three steps. First the spatial domain of the imagery (BV) is transformed into the frequency domain using a Fourier theorem. Secondly, the frequency transform is filtered using a frequency domain filter. Lastly, the filtered frequency domain image is transformed back into a spatial domain (or satellite image) using the inverse Fast Fourier Transform algorithm.

Although very complex, the Fast Fourier transform filtering process is able to remove periodic errors in an image better than a convolution filter (Jensen, 1996).

2.6.4 Image Classification Techniques

Remote sensing data in its raw state is not very useful unless it is classified into polygons or areas of similar reflectance. Once areas of similar reflectance are identified, the analyst can use this information for further analysis. Two types of classification methods exist; supervised and unsupervised classification methods. Supervised classification methods use ground truth data to identify the reflectance values on small parts of the imagery and by applying clustering algorithms, the entire imagery can be classified. When ground truth data is not available, analysts have to revert to unsupervised classification techniques to segregate the imagery into areas of similar reflectance. Once the unsupervised classification process is done, the analyst has to identify to what each area corresponds on the imagery. This unsupervised classification method requires the analyst to have a great knowledge of the area analyzed in order to be accurate (Jensen, 1996).

One unsupervised classification method employed commonly in remote sensing is the Iterative Self-Organizing Data Analysis Technique or ISODATA. This clustering technique requires the analyst to specify the number of clusters desired, number of iterations of calculations, and several other cluster mean calculation parameters. The first iteration done by the software is to calculate a cluster mean for each user specified number of classes based on the range of BV in the image. Then, each pixel in the image is compared to each cluster mean and assigned to the nearest cluster mean to which it belongs. Once the first iteration process is done, a new cluster mean is calculated for

each class and based on the analyst's clustering parameters, the whole process is repeated. The end result is a set of defined classes of BV that the analyst can interpret based on his knowledge of the terrain studied (Jensen, 1996).

As real-world problems are complex in their nature, fuzzy k-means unsupervised classification is commonly used to classify remote sensing images of mixed reflectance areas. The fuzzy k-means classification algorithm first randomly assigns pixels to k clusters, where k is user defined. The center of each cluster is then calculated as the average of BV of the pixels assigned to each cluster. Then pixels are reallocated among the classes based on the relative similarity between pixels and clusters, where the similarity index is a function of distance between cluster mean and BV of pixel. The distance is calculated using euclidian, diagonal or malahonabis algorithm. This process is iterative and will stop when similar pixels are grouped within the same class (Burrough and McDonnell, 1998).

2.6.5 Image Classification Accuracy Techniques

Once the satellite imagery has been classified, there is a need to verify the accuracy of the classification process. The most commonly used classification accuracy assessment method is a pixel by pixel comparison of ground truth reference data to classes delineated from the imagery. An error matrix is then created with reference information pixels in the columns and the classified image pixels in the rows of the matrix. Accuracy assessment is done with the use of descriptive evaluations and discrete multivariate techniques derived from the error matrix. Descriptive statistics such as overall accuracy, producer's and user's accuracy become useful to the analyst and the user of the classified data.

Overall accuracy is computed as the sum of all correctly classified pixels in each class divided by the total number of pixels in the image. Although overall accuracy is a good representative of the classification accuracy, it does not explain the misclassification errors.

The producer's accuracy is computed as the number of correctly classified pixels in a category divided by the total number of pixels in that category as derived from the reference data (column data). This descriptive evaluation is also called error of omission as it indicates the probability of a reference pixel being correctly classified. The producer's accuracy is a good indicator of how well the analyst classified the imagery.

The user's accuracy is computed as the number of correctly classified pixels divided by the total number of pixels in that category as derived from the classified data (row data). This descriptive evaluation is also called error of commission as it represents the probability of a classified pixel on the image to represent that category on the ground. The user's accuracy is a good indicator to the user of the classified data of how accurate the classification was (Jensen, 1996).

Without a Kappa statistic, classification accuracy would not be complete. A Kappa value is a discrete multivariate statistic that is calculated using all pixels of the image, thus incorporating all classification errors (omission and commission). An overall Kappa statistic of 85% for an image classification is considered accurate according to Jensen (1996).

3 MATERIALS AND METHODS

3.1 The Study Area

3.1.1 Soils Description

Fields 1, 2, 3 and 5, located in the south central part of the RM of Indian Head (Table 3.1), were of a loam to silt loam textured soil developed from morainal surface deposits. General surface landform trends were hummocky with slope gradient ranging from 2% to 15%. Field 4, located north of the town of Indian Head, was a mix of loam, clay and silt clay textured soil developed from lacustrine deposits. The general landscape was classified as gently undulating with very gentle to gentle slopes ranging from 0.5% to 5% (Saskatchewan Soil Survey, 1986).

Table 3.1 Description of field sites.

.	Legal Land Location (Section-Township-Range)	Landscape Type	Average slope %
Field 1	SW-5-17-12 West of 2nd Meridian	Hummocky	5 to 15
Field 2	SE-7-17-12 West of 2nd Meridian	Hummocky	2 to 5
Field 3	NW-7-17-12 West of 2nd Meridian	Hummocky Dissected	2 to 10
Field 4	NW-25-18-13 West of 2nd Meridian	Undulating	0.5 to 5
Field 5	NE-6-17-12 West of 2nd Meridian	Hummocky	5 to 15

Soils in Field 1 were classified as mainly Orthic Oxbow soils on mid-upper slopes with Orthic Cudworth soils on mid-lower slopes and calcareous Oxbow soils on knolls. Soils found in Field 2 and 5 were mainly Orthic Oxbow with calcareous Oxbow soils on

knolls and upper slopes. Soils in Field 3 were classified as mainly Orthic Glenavon soils, with calcareous and eroded Glenavon soils on upper slopes, knolls and circular ridges, and poorly drained soils in depression areas. Soils in Field 4 were mainly Orthic Edgeley soils, with calcareous Edgeley soils on knolls and calcarous Indian Head soils (Saskatchewan Soil Survey, 1986).

3.1.2 Cropping Practices

All the fields, except for Field 5, were in a minimum till direct seeding continuous cropping system where annual crops were seeded directly into the previous year's crop stubble using a low disturbance, shank type air seeder.

Field 5 had been in a wheat-till fallow seeding system for the past 10 years where tillage of the land was done prior to seeding with a conventional disc seeder. Every second year the land was not seeded and tilled twice during the growing season using conventional tillage tools.

In 2000, Field 1 was seeded to canola and barley (Figure 3.1); Field 2 was seeded to canola (Figure 3.2), and Field 3 was seeded to field peas and spring wheat (Figure 3.3). In 1999, Field 4 was seeded partially to flax with some chemical fallow present (Figure 3.4) and in 2000, Field 5 was in fallow therefore the soil was tilled and exposed (Figure 3.5). The presence of different crop stubble, harvest management practices, snow and/or burnt areas were clearly visible in all images.

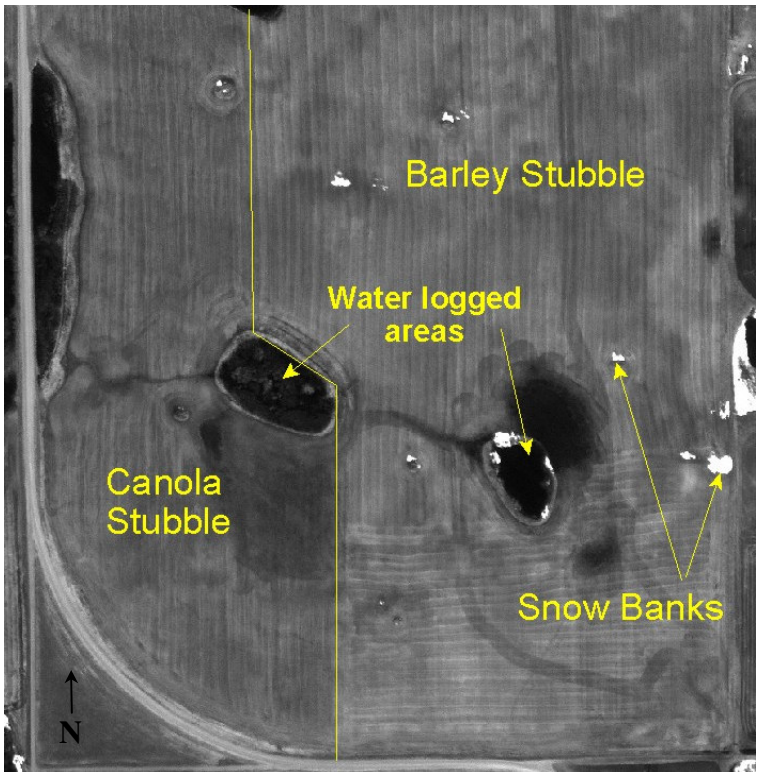

Figure 3.1 IKONOS panchromatic image of Field 1(April 24, 2001).

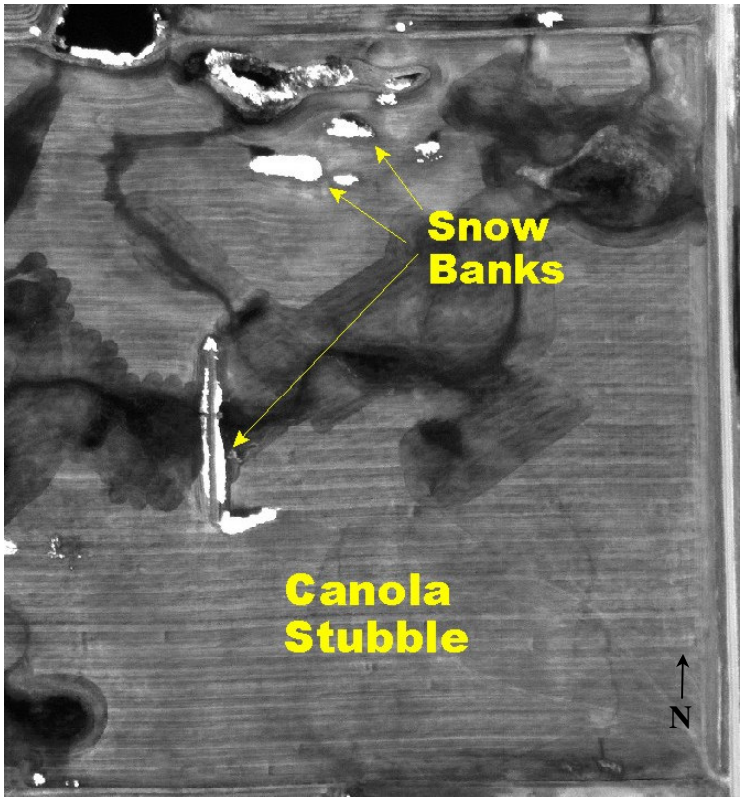

Figure 3.2 IKONOS panchromatic image of Field 2 (April 24, 2001).

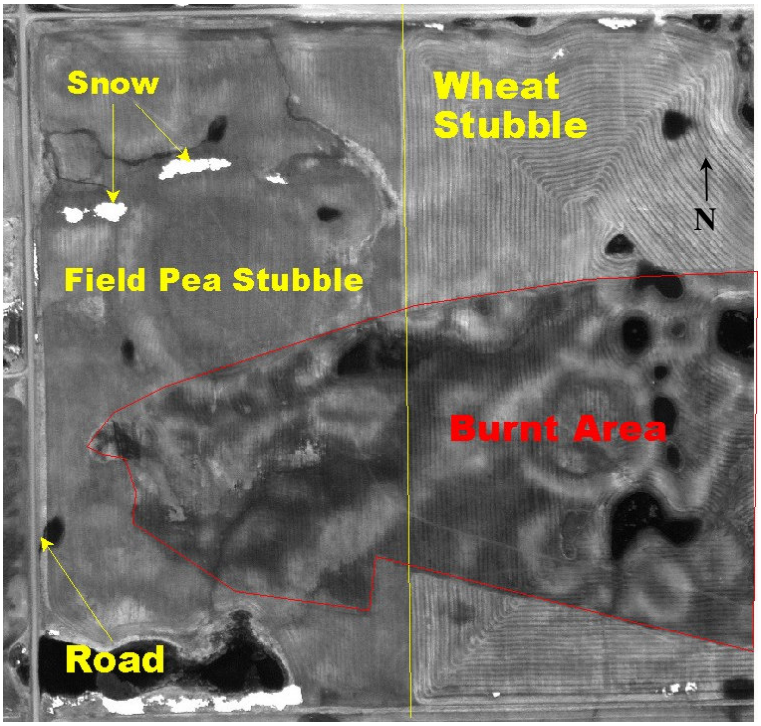

Figure 3.3 IKONOS panchromatic image of Field 3 (April 24, 2001).

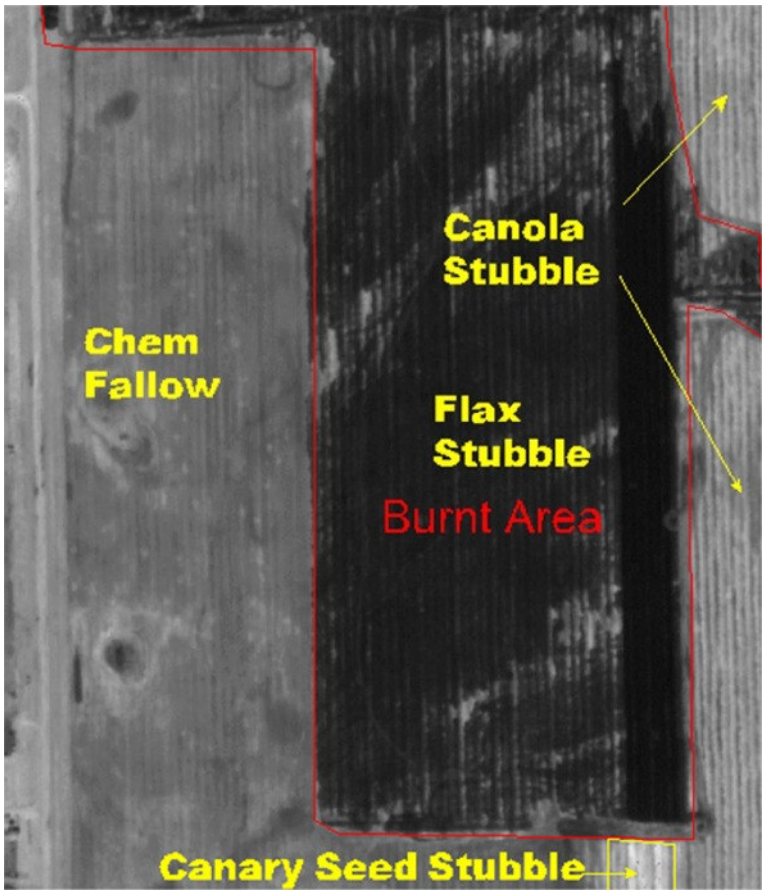

Figure 3.4 IKONOS panchromatic image of Field 4 (May 17, 2000).

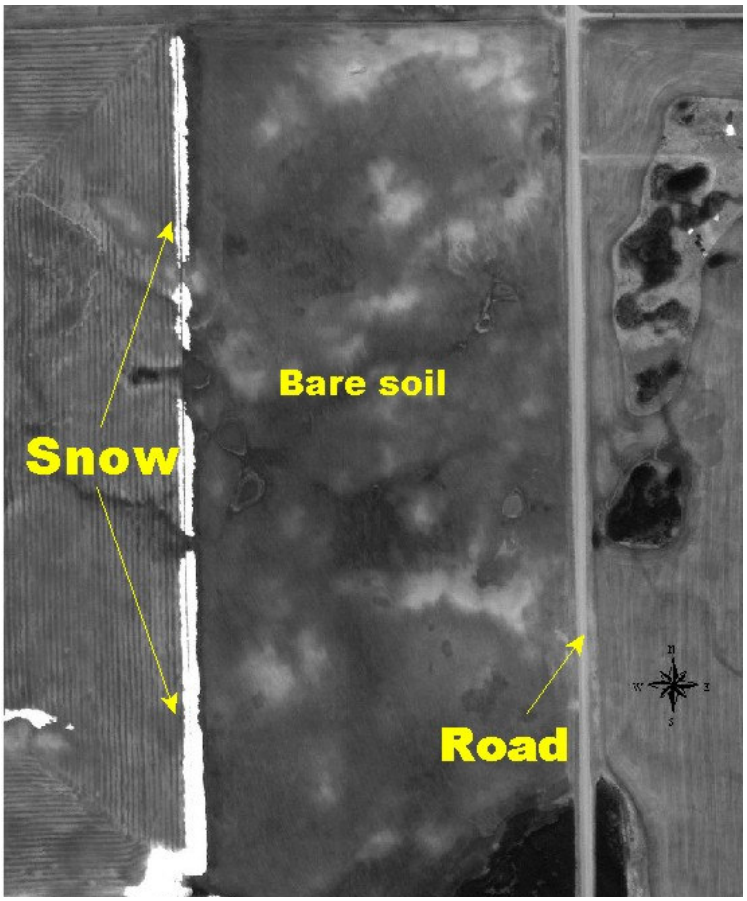

Figure 3.5 IKONOS panchromatic image of Field 5 (April 24, 2001).

3.2 Surveying Equipment

The Trimble RTK GPS survey equipment consisted of a base station and a roving unit. The base station was set up on the highest elevation point of the field to be mapped and the roving station was installed on a John Deere 6410 Tractor (Figure 3.6).

The Base station consisted of a Trimble MS-750 High Accuracy dual frequency RTK GPS Receiver and a Trim Com 900 M Base radio broadcasting antenna. At the base station, the GPS antenna calculated the positional error from the standard code and

carrier phase signals of the GPS satellites and broadcasted the positional correction signal via compact measurement record (CMR) signal using the Trim Com radio antenna.

The roving station consisted of a Trimble AgGPS 214 Dual Frequency GPS Receiver as well as a Trim Com 900 Rover Radio. The dual frequency roving receiver acquired the standard code and carrier phase signals from the GPS satellites as well as the CMR signal from the base station to provide centimeter accuracy in the x,y,z direction. The base station was set up in each field so the maximum distance between the roving unit and base station would not exceed 1.6 km (1 mile) in order to optimize the accuracy of the mapping system.

On board the tractor, a Trimble guidance system connected to an AgGPS 170 field computer with mapping software was used to record elevation data. The tractor speed and data point collection interval was set-up so elevation points would be recorded at approximately every 10 meters along track and between tracks.

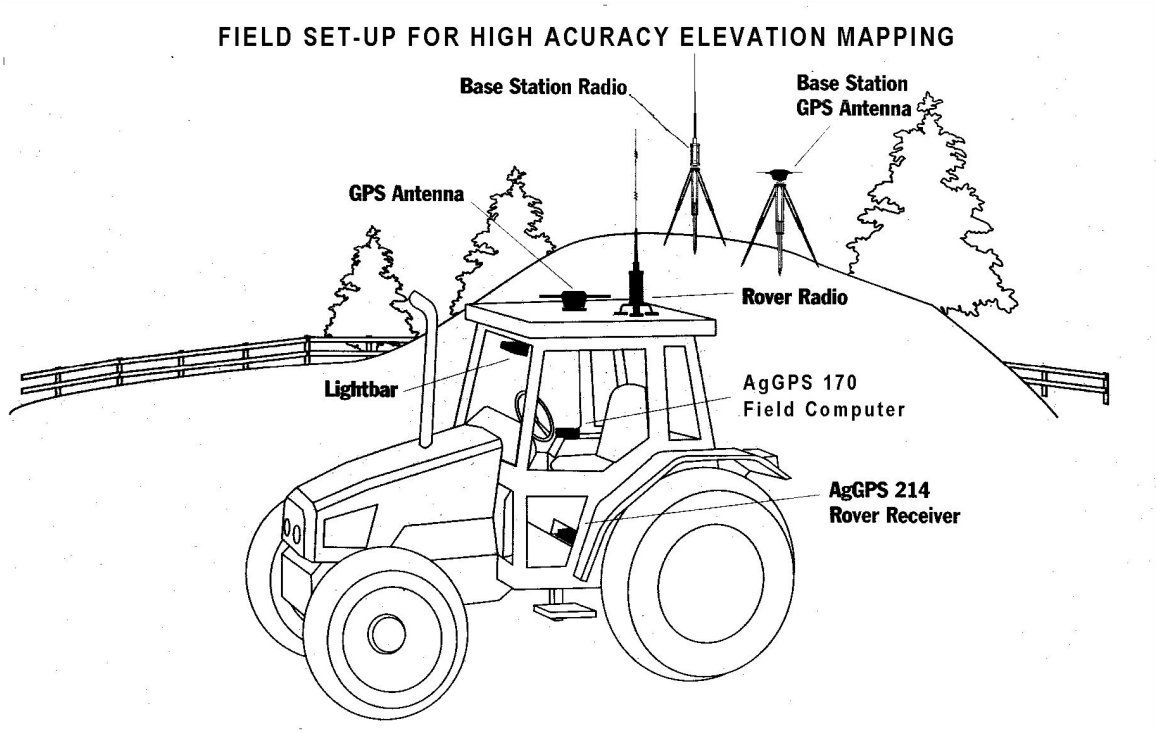

Figure 3.6 Trimble RTK GPS surveying equipment set-up diagram.

3.3 Elevation Data Processing

The raw elevation data collected with the Trimble RTK system had to be re-projected from a geographic coordinate system based on a WGS 84 datum to a Universal Transverse Mercator (UTM) Zone 13 coordinate system based on NAD 83 datum. The re-projection was done using ArcView GIS™.

The raw elevation was interpolated into a smooth continuous surface called a digital elevation map (DEM) before landform elements could be defined. The first step involved in creating a DEM was to eliminate elevation data points that were not included in the study area. The remaining elevation points were rasterized into a 10 meter grid continuous surface using a block- kriging method.

Block kriging has been well described in the literature (Bishop and McBratney, 2002, Robertson, 2000). Block-kriging is a weighted moving average method of interpolation that provided the best local estimate of the mean value of an elevation point based on spatial dependence of measured points. Weights of surrounding measured points were calculated using the distance between measured points and predicted points as well as the spatial autocorrelation of measured points. The spatial autocorrelation, or statistical dependence, was calculated with variograms and covariance functions which depended on a model of autocorrelation (linear, exponential, Gaussian, spherical). Kriging was done in two parts:

1) The semivariance was used to estimate the shape of the variogram. The semivariance was a measure of the degree of spatial correlation among sample data points as a function of the distance and direction between sample data points. The independent variable was the distance between pairs of points and the dependent variable was the (semi) variance of the differences in the data values for all samples given the distance apart. The variogram described the spatial relationship between data points.

2) The estimated semivariance function was used to determine the weights needed to define the contribution of each measured sample point to the interpolation. The closest sample points to the estimated sample point had the highest weight in the interpolation. The result was a regularly spaced 10-meter grid of estimated elevation points for each study area.

3.4 Landform Element Delineation from DEM

The delineation of landform elements (LE) from the DEM of each field was done using the LandMapper™ software developed by MacMillan et al. (2000). The LandMapper™ program first calculated a slope gradient, aspect, profile and curvature value for each cell of the DEM based on calculations done within a 3 by 3 window passed over the entire dataset (MacMillan et al., 2000). The terrain derivatives were then converted into 15 definite landform classes through the application of a set of default rules (Table 3.2) by means of fuzzy logic. The resulting 15 classes were aggregated into four classes based on typical landscape positions (Upper slope, Mid-slope, Lower slope and Depression areas) to simplify the LE thematic map.

Prior to segregating the DEM into LE, the elevation data for all fields had to be re-scaled to a 25-meter range using this formula:

$$Elev = \left(\frac{Z_{xy} - Z_{\min}}{Z_{\max} - Z_{\min}} \right) * 25$$

where Z_{xy} is an elevation point, Z_{min} and Z_{max} are the minimum and maximum elevation within the field. Through the re-scaling process, the LandMapper™ software was able to differentiate LE for very low relief elevation (< 1m), low slope gradient (< 1%) and low curvature (5^0 / 100 m). Otherwise, many areas would have been classified as level or depression areas as the software was designed to delineate LE from landscapes with relief range of 15 to 25 meters (Macmillan et al, 2000).

LE classes included in a different class than their respective class were removed using a 3 x 3 average filter to create four crisp LE classes. The classes were renamed within ArcView GIS™ as class 1 = Depressions, class 2 = Lower, class 3 = MID and class 4 = Upper areas for further analyses. The re-classified DEMs were converted to an ArcView GIS™ grid file for further processing.

Table 3.2 LandMapR[tm] rules for landform element class delineation (adapted from MacMillan et al., 2000).

3.5 IKONOS Images

On May 7th, 2000 and April 24th, 2001, IKONOS panchromatic images were acquired over two different areas in the RM of Indian Head. The first footprint was centered on the town of Indian Head, SK. and the second footprint on Deep Lake, SK, seven miles

south of the town of Indian Head. The panchromatic images had a 1-meter pixel resolution and 11 bit radiometric resolution that allowed 2048 brightness values to be represented in the gray scale. Snow banks present on the April 24th, 2001 footprint had the brightest reflection (white) and sloughs or waterlogged areas had the lowest reflection (dark) in the images.

3.6 IKONOS Image Processing

3.6.1 Image Geometric Rectification and Re-projection

The IKONOS imagery was pre-ordered from Space Imaging Inc. already geo-rectified to a WGS84 datum and projected in a UTM zone 13 coordinate system. However, for the DEM to overlay precisely onto the imagery, geo-rectification or "rubber-sheeting" of the imagery, was performed using PCI Geomatica™ software.

The first footprint was geometrically corrected using ground control points extracted from a geo-referenced Quickbird™ panchromatic image that was acquired in July 2003. The Quickbird imagery had been geometrically rectified using GPS ground control points that were post-processed for sub-centimeter accuracy purposes by the Canada Center for Remote Sensing (CCRS) in Ottawa, Ontario, Canada. The Quickbird™ image root mean square error (RMS), a measure of error of distance between actual and projected points, was less than a meter. Once geo-rectified to the Quickbird image, the RMS of the IKONOS image was 0.51 m in the easting direction (X axis) and 0.8 m in the northing direction (Y axis) using six ground control points.

The second footprint was geometrically rectified using ground control points collected with a handheld GPS system (Trimble AgGPS 132 with Omnistar DGPS). The

GPS system accuracy was at the sub-meter level. The final RMS error for the second footprint was 1.47 m in the easting direction (X axis) and 1.7 m in the northing direction (Y axis) using seven ground control points.

Once both footprints were geometrically rectified, the imagery was re-projected to a NAD 83 datum so that all dataset would be on a common datum (NAD 83) and coordinate system (UTM, Zone 13) for further analyses.

3.6.2 Image Filtering

In order to make more efficient use of computer power, each field was cutout from the image footprint and saved under an individual field name. The raw images were classified into four different classes using the ISODATA unsupervised clustering method to test if an image processing method should be used prior to image classification. Preliminary results showed that the effects of harvest management practices (swath, residue spread coverage, vehicle tracks, burnt areas) and the presence of snow skewed the classification process. To eliminate the effects of snow on the image classification, bitmap masks were created over the snowed areas in order to eliminate the pixel's brightness value from the classification process. To mask the crop residue cover effects, vehicle tracks and presence of different stubble types, convolution filters and frequency filters were applied to each field prior to classification.

3.6.2.1 Convolution Filters

Convolution filters calculated a new brightness value for the middle pixel in group of pixels included within a square kernel (filter size) and assigned the calculated value to the pixel located in the middle of the kernel. The kernel moved over each pixel of the

image thus changing all brightness values of the image based on a specified filtering algorithm. All convolution filters had the effect of smoothing the images and thus eliminating systematic patterns that were affecting the classification process (PCI, 2002).

Each raw IKONOS image was submitted to one filtering process to determine which filtering method would be best in eliminating crop residue and other systematic errors in the images. The convolution filters used were: average, Gaussian, median and mode, with different size of kernel: 5x5, 7x7, 9x9, 11x11 and 21x21 pixels for the average and Gaussian filters, and 3x3, 5x5, 7x7 pixels for the other filters. The size of one pixel was 1m by 1m.

The mean, mode and median filter computed the mean (average), mode and median value of the brightness values within a square filter respectively and assigned the calculated value to the center pixel of the kernel (PCI, 2002).

The Gaussian convolution filter computed the weighted sum of the brightness values within a square filter window surrounding each pixel. The filter window size was determined by the equation: 2 * sigma +1. For example, if a 5 by 5 filter was desired the sigma = 2 where 2*2 + 1= 5. The weights were calculated using the following Gaussian function:

$$G(i,j) = \exp\left(\frac{-((i-u)^2 + (j-v)^2)}{\overline{2}\ \overline{sigma^2}}\right)$$

where (i,j) was a pixel within the filter window, (u,v) was the center of the filter window, and Sigma^2 was the parameter sigma. The filter weights W (i, j) were calculated as the normalized values of G (i, j) over the entire window hence the sum of all weights was equal to 1. The new filtered brightness value of the center pixel of the window would be calculated as W (i, j)*V (i.j), where V (i, j) was the original pixel (PCI, 2002).

3.6.2.2 Frequency Filtering

Another filtering method commonly used in remote sensing to remove periodic noise due to satellite sensor errors is Fourier analysis. Fourier calculations are well explained in the literature (Jensen, 1996) and consist of three separate steps. The first step was to convert the spatial image into a frequency domain. The second step involved the application of frequency filters to remove high frequency noise and thus enhance the low frequency which acts as a smoothing effect. The third step was to convert the filtered frequency image back to the spatial domain image. In this case, two types of low frequency filters were used, Gaussian and Butterworth at two different frequency cut-off values (0.1 and 0.05 Hz).

All filter types and sizes were used on each image which produced 20 different images per field prior to classification

3.6.3 Image Classification

Satellite images are composed of an array of numbers depicting the spatial distribution of several attributes. These arrays are referred to as raster grids and are composed of rows and columns of pixels. Each pixel is assigned a digital number which represents a brightness value which in turn represents a specific attribute on the ground.

As satellite images cover a big area composed of a variety of attributes, it is common to cluster pixels by their brightness values to make simple thematic maps for different attributes. Two different pixel clustering algorithms were used to delineate four classes from each filtered image: 1) unsupervised ISODATA clustering and 2) unsupervised fuzzy k-means clustering method.

The Iterative Self Organizing Data Analysis Technique (ISODATA) clustering algorithm is based on detailed user defined procedures incorporated into an iterative scheme to cluster pixel brightness values into a specific number of clusters. The entire range of brightness values on each field was divided by the number of desired classes and preliminary clusters means for each group were calculated. Each pixel was then associated to a cluster mean based on the average distance between the pixel value and the cluster means. The entire process was repeated until all user-defined parameters were met (number of iterations, percent change in cluster, etc.) The procedure is well documented (Tou and Gonzalez, 1974).

The fuzzy k-means unsupervised clustering method was similar to the ISODATA but pixels were clustered together based on fuzzy membership to cluster means. The range of brightness values on each field was first divided into the desired number of classes and cluster means were calculated. Secondly, pixel degree of membership to each cluster center was calculated and thirdly, pixels were assigned to a cluster mean based on their fuzzy membership. This procedure has also been well described (Jensen, 1996).

The classified images of each field were compared to their respective Landform Element thematic map generated from the DEM to assess accuracy of the classification of panchromatic images of zero-till fields into Landform Elements.

3.6.4 Image Classification Accuracy

In order to determine the best combination of filter and classification method for delineating LE from an IKONOS panchromatic image, an error matrix between each classified IKONOS image and respective LE thematic map was done. The error matrix allowed the calculation of the user, producer and overall accuracy as well as Kappa statistic to determine the degree of accuracy of the classification method.

The overall accuracy was calculated as a ratio of correctly classified pixels over the total number of pixels in the image. The producer's accuracy was calculated as a ratio between the total number of correct pixels in a category over total number of pixels found in that category as derived from the reference data (column). This statistic indicated the probability of a reference pixel being correctly classified and was also a measure of the error of omission (or error of exclusion). The user's accuracy was calculated as a ratio of total number of correct pixels in a category over the total number of pixels that were actually classified in that category (row). This statistic indicated the probability of a classified pixel on the map to actually represent that category on the ground and was also called error of commission (or error of inclusion).

Discrete multivarariate statistics are also used in remote sensing to describe classification accuracy. Since remote sensing data are discrete rather than continuous and most often binomially or multinomially distributed rather than normally distributed, multivariate analysis such as the Kappa statistic for measuring agreement accuracy is used. The Kappa statistic is a discrete multivariate technique used in accuracy assessment between classified images and ground truth data.

The Kappa was calculated by Jensen (1996) as:

$$K_{hat} = \frac{N\sum_{i=1}^{r} x_{ii} - \sum_{i=1}^{r} (x_{i+} * x_{+i})}{N^2 - \sum_{i=1}^{r} (x_{i+} * x_{+i})}$$

where r was the number of rows in the matrix, x_{ii} was the number of observations in row i and column i, and x_{i+} and x_{+i} were the marginal totals of row i and column i, and N was the total number of pixels present in the image. The Kappa statistic incorporated the omission and commission errors in the accuracy assessment contrary to the overall accuracy that took into account the correctly classified pixels only. A representation of the user, overall accuracy and Kappa statistic was used to assess the classification accuracy of the IKONOS panchromatic image for estimating LE.

4 RESULTS AND DISCUSSION

4.1 Elevation Data Statistics

Descriptive statistics on the raw elevation data collected with the Trimble RTK GPS were generated using ArcView GIS (Table 4.1). Elevation points in all five fields were normally distributed, as the mean, mode and median values were very similar. Field 2 had the greatest elevation range (16.565 m) followed by Field 5 (15.362 m), Field 1 (13.041 m), Field 3 (12.799 m) and Field 4 (4.903 m).

Table 4.1 Descriptive statistics of raw elevation data for all study fields.

	Field 1	*Field 2*	*Field 3*	*Field 4*	*Field 5*
Area (ha)	61	48.6	59.5	52.6	34.1
Mean (m)	669.137	657.028	654.099	580.762	668.914
Median	669.192	656.276	653.032	580.744	668.468
Mode	669.224	654.764	650.562	579.477	667.569
Range	13.041	16.565	12.799	4.903	15.362
Minimum	663.554	652.785	646.152	578.325	664.803
Maximum	676.595	669.350	658.951	583.228	680.165
Total# of points	6320	6000	6723	5928	3377

4.2 Field 1.

4.2.1 TIN Surface Representation.

Using ArcView GIS™, along with the Spatial Analyst™ and 3D Analyst™ extension, the raw elevation data of Field 1 was converted to a 3D Triangulated Irregular Network (TIN) surface with a vertical exaggeration factor of 10 (Figure 4.1). The vertical exaggeration factor was achieved by multiplying each elevation data point by a factor of 10 to accentuate the existing landform features for better visual representation.

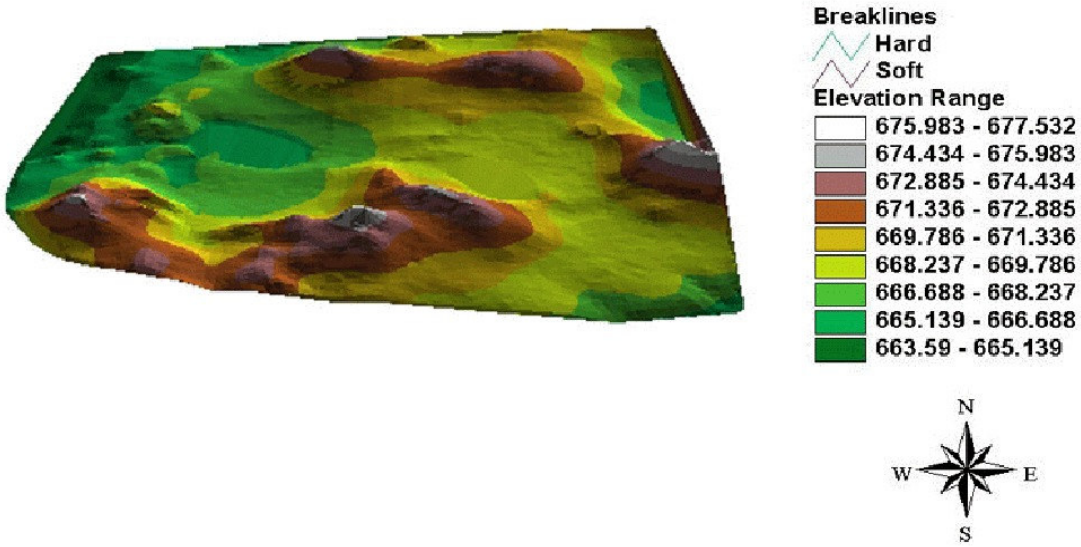

Figure 4.1 3D DEM of Field 1 with a vertical exaggeration factor of 10.

4.2.2 Landscape Feature Quantitative Description.

The TIN surface illustrated the hummocky landscape present in the study area where distinct knolls in the north, south and east edge of the field were clearly dominating the landscape, and where depression areas in the center and west edge were

clearly visible. The general gradient of the terrain was oriented from southeast to northwest with a major run-off collecting basin on the western edge of the field.

The semivariance analysis (Figure 4.2) showed that elevation data best fit an exponential model (r^2 = 0.985) which confirmed the presence of several different landscape features in the field (Burrough and McDonnell, 1998). Spatial patterns were close to each other as indicated by the range value of 438 meters, which agrees with the hummocky landscape classification found in the Saskatchewan Soil Survey for that field (Saskatchewan Soil Survey, 1986).

Terrain derivatives calculated from the LandMapR™ analysis for each grid cell of the DEM were summarized to characterize and quantify the existing landform features. Results showed that 80.1 % of the dominant slope gradient was between 0.5 to 5 degrees with the majority in the 2% to 5% range (Figure 4.3). Slope length distribution was divided in equal proportions between 175 meters and 600 meters (Figure 4.4) and the descriptive relief, which is calculated as the difference in relative elevation of each peak to the closest pit or depression area, was predominantly 5 to 10 meters (Figure 4.5). Results from the LandMapR™ analysis confirmed the presence of a variety of landform features and the low relief hummocky characteristic of the landscape.

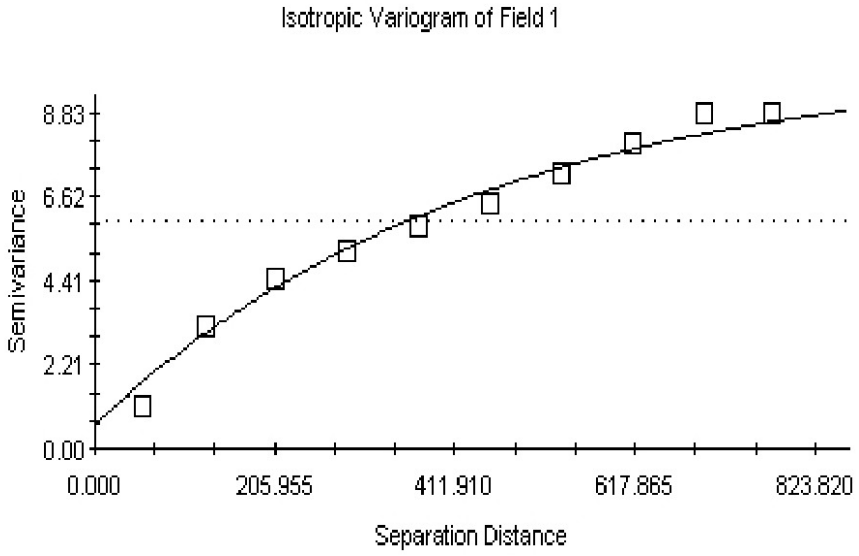

Exponential model (Co = 0.6100; Co + C = 10.2290; Ao = 438.000; r2 = 0.985; RSS = 1.07)

Figure 4.2 Variogram of Field 1.

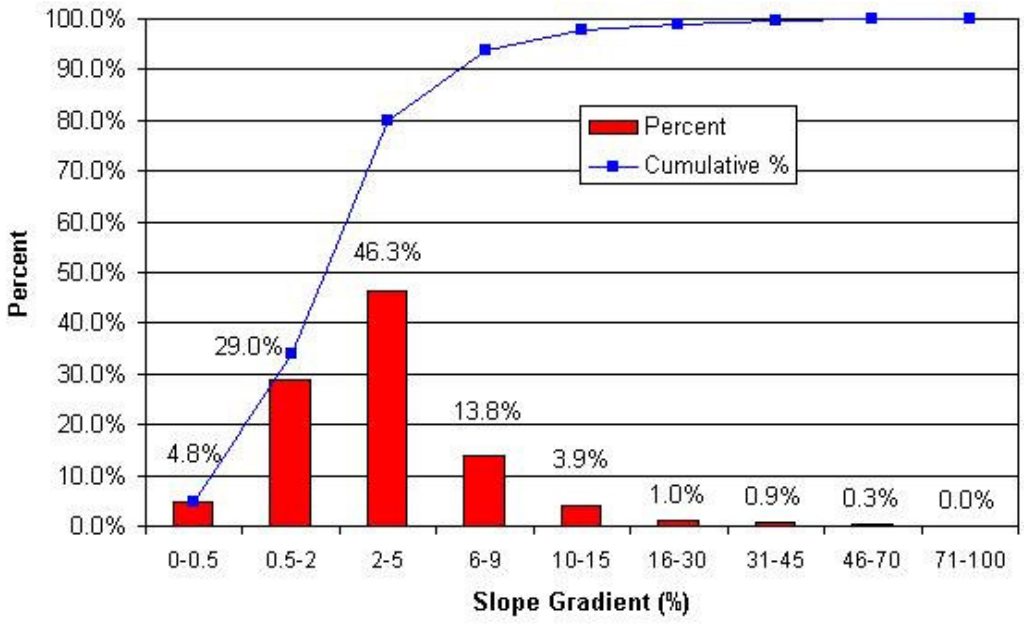

Figure 4.3 Slope gradient distribution in Field 1.

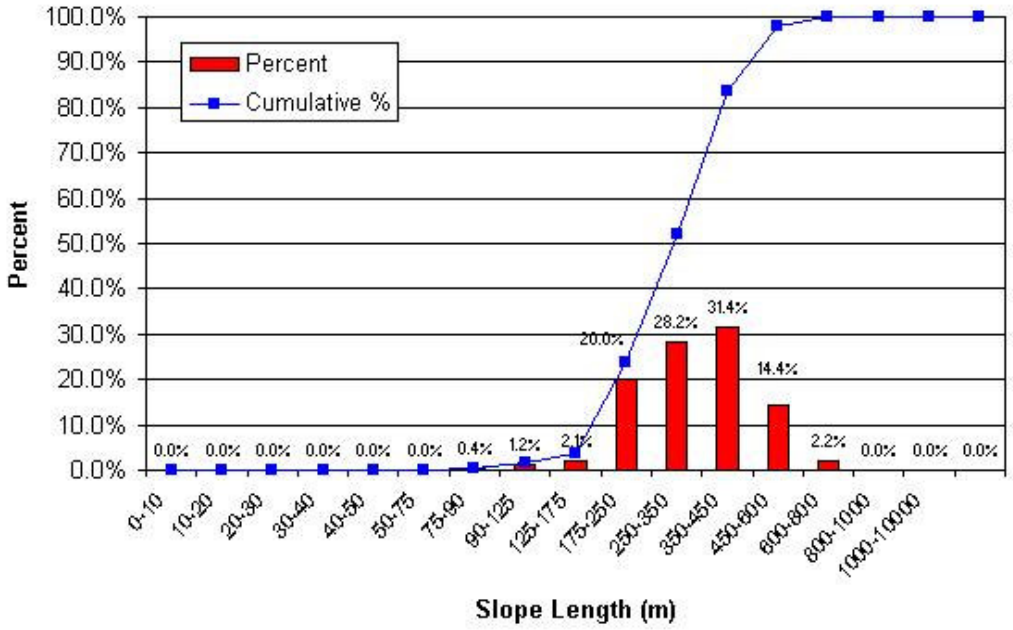

Figure 4.4 Slope length distribution in Field 1.

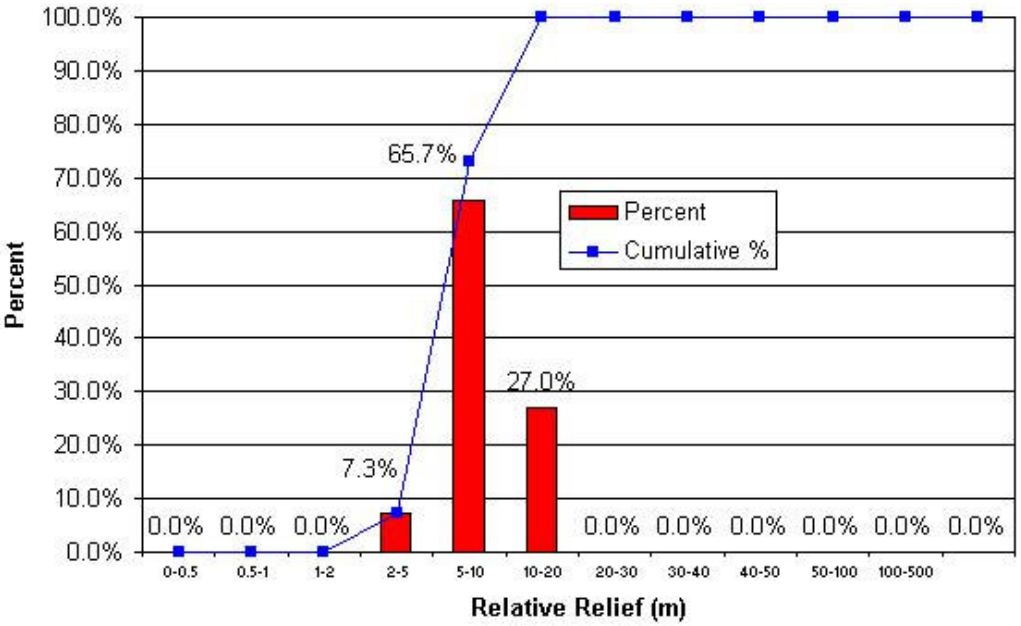

Figure 4.5 Relative relief distribution in Field 1.

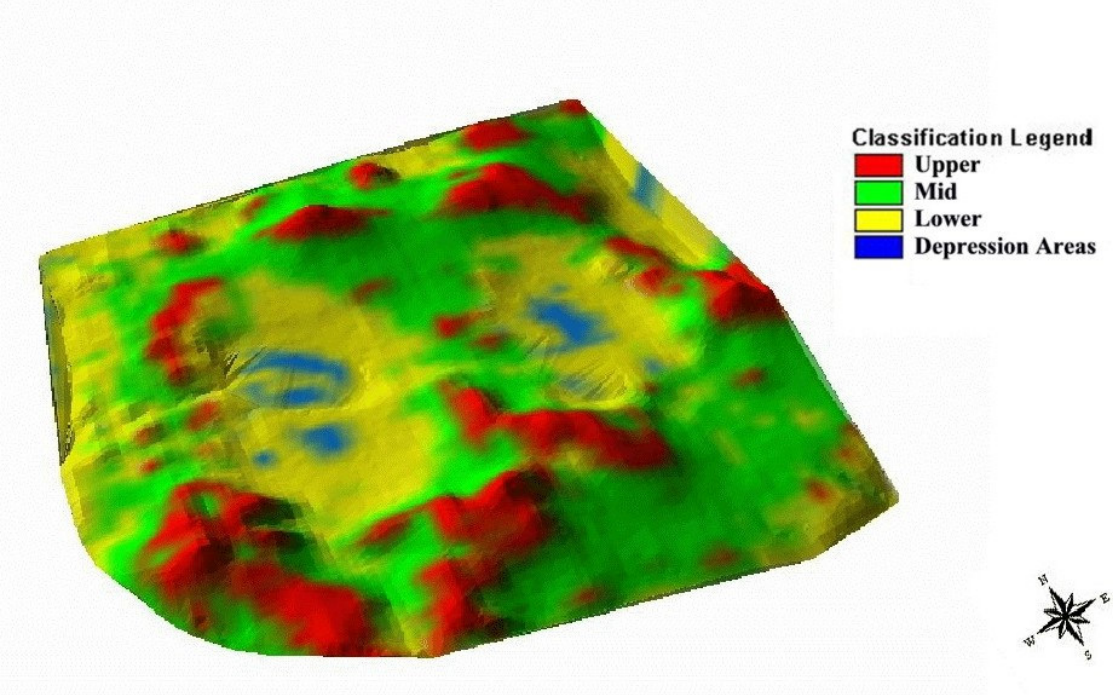

Figure 4.6 3D Landform element map of Field 1.

4.2.3 Landform Element Classification

Classification of the landscape into LE was done using the re-scaled elevation data to better enhance the differences in slope gradient, plan profile and curvature. Four distinct classes emerged from the classification as shown in Figure 4.6.

Upper LE class represented 18.7% of the landscape, Mid LE class represented 41.5%, lower LE class 36% and depression areas 3.8% (Figure 4.7).

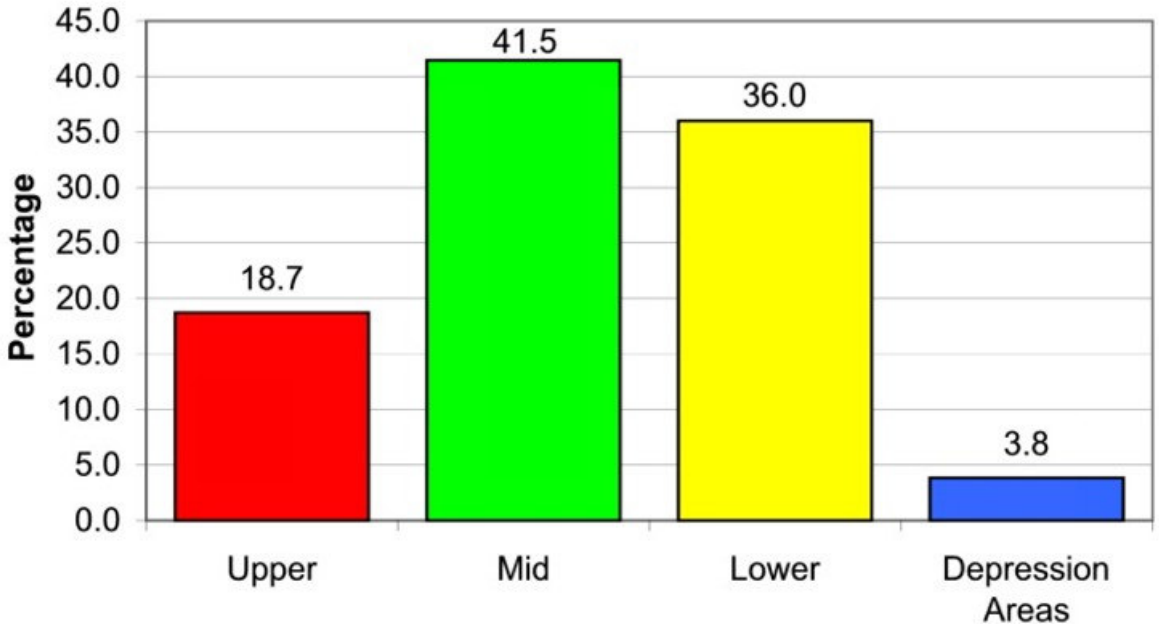

Figure 4.7 Landform element distribution in Field 1.

4.2.4 Land Cover Description

To best describe the land cover present in Field 1, the imagery was separated into three parts as illustrated in Figure 4.8. Part 1, located on the western side of the field, was covered by canola stubble. The canola crop was harvested in the north-south direction leaving stubble strips on the ground which were apparent in the image. On the east side of part 1, the canola crop was harvested around a permanent slough, which created concentric strips around the depression area. As well, a natural drainage channel, which connected the slough to the west side of Field 1, was clearly visible in the image. Furthermore, the area just south of the permanent slough appeared darker than the surrounding area as this area was nearly level and acted as a transition area for the run-off water.

Part 2 and 3 of Field 1 were seeded to barley but Part 3 was harvested earlier than Part 2 and in a different direction. The results were that Part 3 appeared as a lighter gray

tone than Part 2, that distinct stripping effects in the east-west direction were visible in Part 3 and, in the north-south direction in Part 2. The lighter gray tone of Part 3 might be due to the sun angle at the time of image acquisition where the sunlight might have had a greater reflectance off the east-west stubble direction than in northeast stubble direction. Furthermore, on the south side of Part 2 a permanent slough was clearly visible as it appeared darker in the image.

In the fall of 2000, the area around the slough in Part 2 was heavy harrowed by the producer which was clearly noticeable in the image as a path of darker tones was left in Part 2 and 3 of the image.

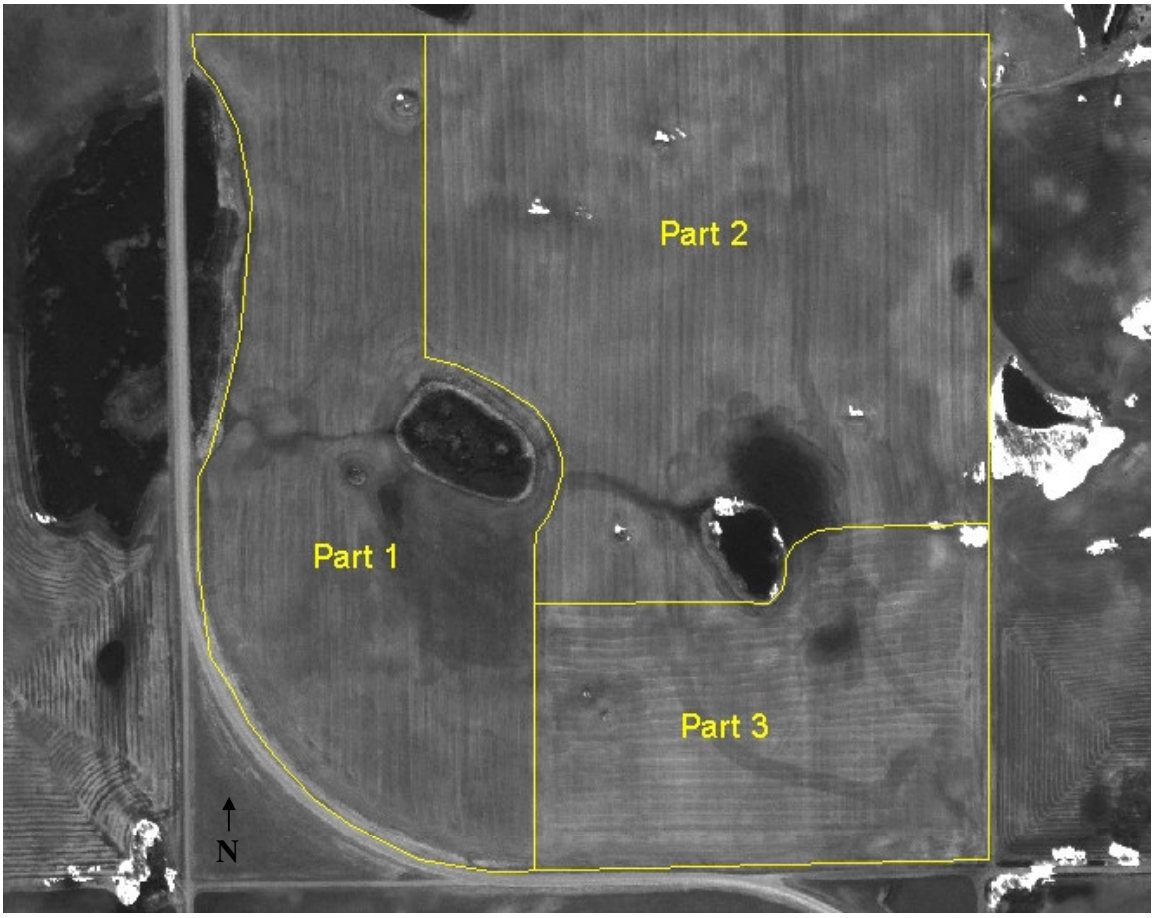

Figure 4.8 IKONOS image of Field 1 (April 24th, 2001).

4.2.5 Image Classification and Map Comparison

Image classification results produced four distinct classes based on brightness values (BV). Class 1 was associated with the lowest BV in the image, class 2, 3 and 4 with the remaining BV where class 4 clustered the highest BV. Therefore, knowing that low reflectance values on the image corresponded with wet low lying areas in the field and high brightness values corresponded to dry convex areas of the field (McCaan, 1995), Class 1 was compared to the Depression class of the DEM, class 2 was compared to Low class of the DEM, Class 3 was compared to the Mid class of the DEM and finally Class 4 was compared to the Upper class of the DEM as shown in Figure 4.9

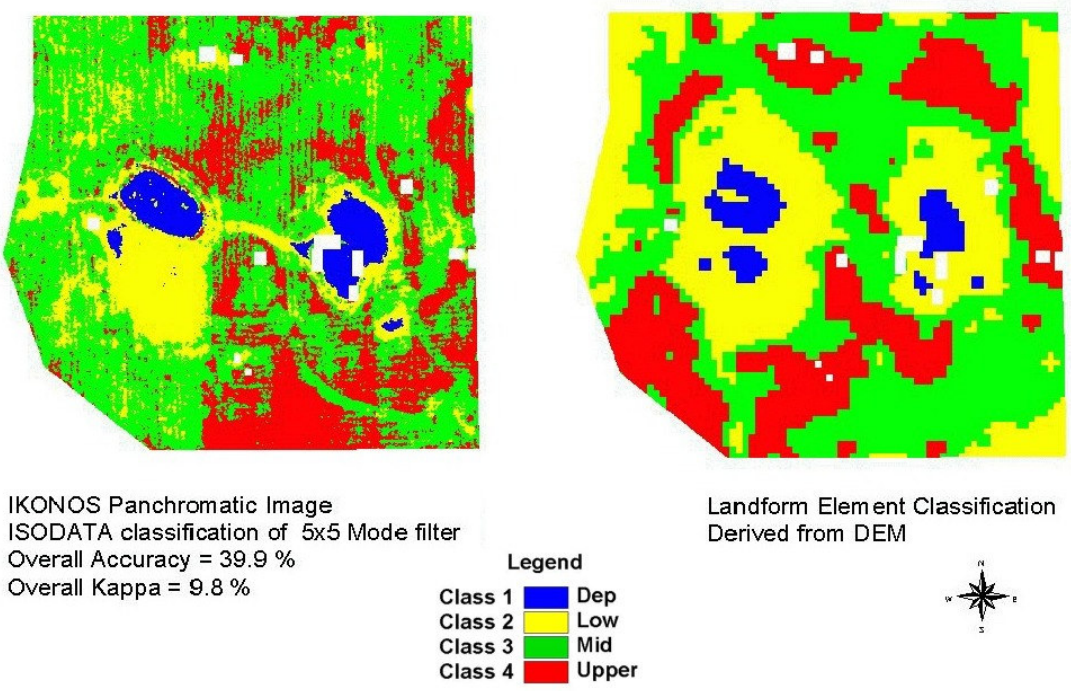

Figure 4.9 Classified thematic map comparison of Field 1.

Image classification results show that treatments (filter type, size) had no effect on producer's and user's accuracy for each class, and no effect on overall accuracy and

Kappa in both classification methodology (Appendix A, table 4.1a, 4.1b). Values for overall Kappa ranged between 7% to 9.8%, which confirmed the lack of agreement between classified image map, and landform element map as a Kappa coefficient lower than 85% is considered poor (Jensen, 1996). For example, producer's accuracy for the Isodata classification was the highest for the depression (Dep) category (65.5%) followed by Mid (56.4%), Low (24.8%) and Upper (21.1%). User's accuracy was the highest for class 2 followed by class 1, class 3 and class 4.

As treatment had no effects on classification accuracies, the combination of a 5 by 5 mode filter and Isodata classification was selected for further analyses. Distribution of classified IKONOS pixel was plotted for each LE class (Figure 4.10). Results showed that the Dep category was predominantly composed of 66.1% of class 1 pixels, 26.9% of class 2 pixels, 4.6% of class 3 pixels and 2.4% of class 4 pixels. The Low LE was predominantly composed of pixels of class 3 (43.3%), class 2 (30.4%), class 4 (21.2%) and Class 1(5.2%). The Mid category was composed primarily of Class 3 pixels (58.4%), and the Upper category was composed primarily of class 3 pixels (67.3%), class 4 and class 2.

Distribution of LE pixels within each IKONOS class showed similar results as class 1 which was predominantly composed of Dep pixels and Class 3 and 4 were composed primarily of pixels from the Mid category. However, class 2 was predominantly composed of Low category pixels (Figure 4.11).

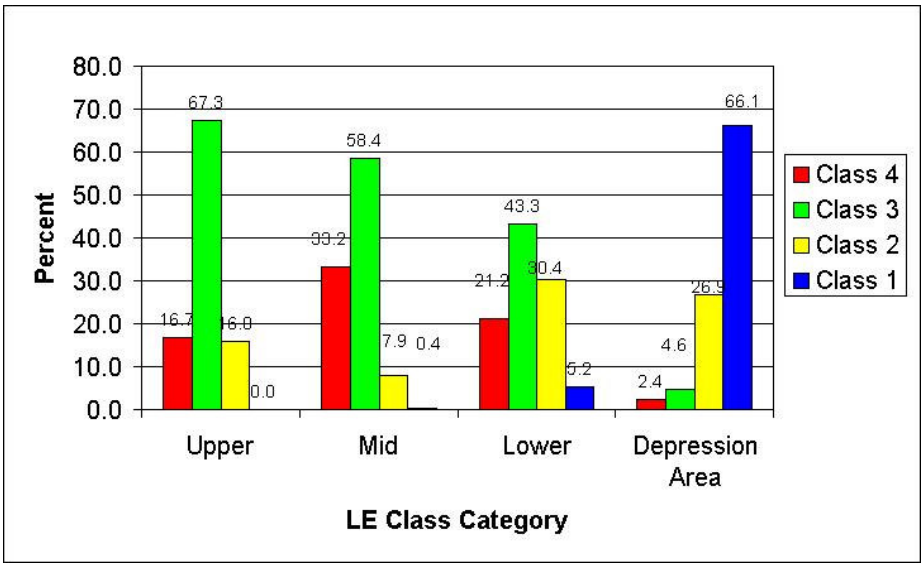

Figure 4.10 Distribution of IKONOS classified pixels within each LE class in Field 1.

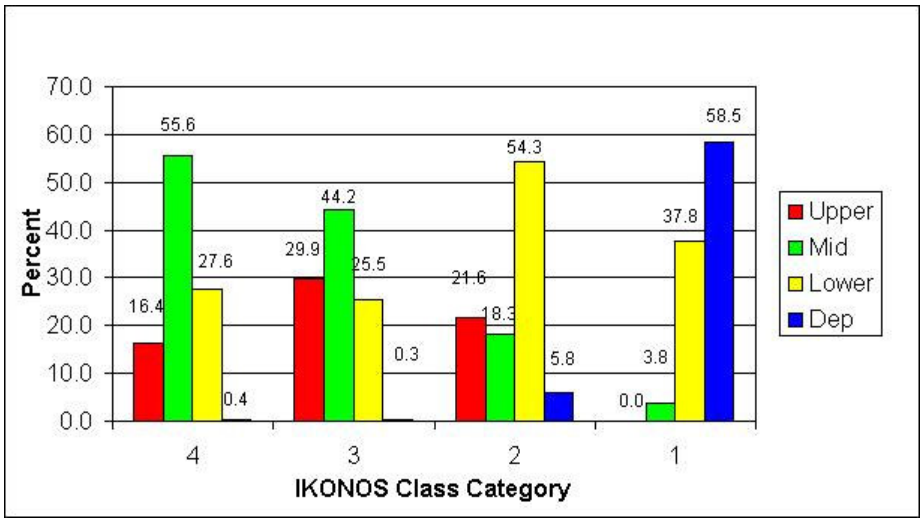

Figure 4.11 Distribution of LE pixels within each IKONOS class in Field 1.

This analysis showed that depression areas for Field 1 could be defined by using any combination of image filter type and size and an unsupervised classification of IKONOS panchromatic image. However, class 2,3, 4 and Low, Mid and Upper categories did not match perfectly. In the Landform map (Figure 4.9), landform categories were well defined with distinct boundaries where as in the IKONOS image

classification map, class boundaries were not well defined. Class 4 was predominantly located in the barley stubble, class 3 in both canola and barley stubble and class 2 in the canola stubble. Furthermore, the image classification process was drastically affected by man made features such as direction of swath rows and drive paths of farm equipment on the ground. Image classes followed regular linear patterns caused by harvesting equipment (swath rows and chaff/straw spreading patterns) which affected the final classification process. An obvious example of man made disturbance was the presence of a temporary road created by farm equipment on the southeast corner of Field 1. The repeated traffic of farm equipment and grain trucks at that location changed the surface roughness of the barley stubble thus changing its reflective properties. The result was a reduction in the reflectance of the barley stubble which lowers brightness values compared to the surrounding undisturbed barley stubble.

4.2.6 Sub Field 1 Analysis

Classification of the IKONOS image in Field 1 produced four distinct classes. However, the spatial distribution of each class was discontinuous as compared to the landform element map created from the DEM. One of the reasons for the erratic spatial distribution was the presence of several different types of ground surface cover in the field. During the unsupervised classification process, the user specified the number of classes desired along with a few other parameters, and the software created the desired number of classes. From Figure 4.8 it was evident that differences in stubble type as well as man made features affected the reflectance of the sunlight, thus affecting the classification process. Features, such as drive path, harvesting direction as well as stubble type and direction were classified instead of soil properties. Therefore a 35.2 ha

part of the field with four landform elements and a relatively uniform canola stubble cover was selected for analysis as shown in Figure 4.12. The IKONOS imagery was cropped, filtered using a 21 by 21 pixel mean filter and classified using an Isodata unsupervised classification. Producer's, user's and overall accuracy calculation as well as Kappa statistic were used to estimate accuracy.

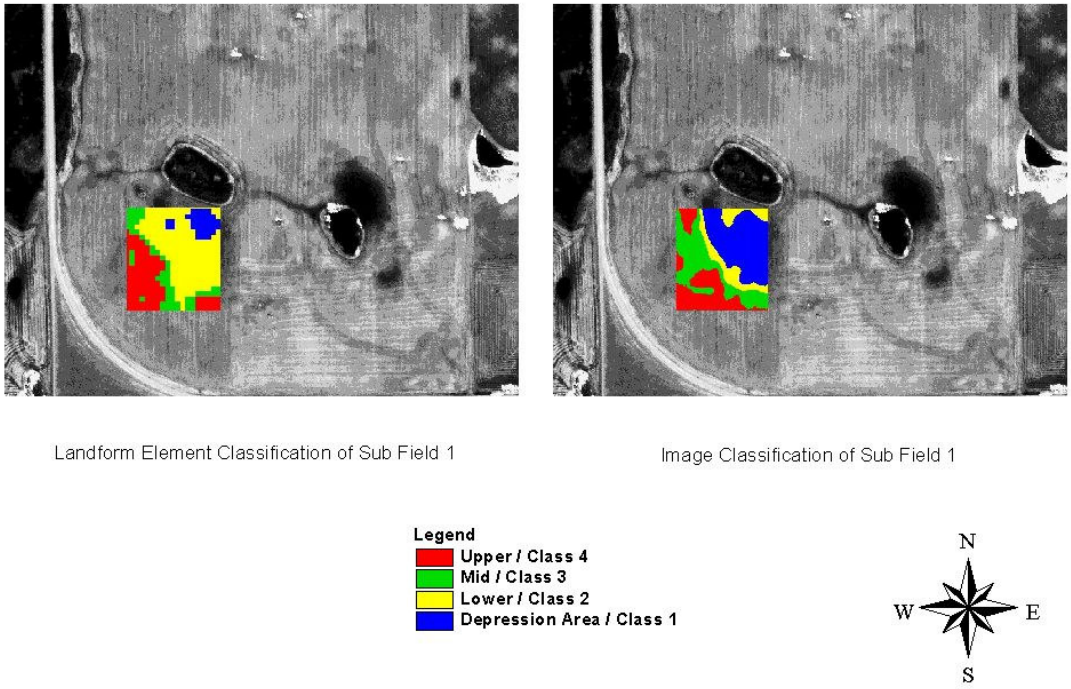

Figure 4.12 Sub-field image classification comparison.

The classification process created four classes with distinct spatial distribution. Pixel distribution analysis showed that, from the producer's perspective (classified image distribution per LE category), depression areas were well classified (86%), followed by Upper (40.1%), Mid and Lower landform positions (Table 4.2)

However, from a user's perspective (LE pixel distribution per IKONOS class) Lower landform position were better classified (82.5%) than the rest of the landform categories. Overall accuracy was slightly lower than the average overall accuracy for the

entire field (34.8% vs 38.3%) and the overall Kappa statistic was twice as good as the average overall Kappa statistic for the entire field at 18.3%. These findings suggest that even if ground cover appears uniform on the raw image, classes created from an unsupervised classification algorithm do not match landform element classes delineated from a DEM.

Table 4.2 Accuracy statistic comparison for Field 1 and sub-field 1.

	Producer's accuracy				**User's accuracy**				**Overall Accuracy**	**Kappa**
	Upper	Mid	Lower	Dep	4	3	2	1		
Sub-field 1	40.1	32.7	22.8	86.0	47.3	19.3	82.5	21.2	34.8	18.3
Whole field average	65.5	24.8	56.4	21.1	60.9	68.5	41.5	60.9	38.3	7.7

4.3 Field 2.

4.3.1 TIN Surface Interpolation

Using ArcView GIS ™ the raw elevation data points of Field 2 were converted to a 3D Triangulated Irregular Network (TIN) surface with an elevation exaggeration of 10 for visual interpretation of the landscape (Figure 4.13).

The TIN surface clearly illustrated the "channel" type of terrain present in the field, where the north and south edges were of higher elevation than the middle part of the field. The area consisted of gently undulating landscape in the middle part of the field, characterized by long slope and a general gradient running east-west, and hummocky areas on the edges of the channel characterized by shorter and steeper slopes.

Furthermore, a depression area (or slough), in the northeast part of the field where permanent water can be found, drained the excess run-off water via a natural draw present at the lowest elevation part of the field.

4.3.2 Landscape Feature Quantitative Description

The semivariance analysis showed that spatial auto-correlation between elevation points best fit a linear to sill model (Figure 4.14) with an r^2 of 0.99 and a range value of 353 meters. The linear to sill model showed the presence of two distinct patterns, which, in this case, would be a hummocky type landscape to the north and south edges of the field, with greater elevation difference and a gently undulating landscape in the middle of the field with small elevation variation.

The LandMapR™ analysis showed that more than 81% of the field was dominated by a slope gradient between 0.5% to 5% and 8.4% of the field was dominated by a slope gradient ranging from 6% to 9% (Figure 4.15). The dominant slope length categories were predominantly in the range of 450 to 800 meters (Figure 4.16) and the dominant relative relief was in the range of 10 to 20 meters (Figure 4.17). These statistics show that the field was made of two distinct landscape features. One could be classified as hummocky with long slope length, steep gradient and high relative relief and the second part as gently undulating with predominantly long slope length, low slope gradient and low relative relief.

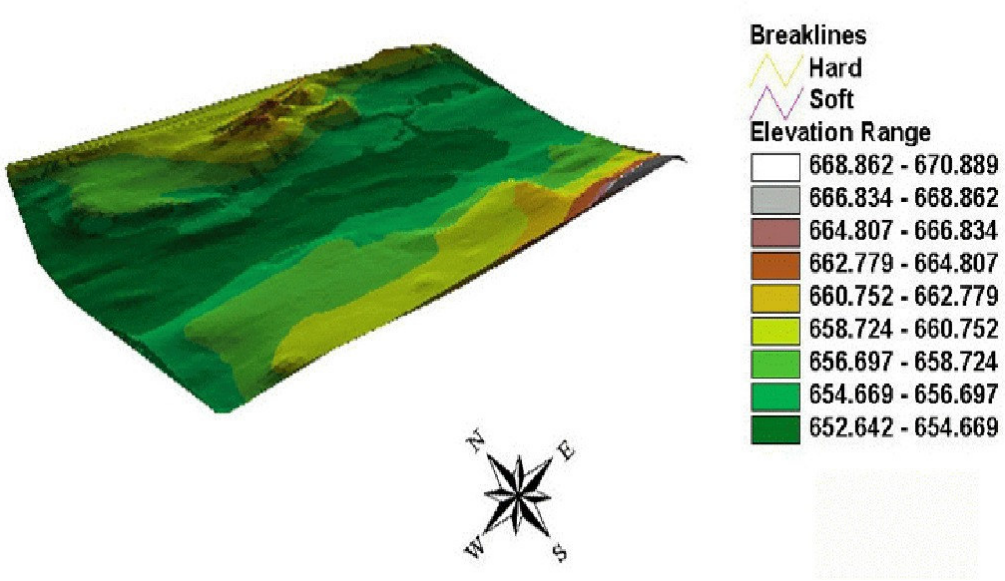

Figure 4.13 3D DEM of Field 2 with a vertical exaggeration factor of 10.

.

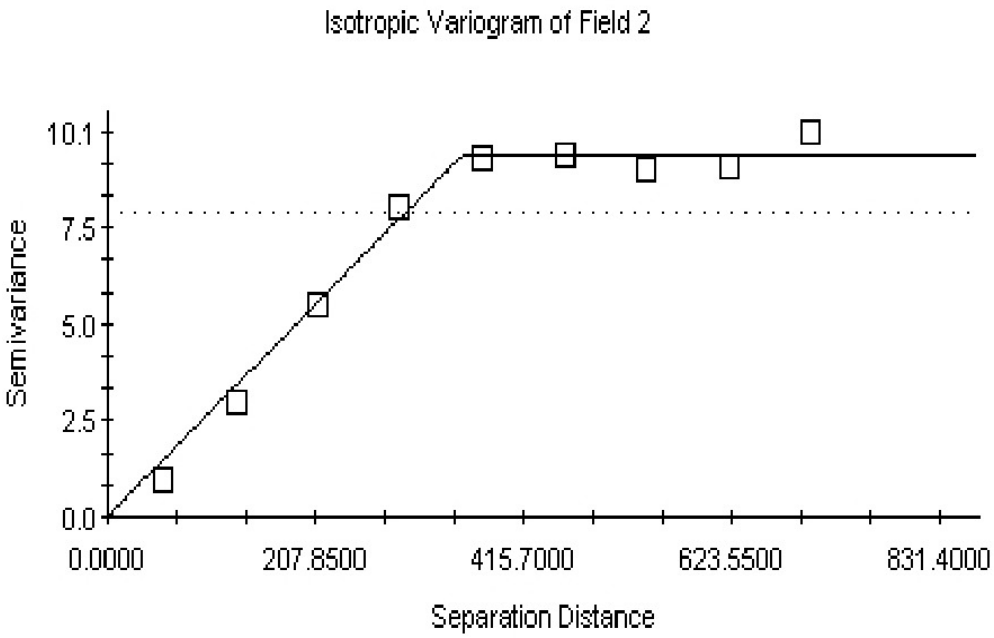

Linear to sill model (Co = 0.0100; Co + C = 9.4000; Ao = 353.0000; r2 = 0.990; RSS = 1.20)

Figure 4.14 Variogram of Field 2.

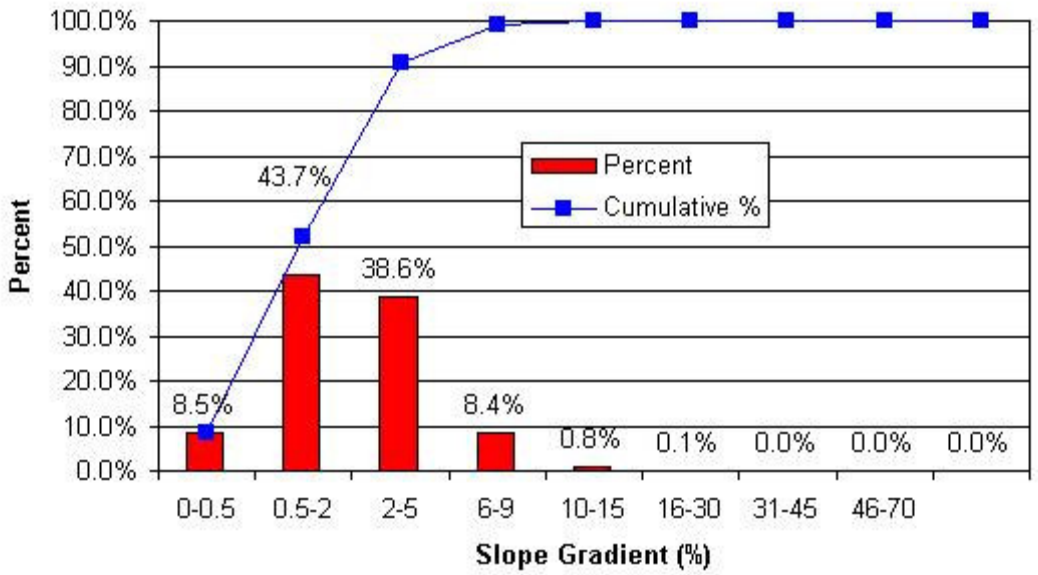

Figure 4.15 Slope gradient distribution in Field2.

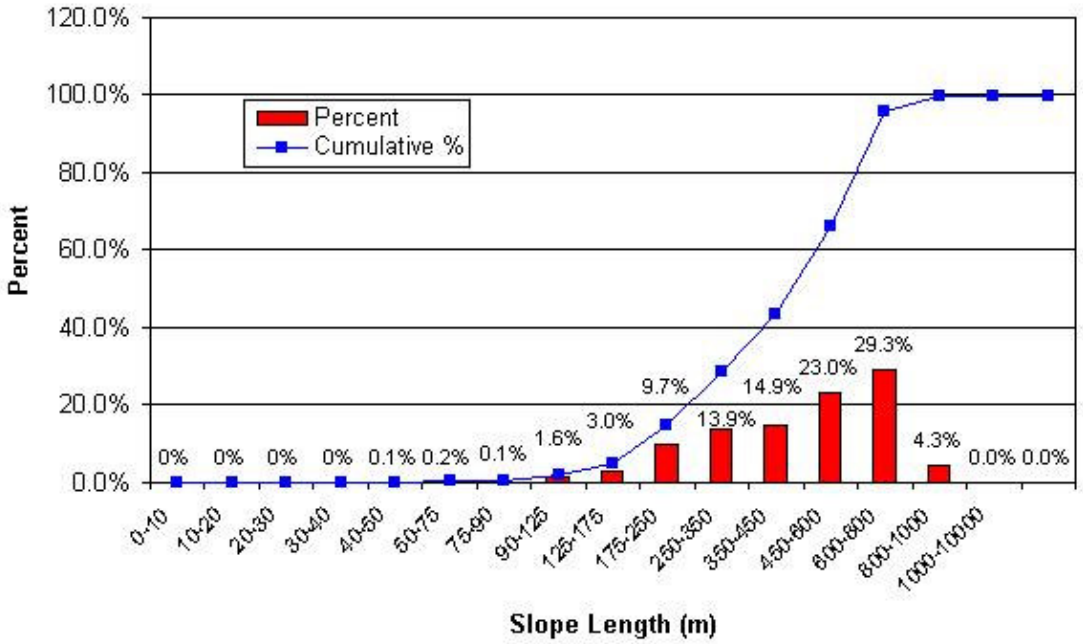

Figure 4.16 Slope length distribution in Field 2.

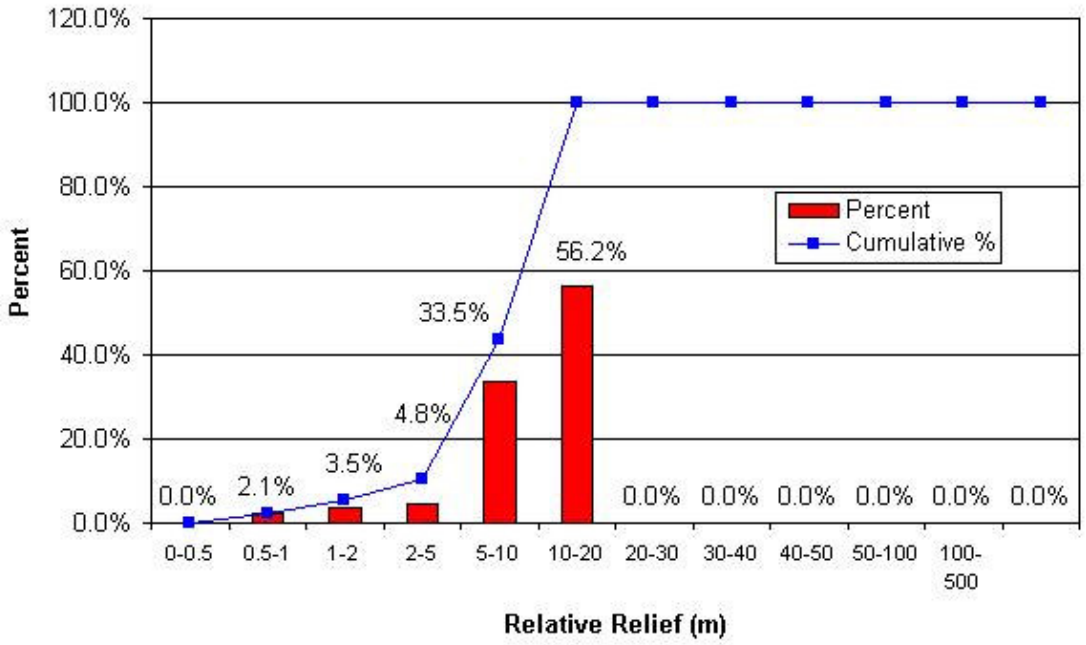

Figure 4.17 Relative relief distribution in Field 2.

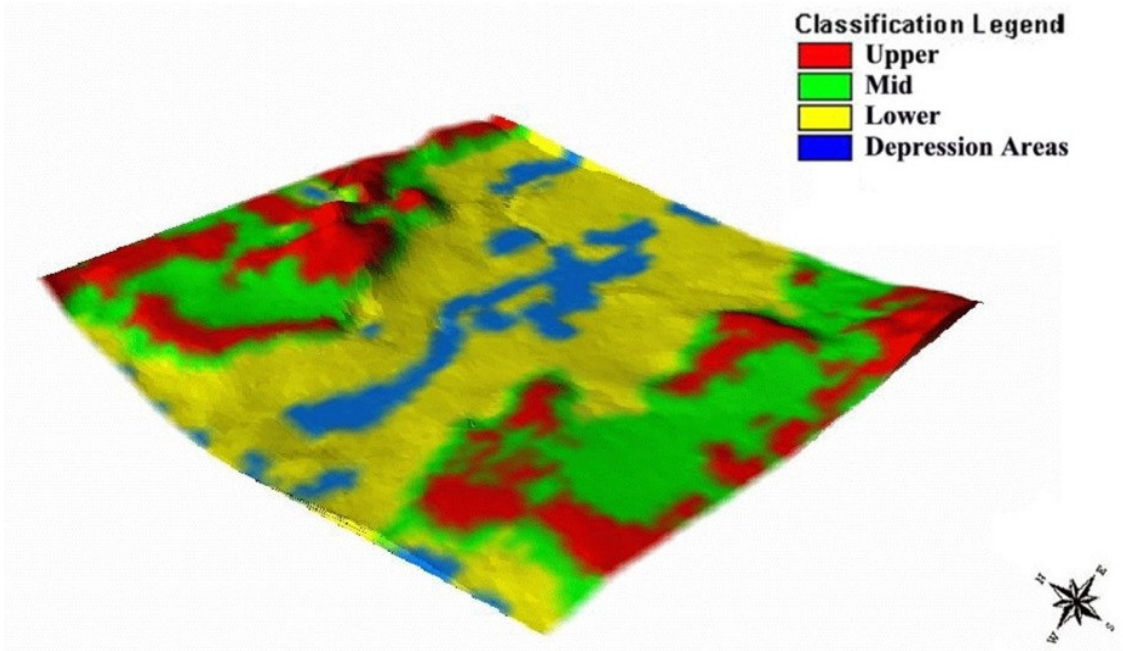

Figure 4.18 3D Landform element map of Field 2.

4.3.3 Landform Classification

Classification of the landscape into LE was done using the re-scaled elevation data. Four distinct classes (Upper, Mid, Lower and Depression areas) emerged from the classification as shown in Figure 4.18. Upper class was clearly evident on the north and south edges of the field with mid, lower and depression areas in the middle part of the field. The landscape was predominantly classified as Lower LE followed by Mid, Upper and Depression areas (Figure 4.19).

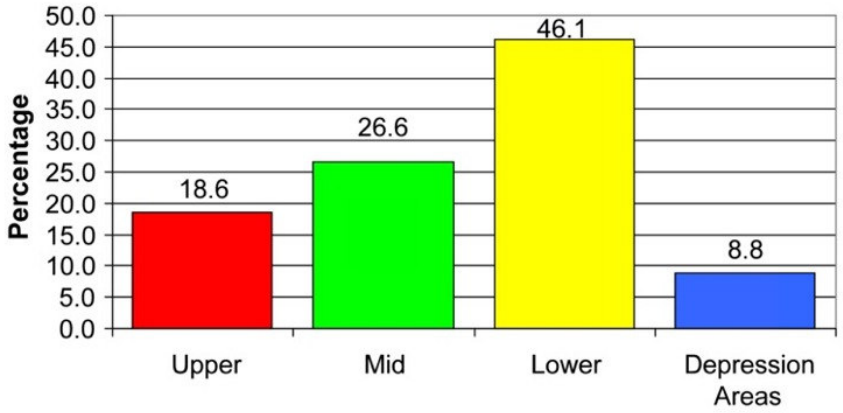

Figure 4.19 Landform element distribution in Field 2.

4.3.4 Land Cover Description

In the Image of Field 2 (Figure 4.20) four distinct features were evident. First, the entire field was seeded to canola and harvested in the east-west direction leaving parallel whiter strips in the image. These whiter strips were caused by a higher density of straw and chaff left in swaths from the harvesting equipment which reflected more light and thus looked brighter in the image. Second, two permanent sloughs, one in the north-east corner and one on the west side, connected via a natural surface drainage channel were clearly visible in the image as both depression areas and channel appeared darker in the

image. Furthermore, a second surface run-off channel connected the north end of the field to the main drainage channel connecting the two sloughs. Thirdly, some mechanical soil tillage or heavy harrowing of areas surrounding both sloughs and natural drainage channels was evident in the image as dark grey parallel strips were clearly visible in those areas. Lastly, a small shelterbelt oriented north-south in the middle of the field was clearly identified as snow accumulated on both sides of it. Furthermore a few snow banks existed on the north end of the field as they appeared very white in the image. The latest items were omitted from the image classification to concentrate the image analysis process on the stubble-covered soil only.

Figure 4.20 IKONOS Image of Field 2 (April 24th, 2001).

4.3.5 Image Classification and Map Comparison

Image analysis classification results showed that treatments (filter type, size and classification methodology) had no effects on classification accuracy (Appendix A, table 4.2a, 4.2b). Producer's accuracy was the highest for the Mid LE followed by Dep, Upper and Lower in both classification method.

User's accuracy was the highest for class 2 followed by class 1, class 3 and class 4. The average overall accuracy for the Isodata classification method was 38.1% and for the fuzzy k-means was 37.9%. Field 2 had the highest kappa statistic of all 5 fields with a classification accuracy of 16.1% to 16.2% depending on the classification method used. Visual comparison of the classified image map and landform element map revealed the similarity in spatial patterns of class 1 and depression category in the low lying areas of Field 2 (Figure 4.21). However, an inversion in areal extent of class 2 and 3 versus mid and low category contributed the most to the lack of agreement between both maps.

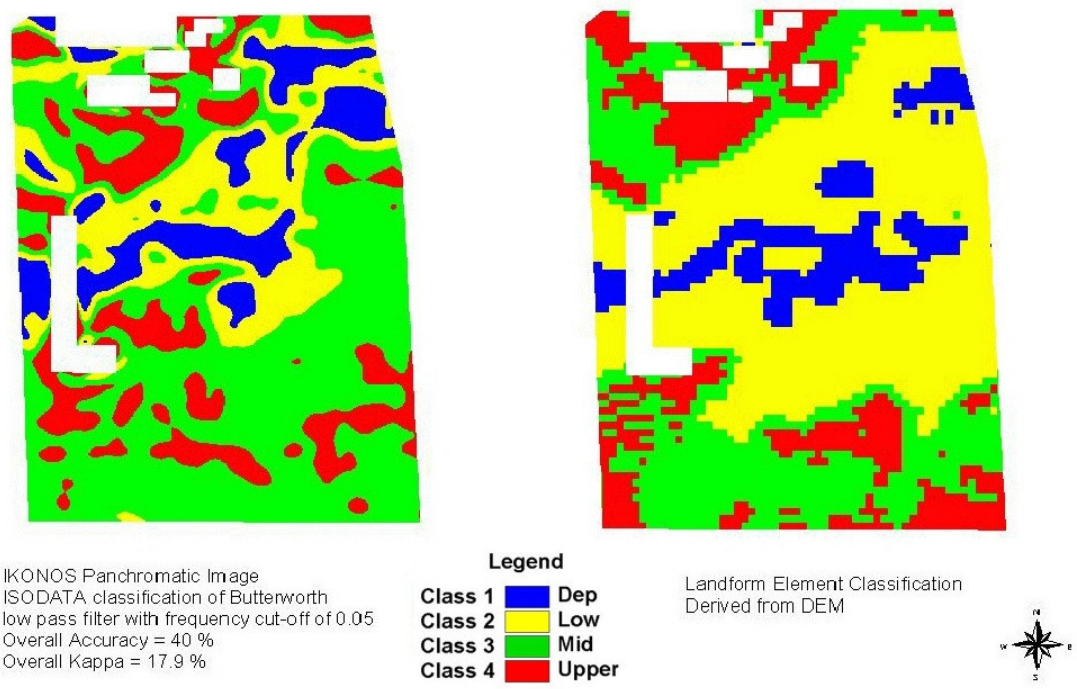

Figure 4.21 Classified thematic map comparison of Field 2.

Further analyses were conducted on the image with the best Kappa statistic (Fast Fourier transformed image with the Gaussian low pass frequency filter and classified using an Isodata algorithm). Results showed that when the landform element categories were assumed as the reference data set (Producer's accuracy), the Dep category was mostly composed of class 1 pixels (46.3%), followed by class 2, 3 and 4 respectively. The Low category was composed of 47.3% of class 3 pixels followed by class 2, class 4 and class 1. The Mid category was composed primarily of class 3 pixels (60.7%), followed by class 4, class 2 and class 1. The Upper category was mostly composed of class 3 pixels, followed by class 4, class 2 and class 1 (Figure 4.22). Therefore, the Dep

and Mid LE were well represented by Class 1 and Class 3 in the image analysis and the upper and lower LE were, in most part, represented by class 3.

When the IKONOS classes were considered as the reference dataset (User's accuracy) in the map comparison process, results differed from the User's accuracy. Class 1 was composed primarily of low (46.5%) and depression area (44%) pixels, class 2 of low category pixels (64.6%), Class 3 of low (40.3%) mid and upper pixels and class 4 of a mix of upper, mid and low pixels (Figure 4.23).

In Field 2, depression areas and class 1 were similar from the user's and producer's perspective . However the spatial patterns of Class 2, 3 and 4 did not match the spatial patterns of the low, mid and upper categories. Nevertheless, distinct patterns emerged from the image classification process which showed that image classification algorithms can be used to delineate areas of similar reflectance.

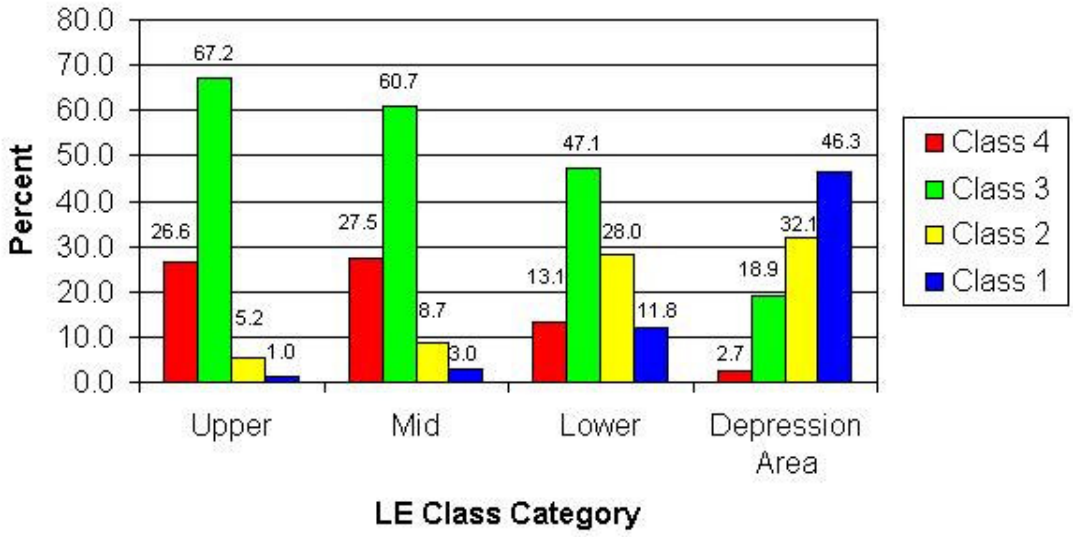

Figure 4.22 Distribution of IKONOS classified pixels within each LE class in Field 2.

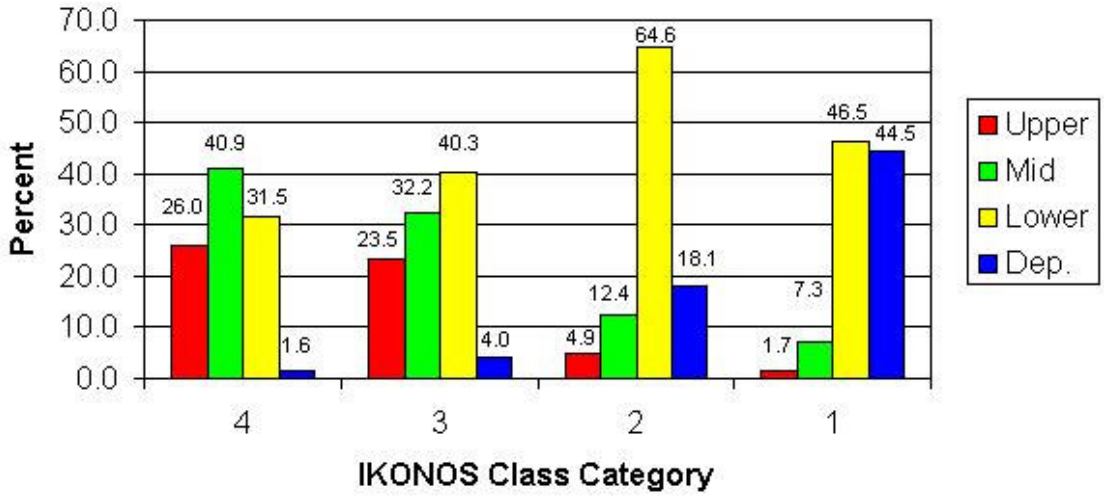

Figure 4.23 Distribution of LE pixels within each IKONOS class in Field 2.

4.3.6 Sub-Field 2 Analysis

As Field 2 did not have uniform ground cover areas where four landform elements were present, no sub-field analysis was done.

4.4 Field 3

4.4.1 TIN Surface Representation

Using ArcView GIS™ the raw elevation data of Field 3 was converted to a 3D Triangulated Irregular Network (TIN) surface with an elevation exaggeration of 10 for visual interpretation of the landscape (Figure 4.24)

The TIN map clearly illustrated the general gradient of the elevation from the east to the west of the study area where higher elevations were found in the eastern part of the field. Visually, the eastern half of the field had a more aggressive landscape with short

slope lengths and steep gradient as compared to the western half of the field where slope lengths were longer and slope gradients were low. There were a few other features of interest: 1) the eroded knoll in the north western part of the field, characterized by the raised edges at the foot of the slope due to soil movement from water and tillage erosion and 2) the depression area located in the south western corner which corresponded to the lowest elevation of the field and acted as a catch basin for surface run-off.

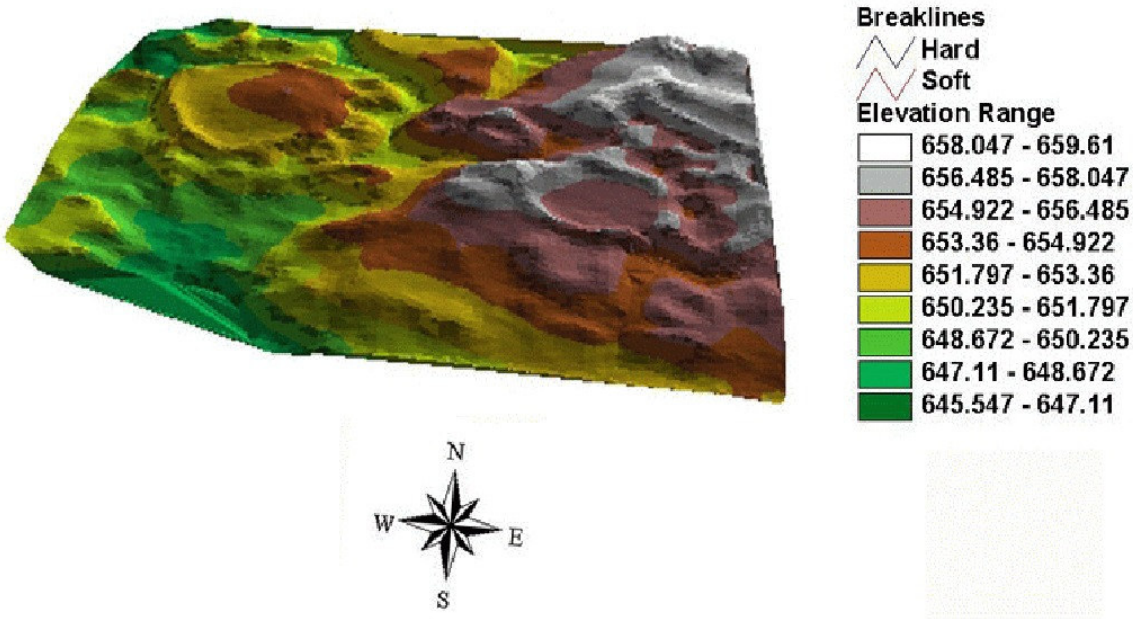

Figure 4.24 3D DEM of Field 3 with an exaggeration factor of 10..

4.4.2 Landscape Quantitative Description

The semivariogram of the raw elevation data best fit a Gaussian model with an r^2 of 0.997 and a range value of 681 meters (Figure 4.25). The Gaussian model expressed the smooth and periodic spatial variation of landscape features throughout the study area (Burrough P.A and McDonnell, 1998) which corresponded with the hummocky dissected

description provided by The Soils of Indian Head Rural Municipality No 156 Saskatchewan, 1988.

The dominant landscape features in the field were found to have a slope gradient of 2 to 5% (Figure 4.26), slope length ranging between 175 to 450 meters (Figure 4.27) and a relative relief ranging from 5 to 10 meters (Figure 4.28).

4.4.3 Landform Element Classification

Classification of the landscape into LE was done using the re-scaled elevation data. Four distinct classes emerged from the classification as shown in Figure 4.29.

The Upper category represented 33.6% of the landscape, the Mid category 37%, the Lower category 28.1% and the Depression areas category 1.3% (Figure 4.30). The even distribution of the first three LE categories also illustrated the regular spatial distribution of the hummocky landscape throughout the entire field.

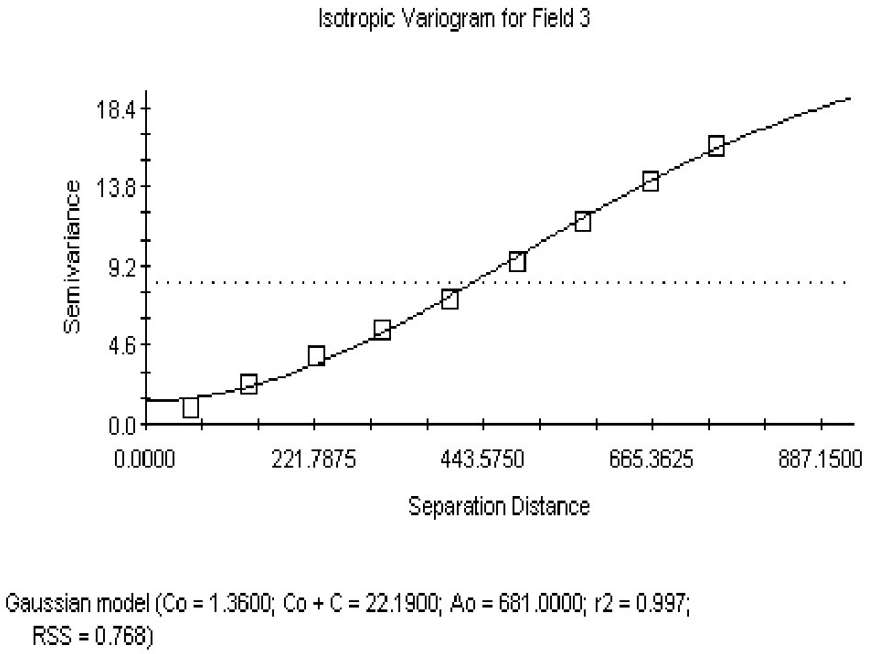

Figure 4.25 Variogram of Field 3.

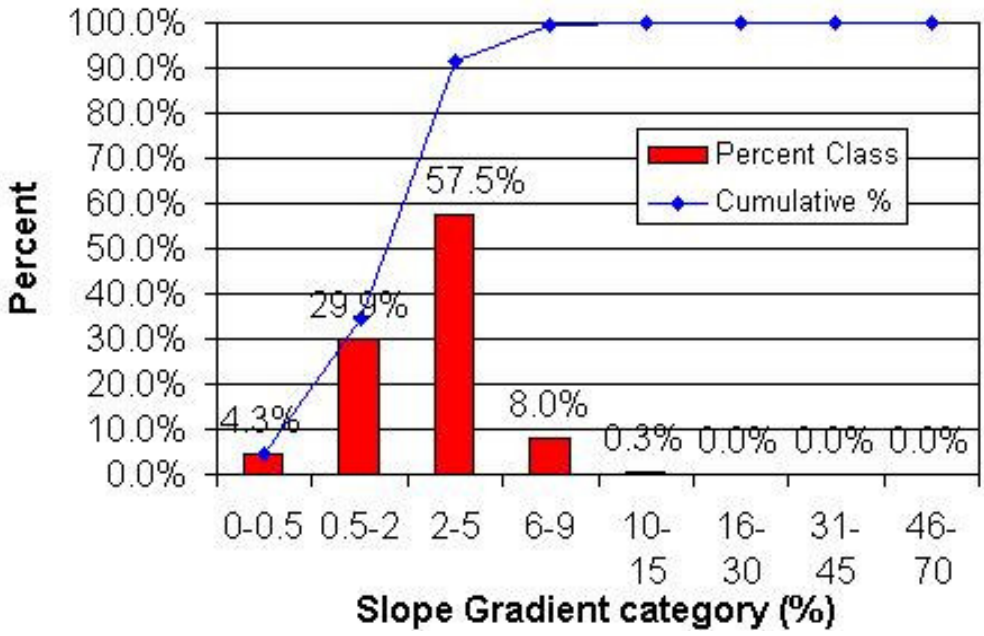

Figure 4.26 Slope gradient distribution in Field 3.

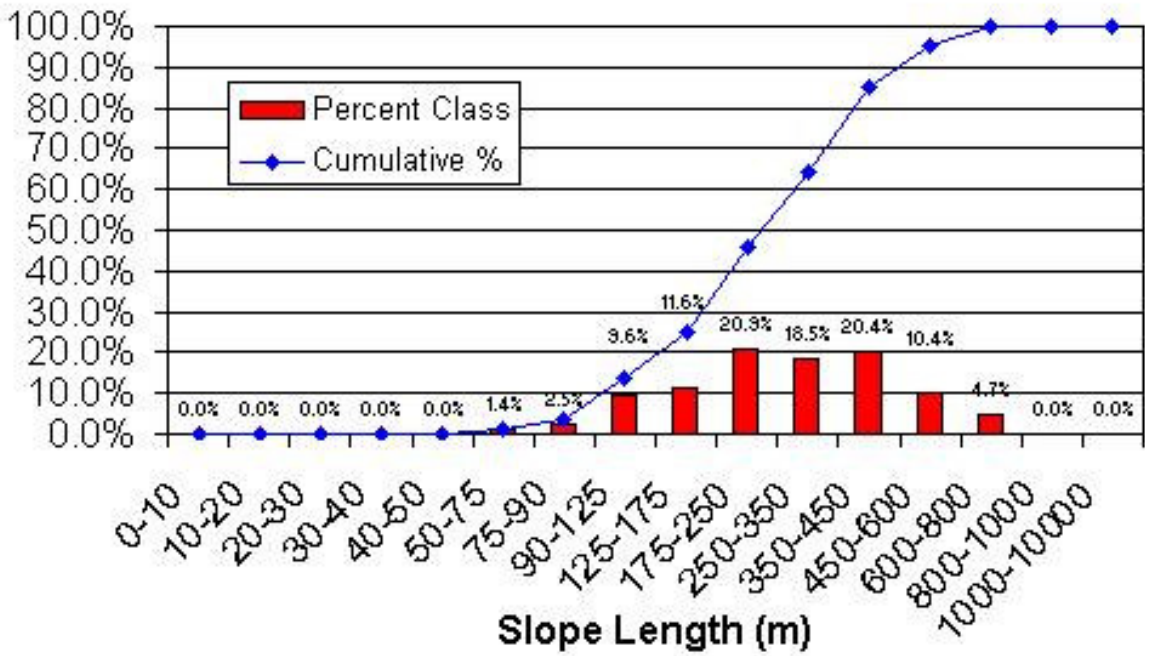

Figure 4.27 Slope length distribution in Field 3.

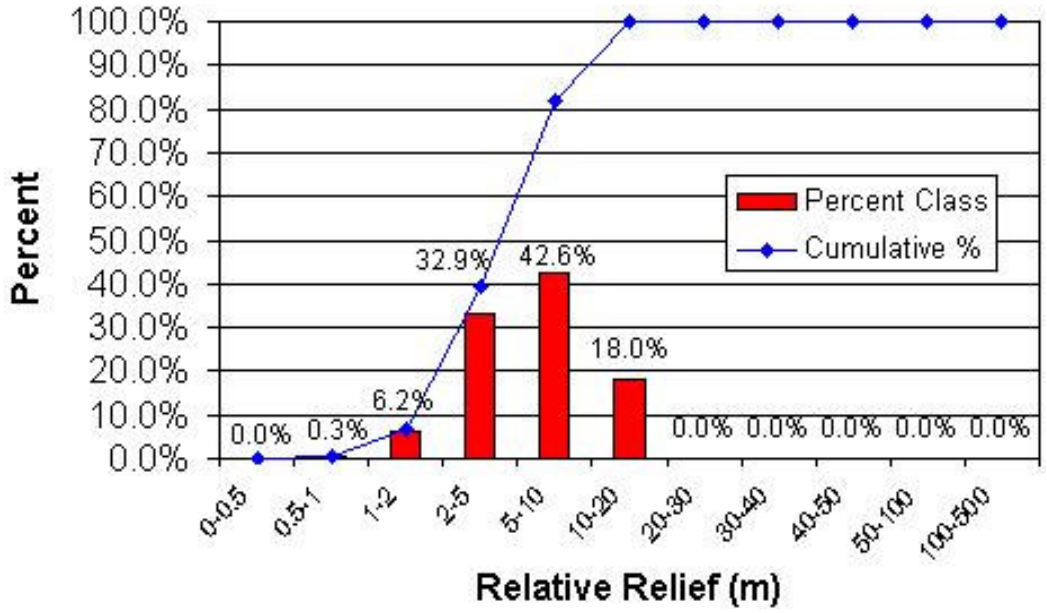

Figure 4.28 Relative relief distribution in Field 3.

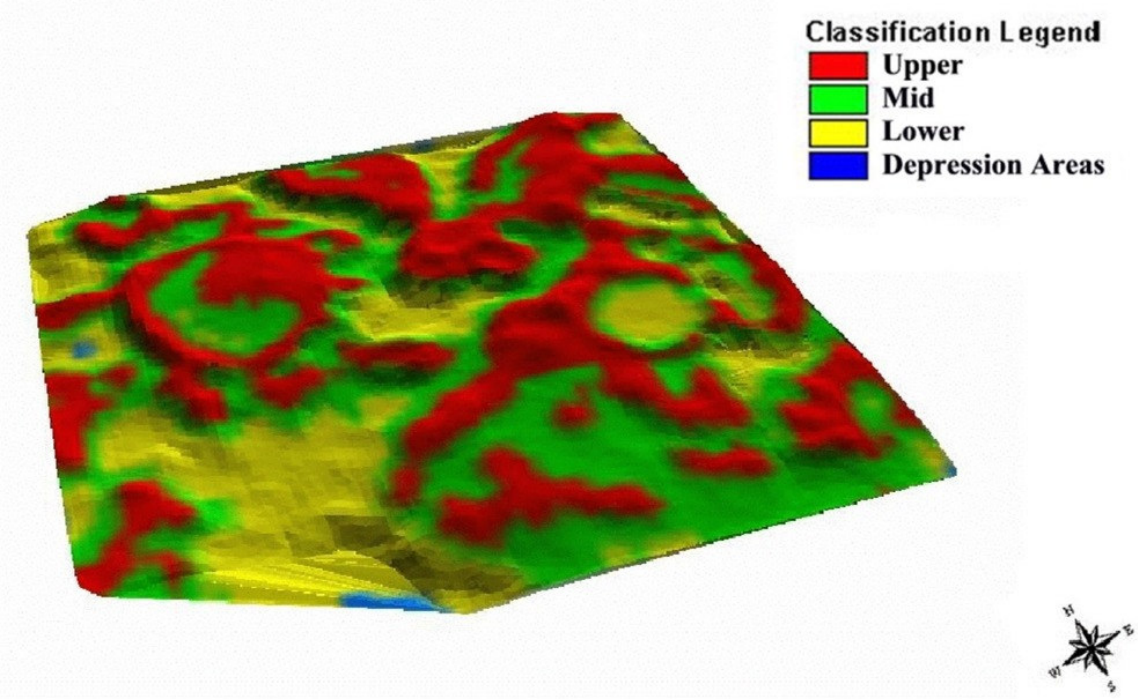

Figure 4.29 3D Landform element map of Field 3.

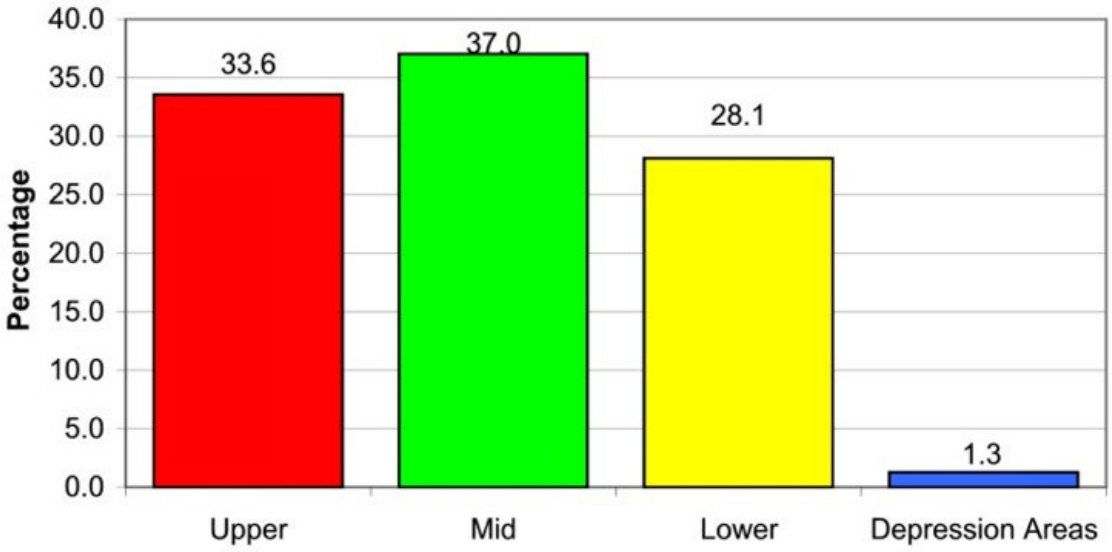

Figure 4.30 Landform element distribution in Field 3.

4.4.4 Land Cover Description

Field 3 was the field with the most ground cover variability. To best describe the existing ground cover, the image was split into four parts (Figure 4.31). Part 1, the west half of the field, was seeded to field peas. When field peas were matured, the plants tend

to fall to the ground. Thus, at harvest, pea plants were cut as close to the ground as possible to minimize grain loss. As a result, the dried field pea stubble was shredded to a fine powder and spread back onto the field which resulted in a smooth gray tone on the image with very little striping effects as is commonly noticed with other types of stubble. Two snow banks were also present in the north end of the field but were masked from the image before analysis. A few small circular black areas were apparent in the image which were identified as permanent wet depression areas.

The east side of the image, Part 2, was seeded to spring wheat and harvested following the contour of the land. As a result, parallel whiter strips were evident in the image as well as the direction the crop was harvested. In general, cereal crops were cut 10 to 20 centimetres from the ground prior to or at harvest (straight combining), and the straw and chaff spread out by the combine. This left large swaths of crop residue on the ground which resulted in clear bright strips in the image. Furthermore, several wet depression areas were detectable as they appeared very dark in the image.

In the fall of 2000, a fire burned the stubble in Part 1 and spread into Part 2 resulting in a distinct black area in the field. Part 3 of the image corresponded to burnt pea stubble, which enhanced the contrast of the land, and Part 4 corresponded to the burnt wheat stubble. Part 3 and 4 showed great contrast in grey tones as compared to the stubble covered area which highlighted the masking effect of stubble coverage on the reflectance of soil. In both Part 3 and 4, distinct bright circular patterns were evident which again proved that crop residue masked a lot of the soil reflectance variability.

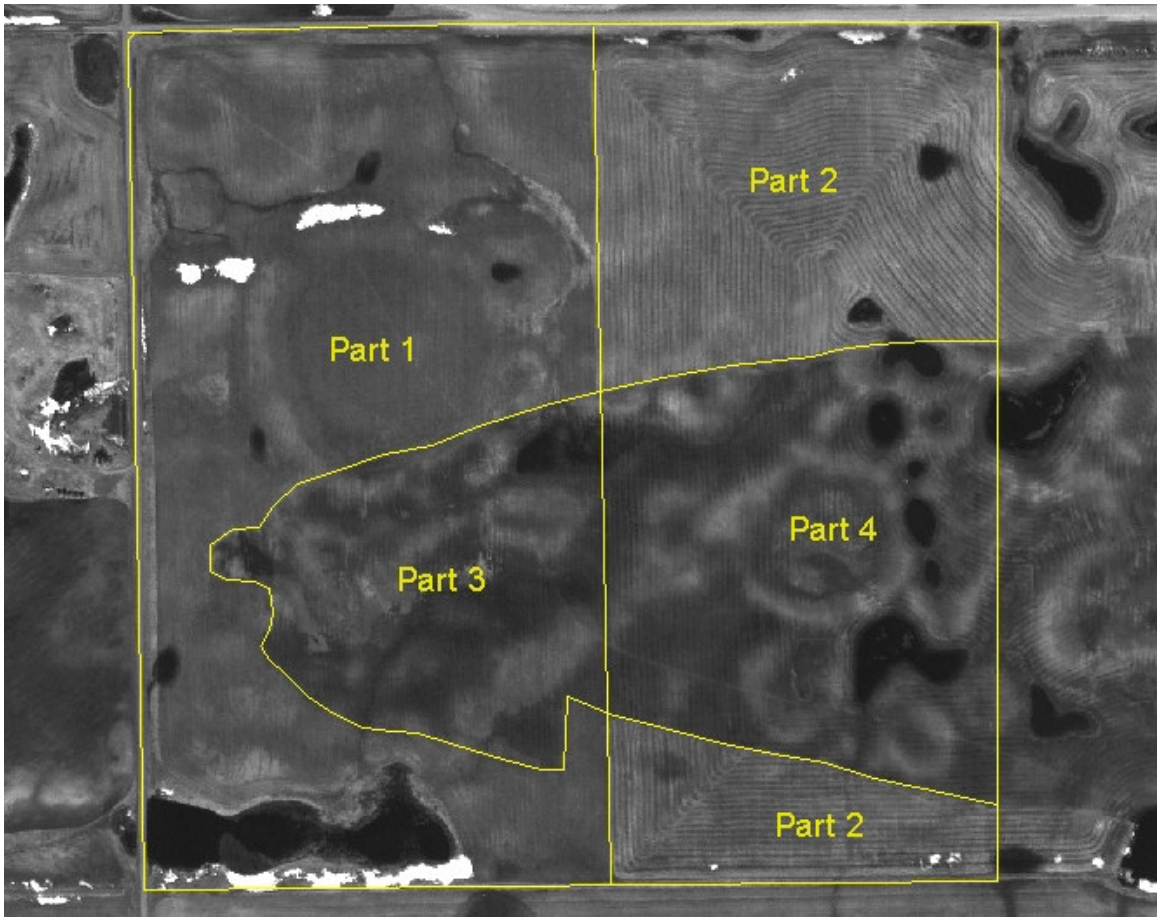

Figure 4.31 IKONOS image of Field 3 (April 24th, 2005).

4.4.5 Image Classification and Map Comparison

Classification results show that treatments and classification method had no effects on producer's, user's, overall accuracy and Kappa statistic (Appendix A, table 4.3a, 4.3b).

In both classification methods, results show that depression area LE had 0% producer's accuracy. The mid and upper category had the highest producer's accuracy followed by Low LE. In both classification methods, the user's accuracy was the highest for class 4, followed by class 3, class 2 and class 1.

Overall accuracy varied from 21.4% to 35.4% for all treatments and classification method and overall kappa varied from 1.2% to 6.0% which illustrated the lack of agreement between the classified maps (Figure 4.32). Visual comparison of the classified image and the corresponding landform element map revealed that spatial distribution of classes created during the image analysis was very different than the spatial distribution of the landform element categories. Classes created during the image classification process more likely represented the type of land cover present on the ground rather than soil properties.

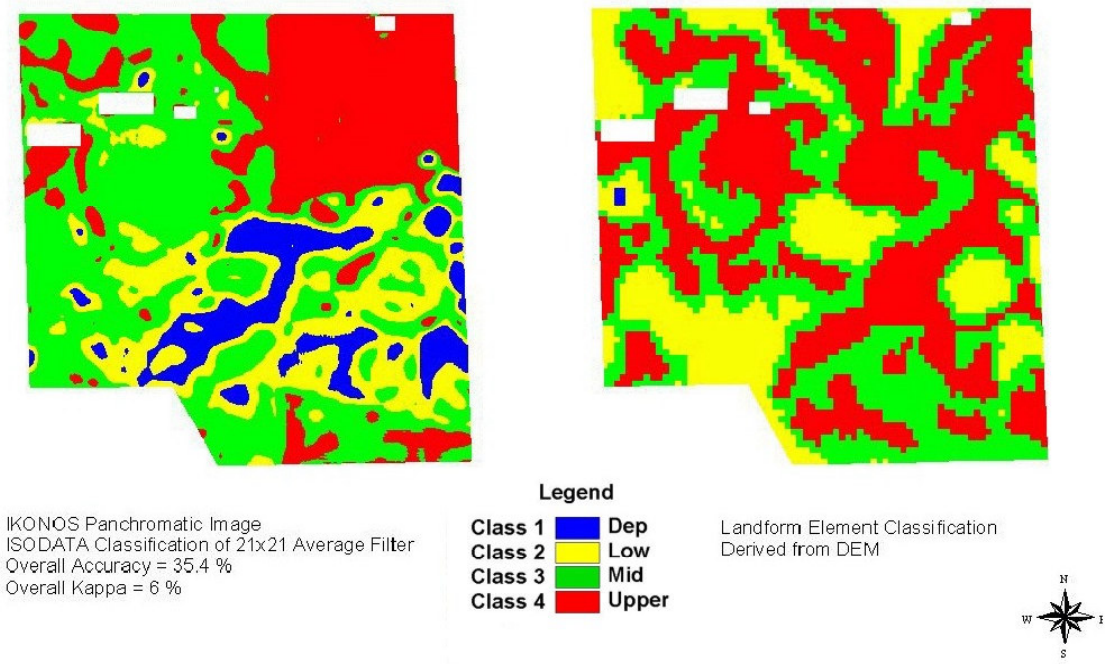

Figure 4.32 Classified thematic map comparison of Field 3.

Further studies were conducted on the IKONOS image filtered using a 21 x 21 mean filter and classified using the Isodata algorithm. Results show that when the landform element map was considered as the reference layer (producer's accuracy), the

Depression LE was composed mostly of class 3 (58.5%) and class 4 (41.5%) pixels, and the Low, Mid and Upper category were composed of all four classes with a dominance of class 3 pixels in all four categories (Figure 4.33).

When the IKONOS classification map was used as the reference dataset (user's accuracy), results showed that all classes were composed of a mix of the Low, Mid and Upper category pixels only (Figure 4.34). Class 1 was dominated by low category pixels (49.9%), class 2 was dominated by pixels of the mid category, class 3 and 4 were dominated by pixels of the upper category and class 4 (48.9% and 60.7% respectively).

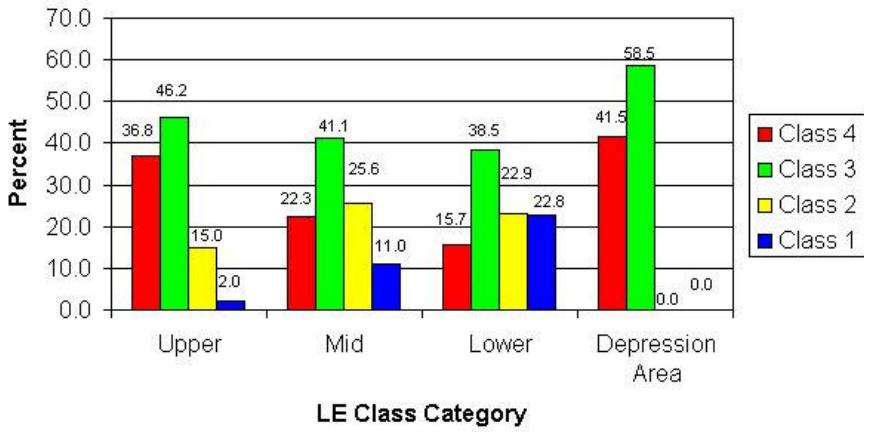

Figure 4.33 Distribution of IKONOS classified pixels within each LE class in Field 3.

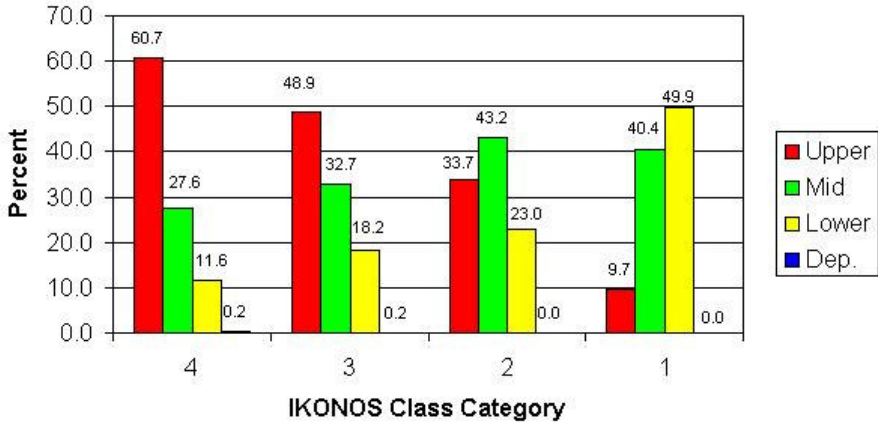

Figure 4.34 Distribution of LE class pixels in each IKONOS class in Field 3.

4.4.6 Sub-Field 3 Analysis

A 24-hectare part of Field 3, located in the pea stubble, was cropped from the entire field image, filtered and classified using an Isodata unsupervised classification algorithm. The four classes created were compared to the landform element categories located in the same area. Producer's, user's, overall accuracies were calculated and reported in Table 4.3.

Table 4.3 Accuracy statistic comparison for Field 3 and sub-field 3.

	Producer's accuracy				**User's accuracy**				**Overall Accuracy**	**Kappa**
	Upper	Mid	Lower	Dep	4	3	2	1		
Sub-field 3	20.7	18.0	61.5	0.0	88.6	18.9	22.1	0.0	26.9	-0.15
Whole field average	31.9	37.8	25.2	0.0	60.6	32.4	22.0	0.0	32.1	4.7

Results show that depression areas were misclassified as producer's and user's accuracy were 0%. However, producer's accuracy for the lower landform element was 61.5% and the user's accuracy for class 4 was 88.6%. Overall accuracy was lower than the overall accuracy for the entire field (26.9% vs. 32.1%) and Kappa statistic was very poor indicating a lack of agreement between the landform element map and the classified IKONOS image as illustrated in Figure 4.35.

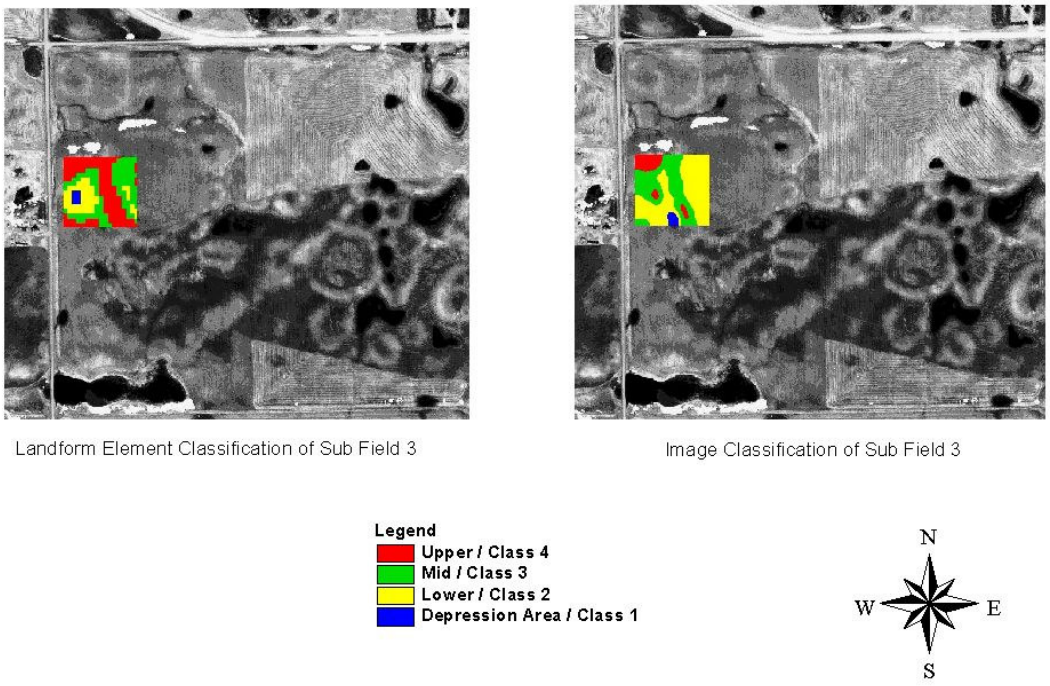

Figure 4.35 Sub-Field 3 thematic map comparison.

4.5 Field 4

4.5.1 TIN Surface Representation

Using ArcView GIS the raw elevation data of Field 4 was converted to a 3D Triangulated Irregular Network (TIN) surface with an elevation exaggeration of 10 for visual interpretation of the landscape (Figure 4.36).

The study area was characterized by a gently undulating landscape with a general slope gradient oriented from the southwest to northeast. Small elevation differences created depression areas where surface run-off was trapped.

4.5.2 Landscape Feature Description

The semivariogram of the raw elevation data best fit a linear model with an r^2 of 0.98 and a range of 934 meters (Figure 4.37), indicating that the variance between pairs of elevation points linearly increased as the distance between pairs increased thus emphasizing the flatness or lack of relief in the study field.

Landscape features present in the field had a dominant slope of 0.5% to 2% (Figure 4.38) with slope length ranging from 600 to 1000 meters (Figure 4.39) and a dominant relief of 2 to 5 meters (Figure 4.40) which is typical of agricultural fields found in the black soil zone of Indian Head, SK (Saskatchewan soil survey, 1986).

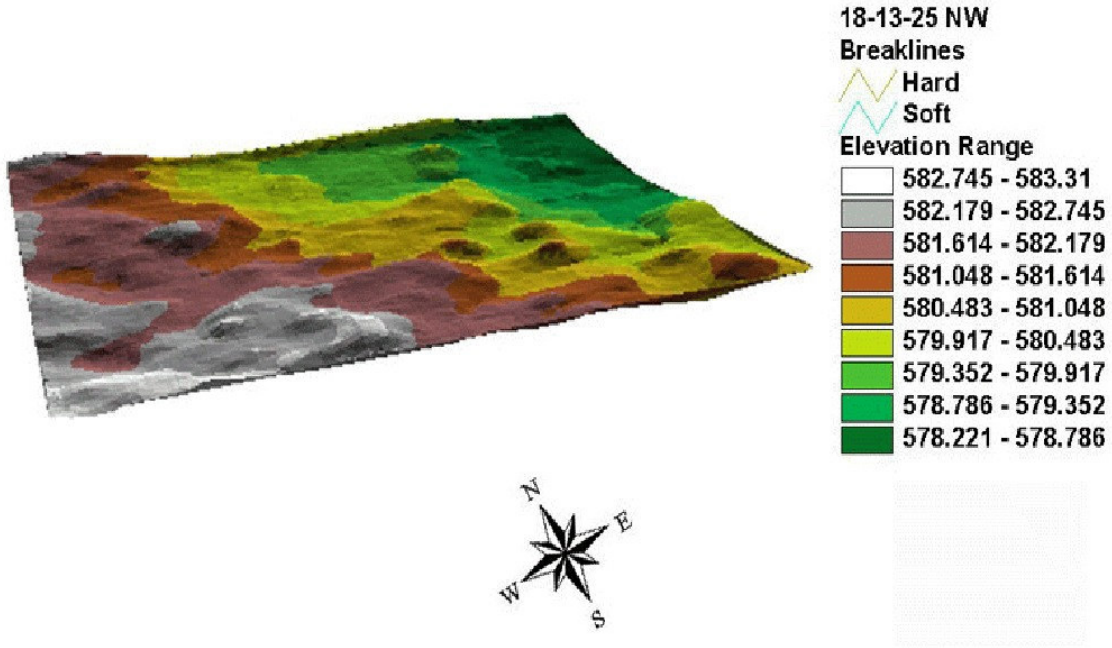

Figure 4.36 3D DEM of Field 4 with an exaggeration factor of 10.

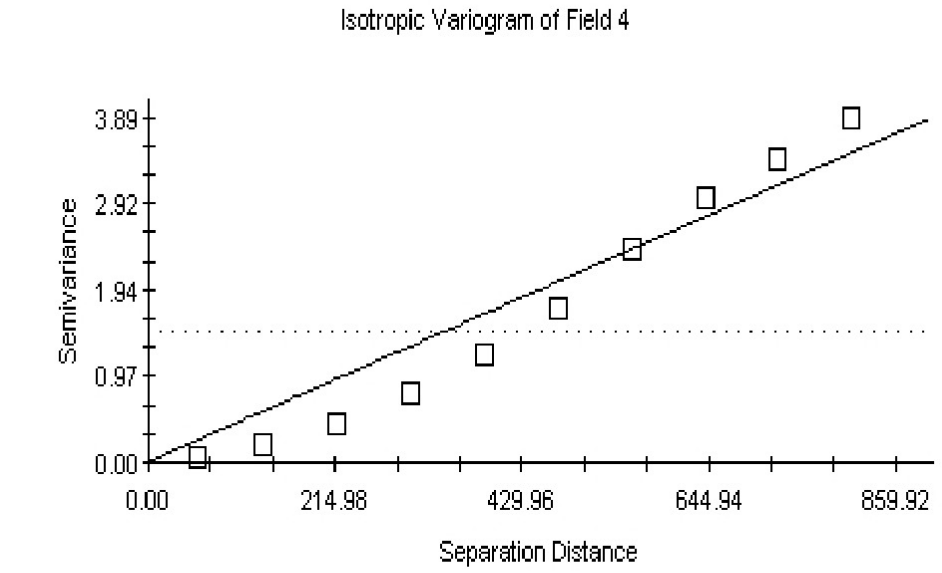

Linear model (Co = 0.01000; Co + C = 4.02900; Ao = 934.00; r2 = 0.980; RSS = 1.28)

Figure 4.37 Variogram of Field 4.

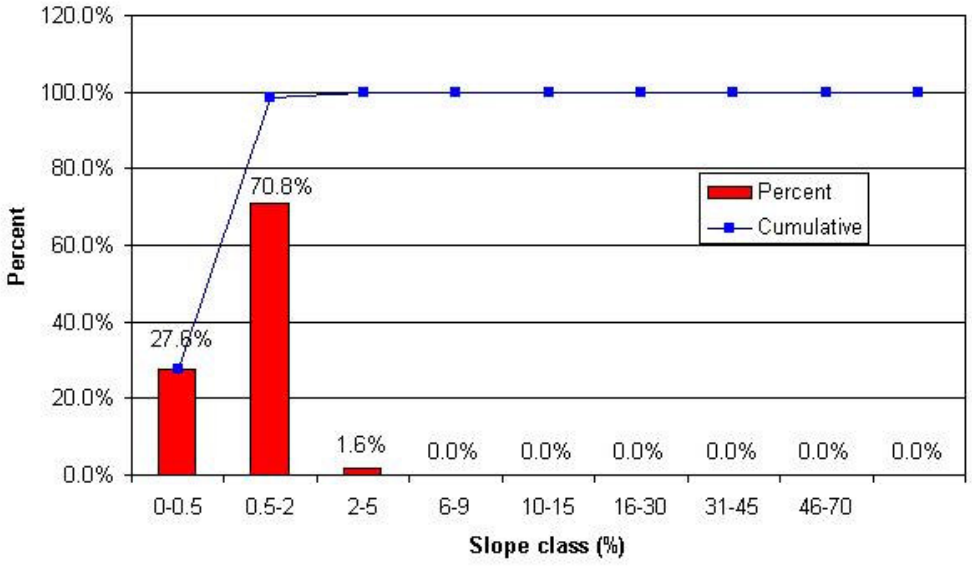

Figure 4.38 Slope gradient distribution in Field 4.

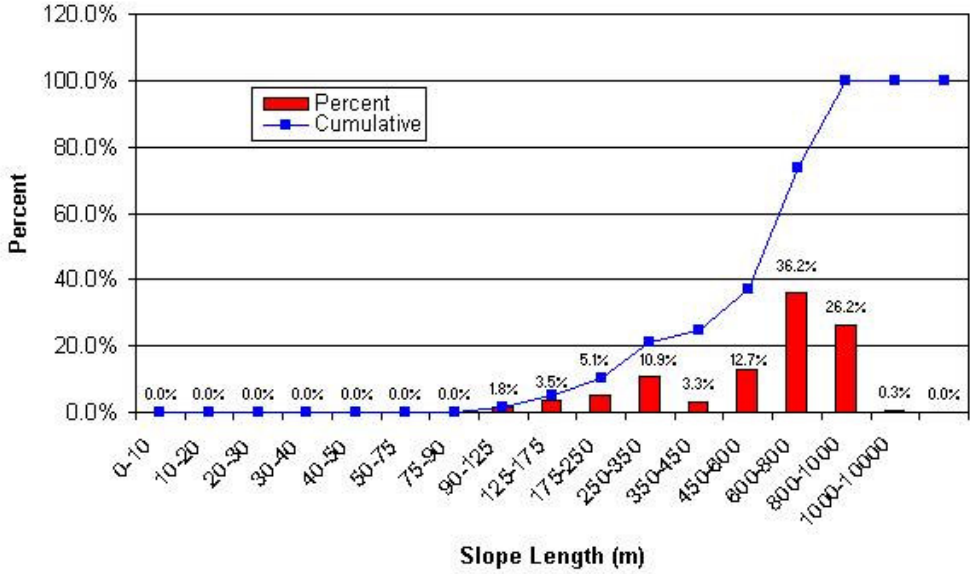

Figure 4.39 Slope length distribution in Field 4.

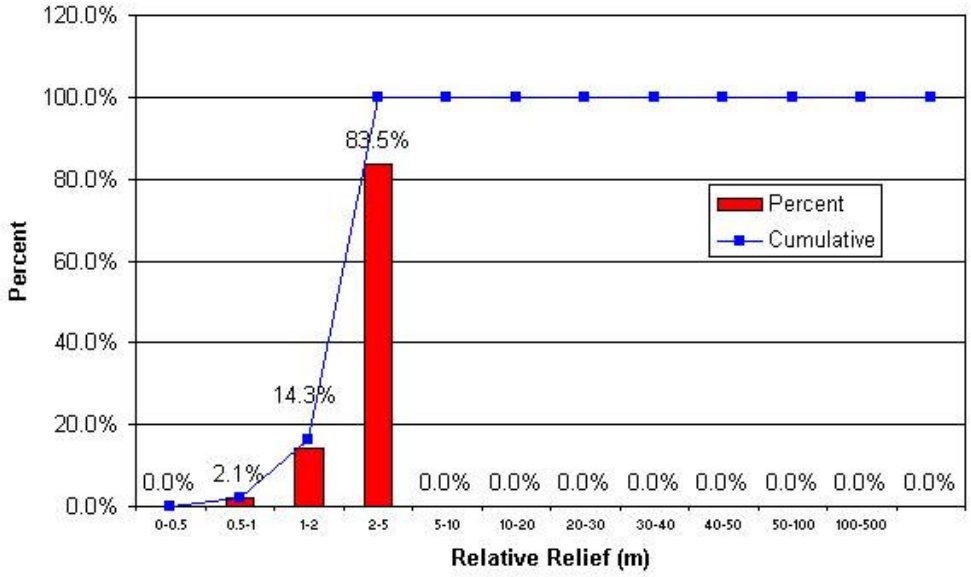

Figure 4.40 Relative relief distribution in Field 4.

4.5.3 Landform Element Classification

LE classification was done using the re-scaled elevation data in order to exaggerate the subtle differences in elevation needed by the software to segregate the DEM into four distinct classes (Figure 4.41).

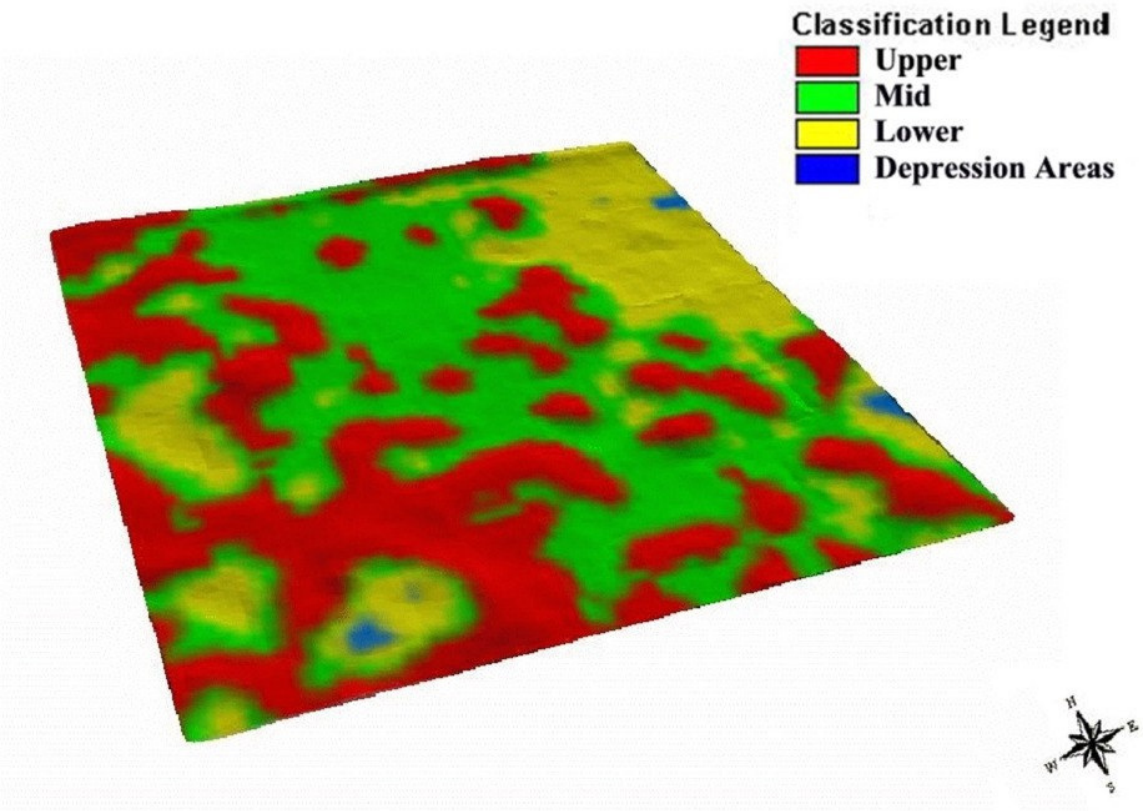

Figure 4.41 3D Landform element map of Field 4.

The Upper LE represented 28.6% of the total landscape, Mid LE 44.6%, Lower LE 25.6% and Depression LE 1.2% (Figure 4.42), which is typical of a gently undulating landscape.

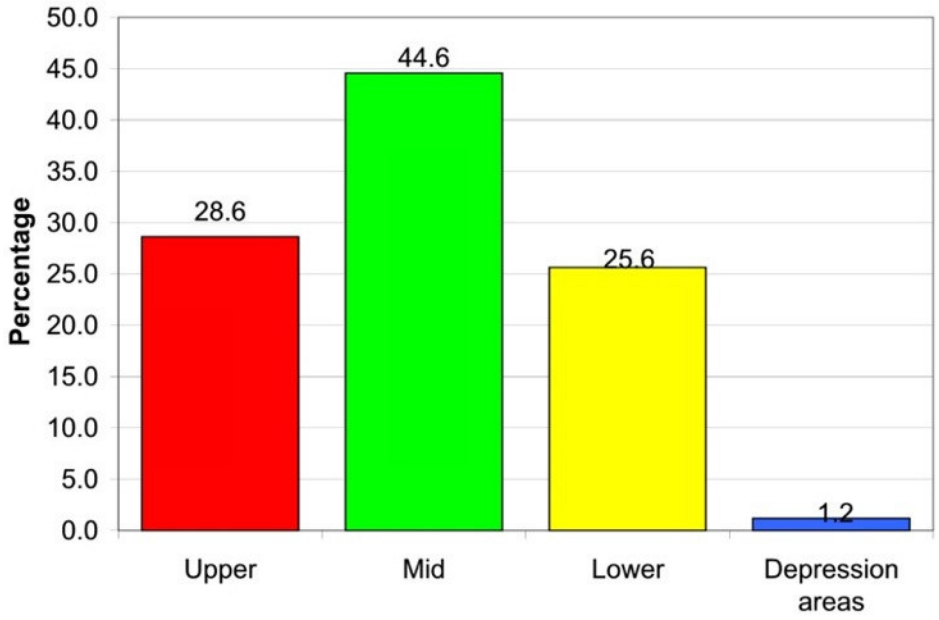

Figure 4.42 Landform element distribution in Field 4.

4.5.4 Land Cover Description

Field 4 was covered with four different types of land cover as illustrated in Figure 4.43. Part 1 was seeded to red lentils in 1998 and was chemically fallowed in 1999 resulting in a mix of senescent plant material covering the soil surface. Part 2 was seeded to flax in 1999 and was burned by the producer in the fall of 1999 resulting in a low brightness value for the area in the IKONOS image. Part 3 was seeded to canary seed in 1999 and was also burned in the fall of 1999 resulting in a black area due to the presence of dark ashes on the ground. Part 4 was seeded to canola which remained un-burnt and thus showed the reoccurring parallel strips in the image due to harvest management practices. However, a small diamond shaped area in Part 4 was burned but the producer used a conventional disker to contain the fire thus leaving several darker strips around the burnt area due to the incorporation of crop residue in the soil and therefore exposing the true color of the soil on the imagery. The un-burned canola stubble had a much higher

reflectance value than the burnt stubble as senescent crop residue reflected more sunlight than burnt crop residue.

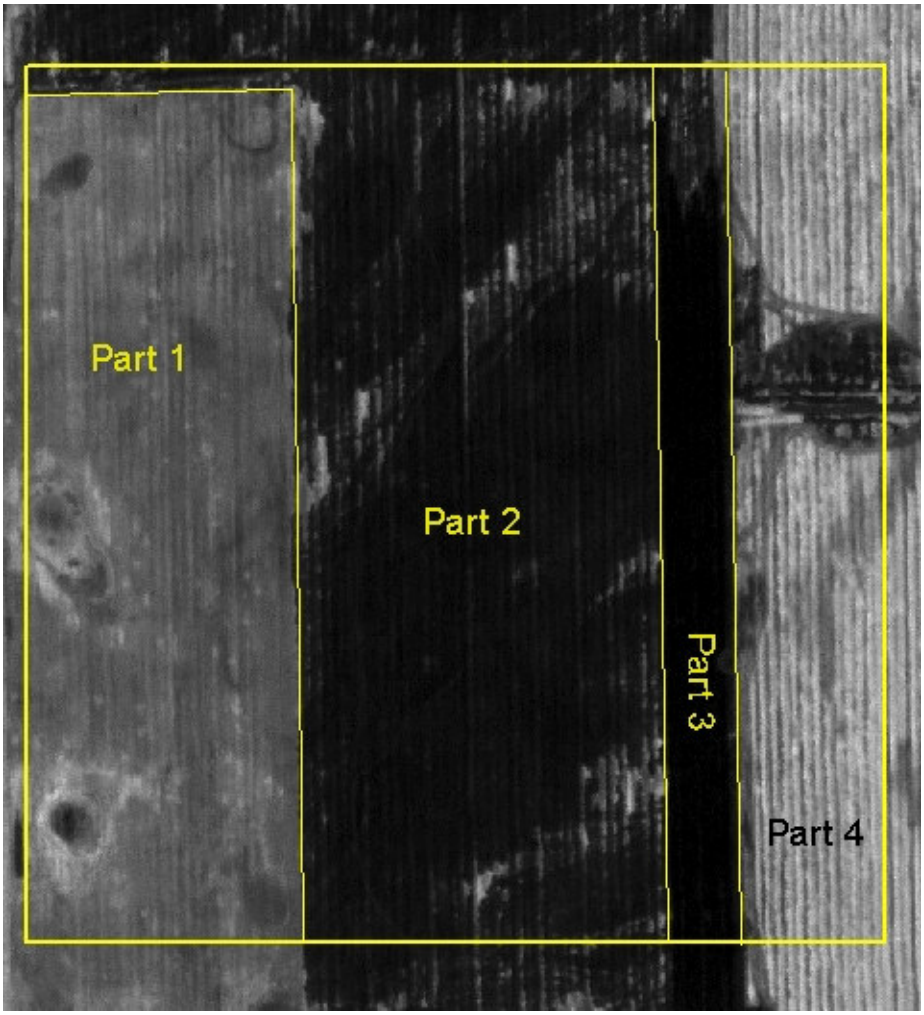

Figure 4.43 IKONOS image of Field 4.

4.5.5 Image Classification and Map Comparison

Classification results of Field 4 showed that treatments had no effect on producer's, user's and overall accuracy as well as overall kappa statistic. Producer's accuracy for the Isodata classification was 0% for the depression category, the highest for the mid category (25.5%), followed by the low category (17.4%) and upper category (8.2%). The overall accuracy was 17.9 % and the overall Kappa was – 5.4% which indicated the lack of agreement between the image classification map and the landform

element classification map (Appendix A, table 4.4a). Similar results were found for the fuzzy k-means classification (Appendix A, table 4.4b). A visual interpretation of the classified maps (Figure 4.44) clearly illustrated the lack of agreement between both dataset due to the existence of several landcover types on the image.

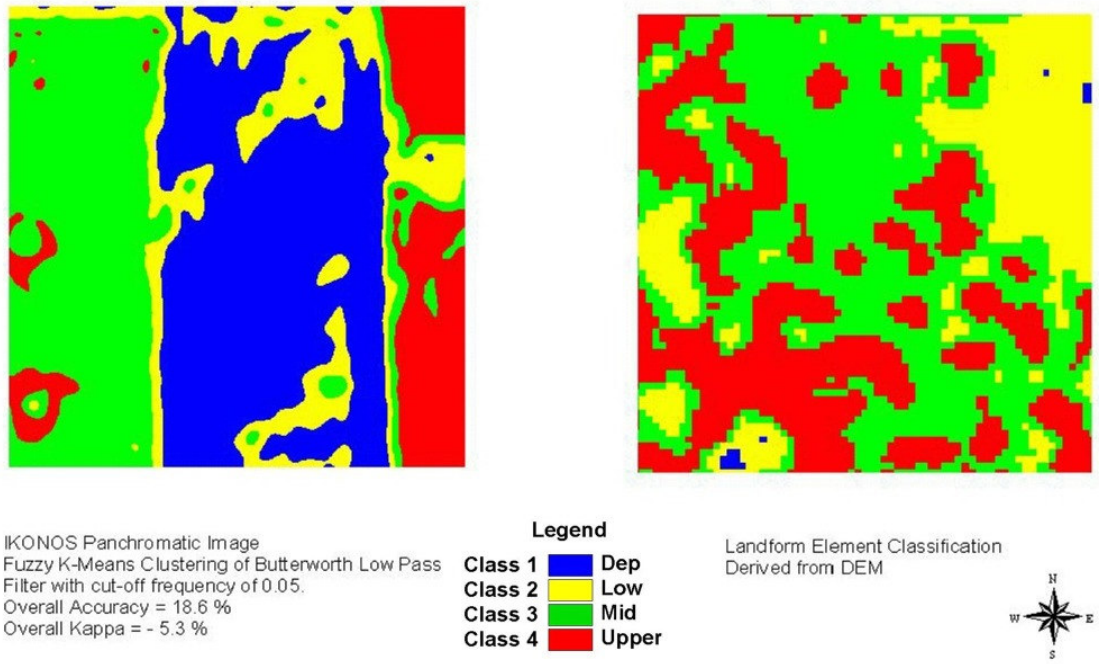

Figure 4.44. Classified map comparison of Field 4.

As treatments had no effect on final accuracy, further analyses were conducted on the Isodata classified image that was modified with an 11 by 11 mean convolution filter. Results show that for the producer's accuracy, the Depression LE was composed of pixels of class 3 and class 4 only. The Low LE category was composed of a mixture of all class pixels with a majority of class 4 pixels (36.2%). The Mid and Upper LE category were composed in majority of pixels of class 1 (49.9%, 42.7%) and class 3 (25.5%, 42.7%) respectively (Figure 4.45).

User's accuracy results show that class 1 was composed mainly of the mid (55.3%) and upper (36.1%) category with no depression category pixels. Class 2 was composed primarily of mid (55.5%), low (28.5%) and upper (16%) pixels. Class 3 of upper (45.1%) category followed by mid (35.9%) and lower (18.3%) category pixels and Class 4 of low (52.5%), mid (27.4%) and upper (19.3%) pixel category (Figure 4.46). Therefore the random distribution of landform element pixels in each class showed the lack of agreement between the two maps.

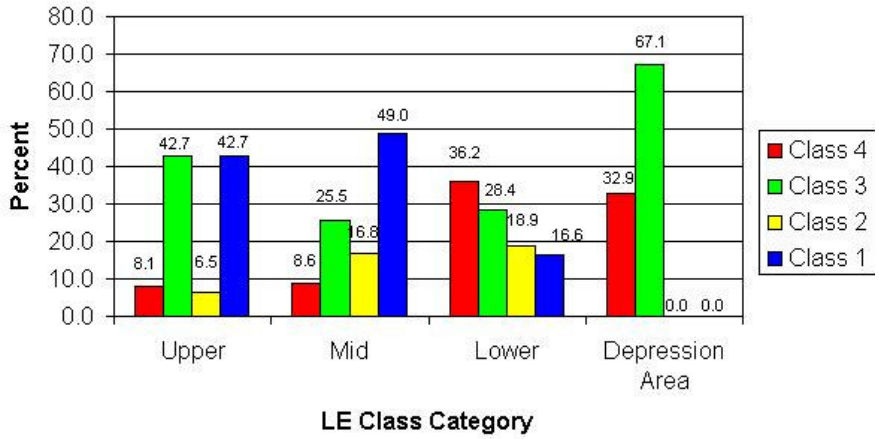

Figure 4.45 Distribution of IKONOS classified pixels within each LE class in Field 4.

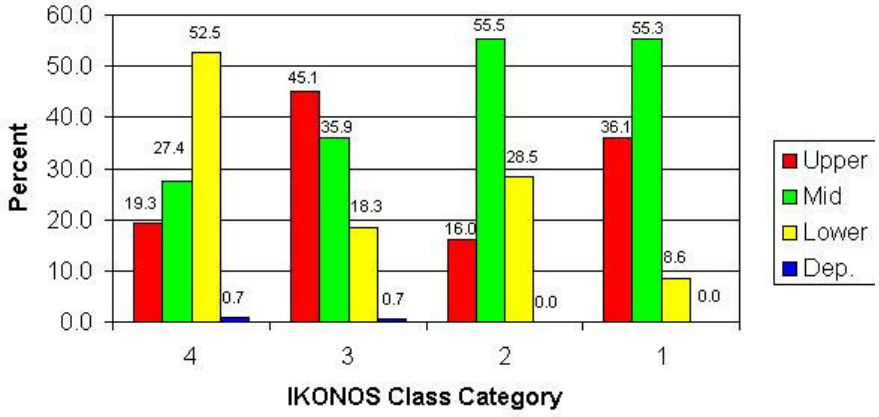

Figure 4.46 Distribution of LE pixels in each IKONOS class in Field 4.

4.5.6 Sub-Field 4 Analysis

A 30 hectare part of Field 4, in the chemical fallow land cover type, was cropped, filtered using a 21 by 21 mean filter and classified using an Isodata unsupervised algorithm. Thematic classes that were created were compared to a landform element map for the same area and accuracy statistics were calculated (Figure 4.47).

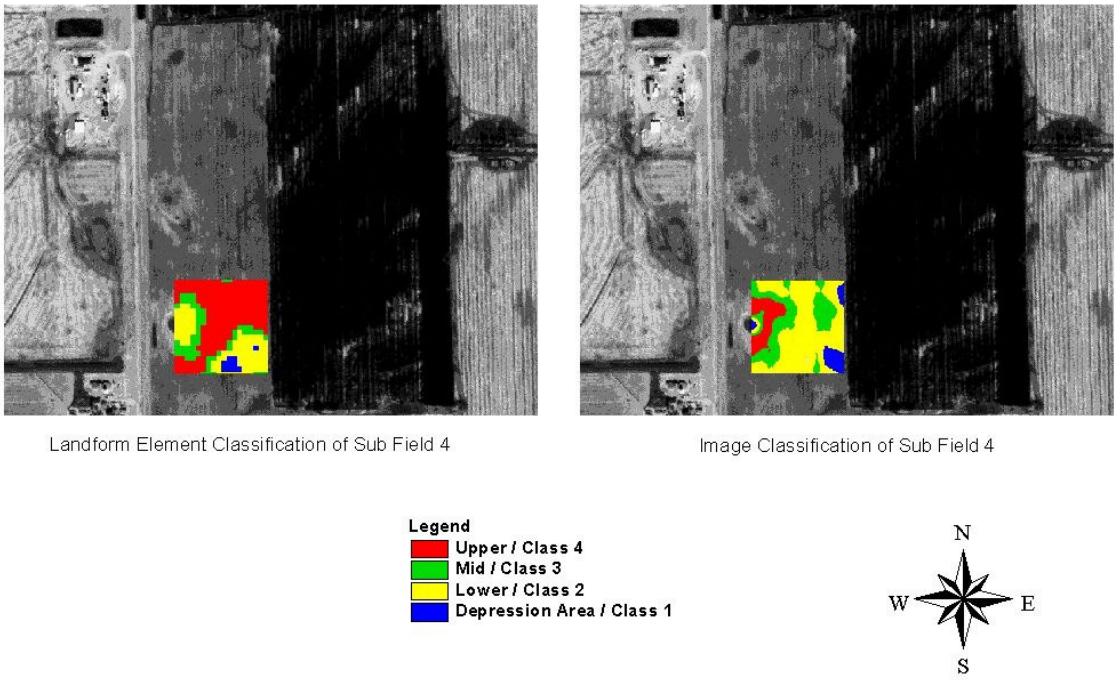

Figure 4.47 Sub-field 4 thematic map comparison.

Results (Table 4.4) showed that producer's accuracy for all landform element classes were higher than producer's accuracy for the entire field, where depression areas were mis-classified in the entire field and were correctly classified up to 5.6% in the sub-field area. User's accuracy for all four classes was lower than user's accuracy of all classes in the entire field. Overall accuracy was higher (20.3%) in the sub field area than for the whole field (17.9%) suggesting that isolating homogeneous ground cover area for

classification would be a good practice. However when classes delineated from uniform ground surface cover are compared to landform elements of the same area, little agreement between thematic maps existed.

Table 4.4 Accuracy statistic comparison for Field 4 and sub-field 4.

	Producer's accuracy				**User's accuracy**				**Overall Accuracy**	**Kappa**
	Upper	Mid	Lower	Dep	4	3	2	1		
Sub-field 4	2.3	39.	49.0	5.6	10.6	24.5	22.3	2.9	20.3	-6.21
Whole field average	8.2	25.5	17.4	0.0	19.8	35.7	27.8	0.0	17.9	-5.4

4.6 Field 5

As ground cover characteristics affected the classification process by creating a different thematic map than the landform element map, a bare soil field was selected to test if delineating landform elements from a panchromatic IKONOS image was feasible on a field without a crop residue cover. The same methodology was used to process the data of Field 5 as for the other study fields.

4.6.1 TIN Surface Representation

Using ArcView GIS™ the raw elevation data was converted to a TIN with an exaggeration factor of 5 for 3D visualization purposes (Figure 4.48). The TIN highlighted the presence of two knolls, one to the south and one to the north of the study area, with a depression area oriented east to west separating both hills.

4.6.2 Landscape Feature Quantitative Description

The variogram of the elevation data best fit a spherical model with an r^2 of 0.875 and a range of 334 meters which indicated the presence of a dominant landscape pattern in the study area (Figure 4.49). Furthermore, the dip at the tail end of the variogram was an indication that the existing landscape pattern extended beyond the study area and therefore could not be encompassed within the field (Burrough and McDonnell, 1998).

The landform features had a dominant slope gradient between 0.5% to 5% (Figure 4.50) with slope length ranging between 175 to 450 meters (Figure 4.51), with a dominant relative relief of 10 to 20 meters (Figure 4.52) thus reinforcing the fact that existing knolls dominated the study area and was in accordance with the hummocky landscape classification from the soil survey (Saskatchewan Soil Survey, 1986)

4.6.3 Landform Element Classification

The LE classification was done using the original kriged data as the elevation range was sufficient for the LandMapR™ software to function properly. A 3D map of the LE classification overlaid onto the TIN map of Field 5 is illustrated in Figure 4.53. Clearly, the dominant LE in the landscape was the Lower area followed by Upper, Mid and Depression area (Figure 4.54).

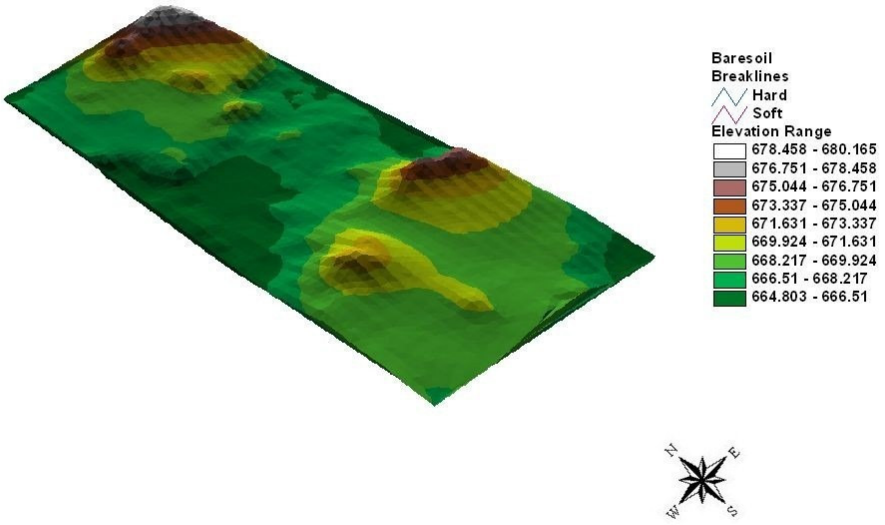

Figure 4.48 3D DEM of Field 5 with a vertical exaggeration of 5.

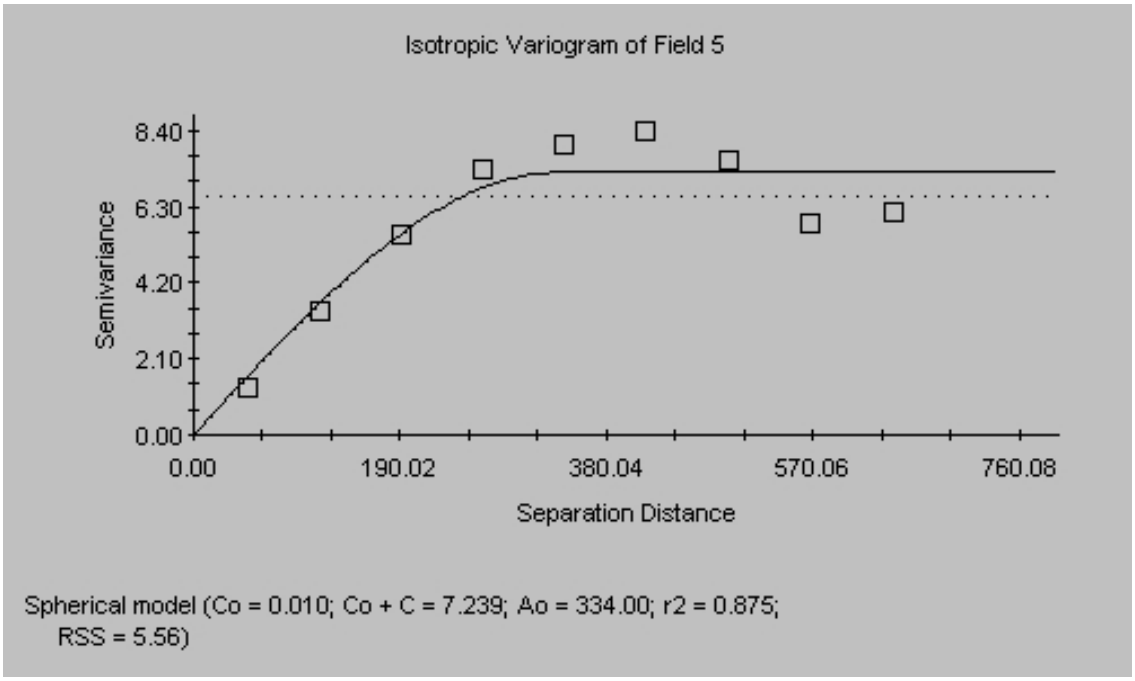

Figure 4.49 Variogram of Field 5.

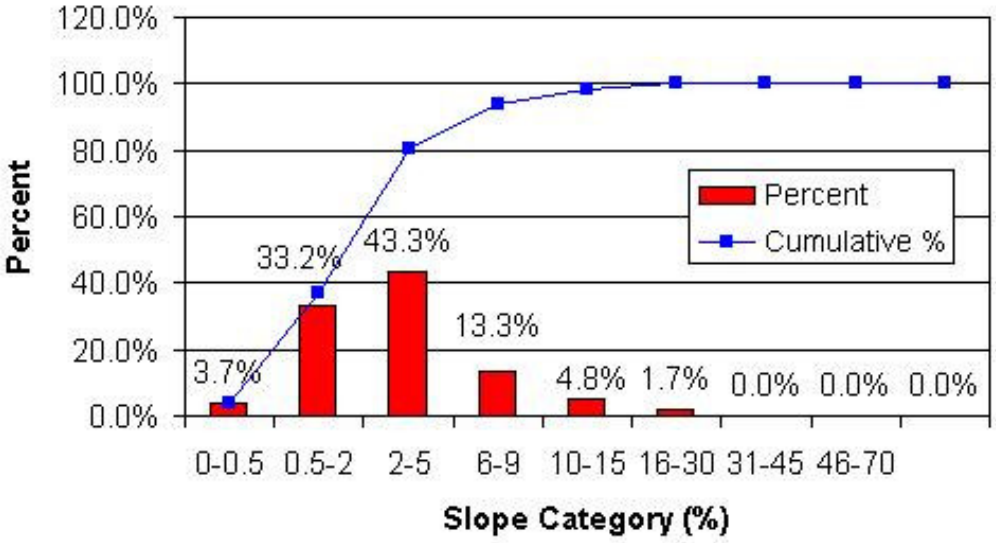

Figure 4.50 Slope gradient distribution in Field 5.

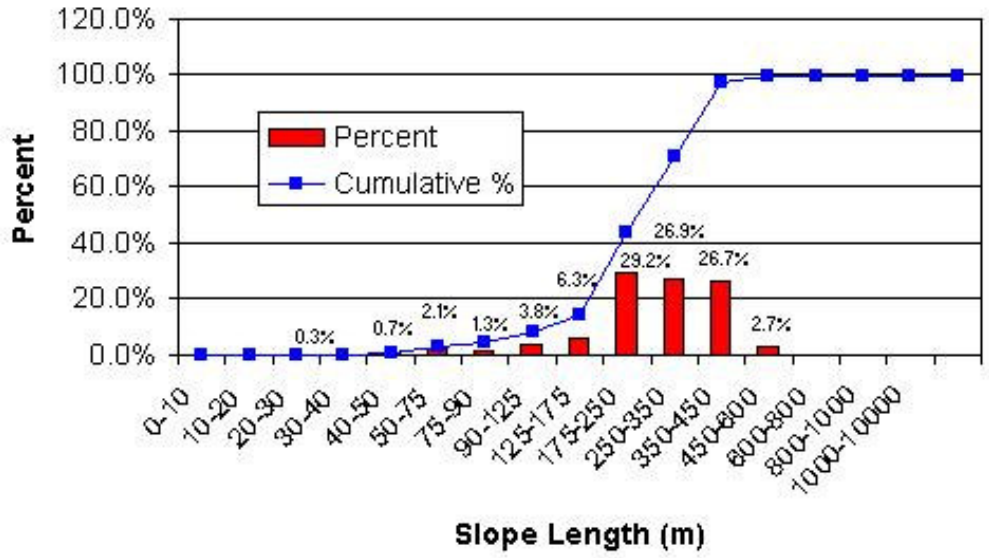

Figure 4.51 Slope length distribution in Field 5.

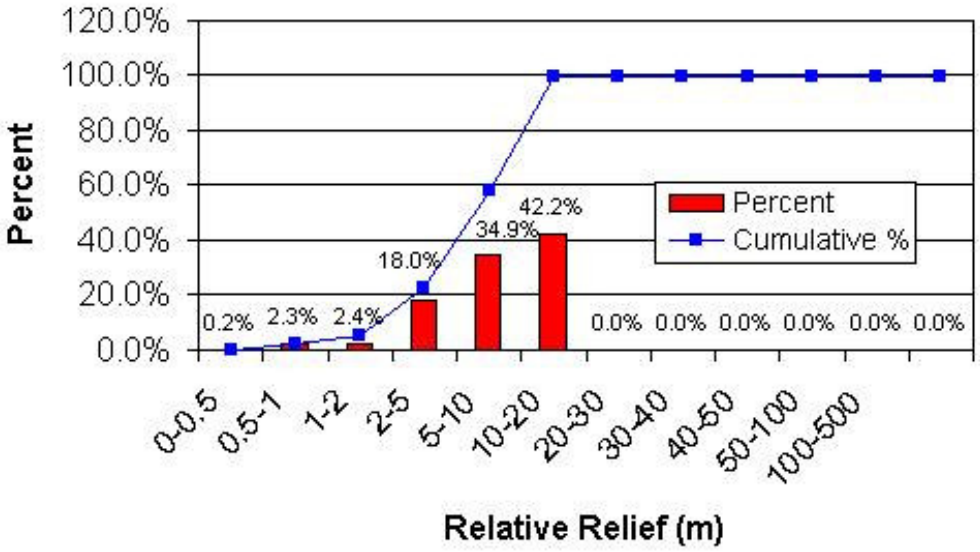

Figure 4.52 Relative relief distribution in Field 5.

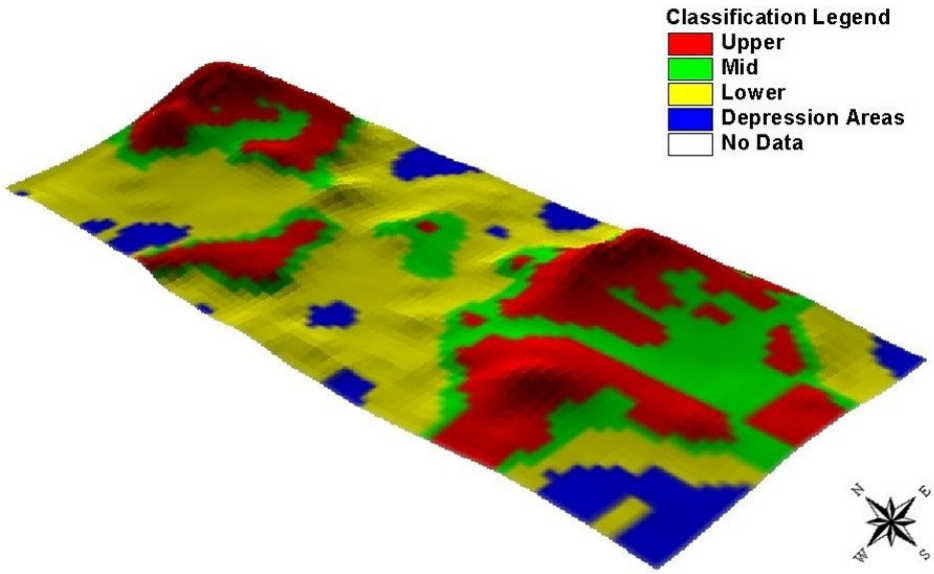

Figure 4.53 3D Landform element map of Field 5.

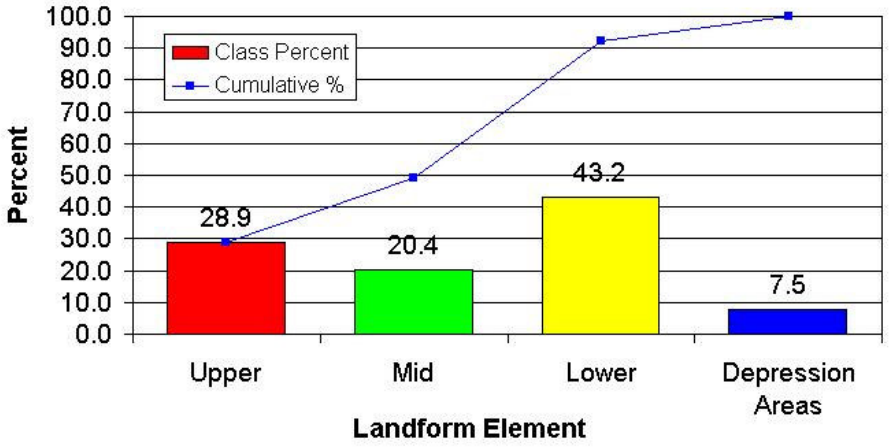

Figure 4.54 Landform element distribution in Field 5.

4.6.4 Land Cover Description

Field 5 was cultivated by the land owner twice in 2000 to remain in summer fallow. As a result, no vegetation or stubble was present in the image. Therefore the true soil reflectance was captured by the IKONOS satellite imagery as illustrated in Figure 4.55 and Figure 4.56. When the IKONOS imagery was draped onto the DEM of Field 5 there appeared to be a good correspondence between color tone of the imagery and landform present in the field. Convex shoulder areas had a lighter shade of grey than the concave backslope and depression areas which were darker in color. This phenomena could probably be associated with the moisture content of the soil surface at the time of imagery as well as organic matter content and also the spatial variability of soil texture within the landscape. McCaan (1995) reported similar findings using gray tone aerial photos.

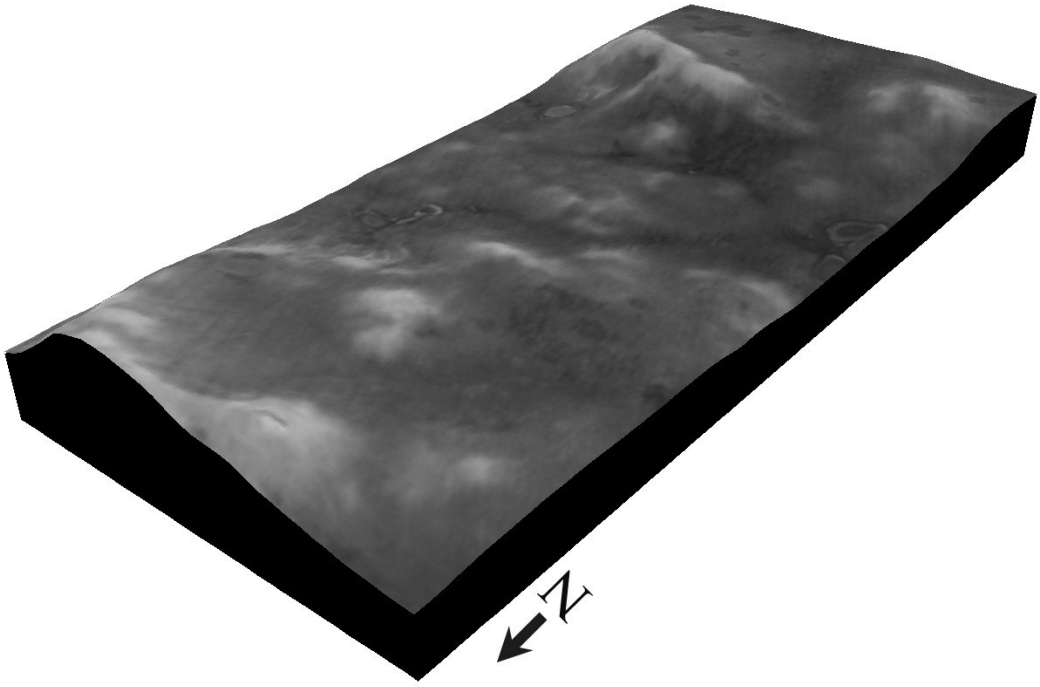

Figure 4.55 3D IKONOS image of Field 5 (North view).

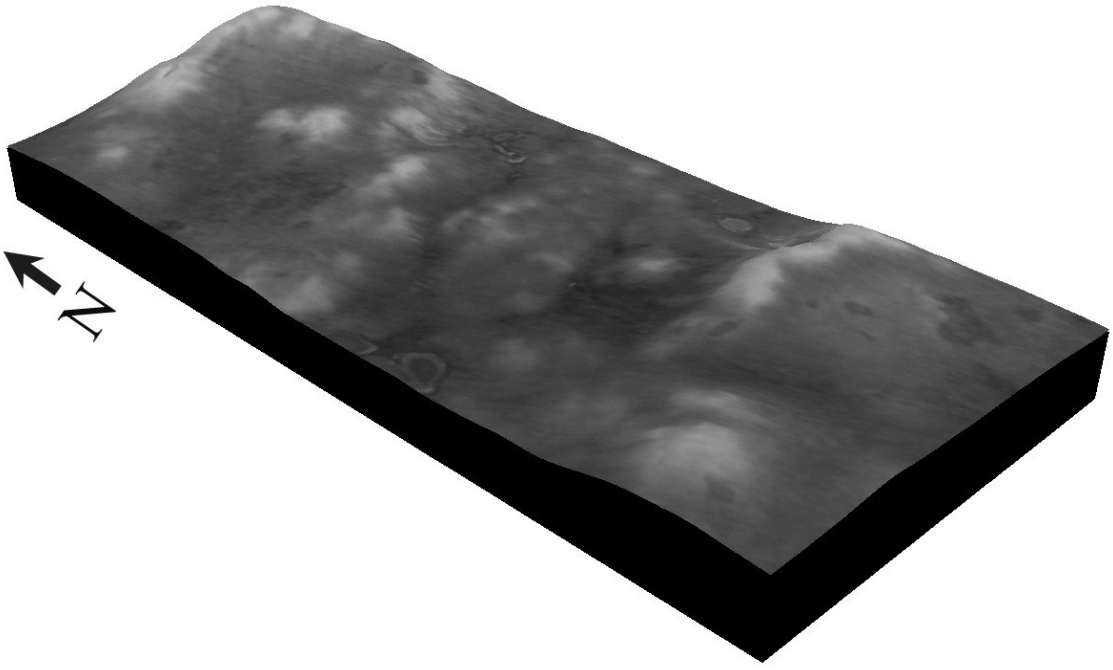

Figure 4.56 3D IKONOS image of Field 5 (South view).

4.6.5 Image Classification and Map Comparison

The image classification process resulted in four well defined classes as shown in Figure 4.57. However the spatial pattern of the classified image and the landform element classification map did not match properly.

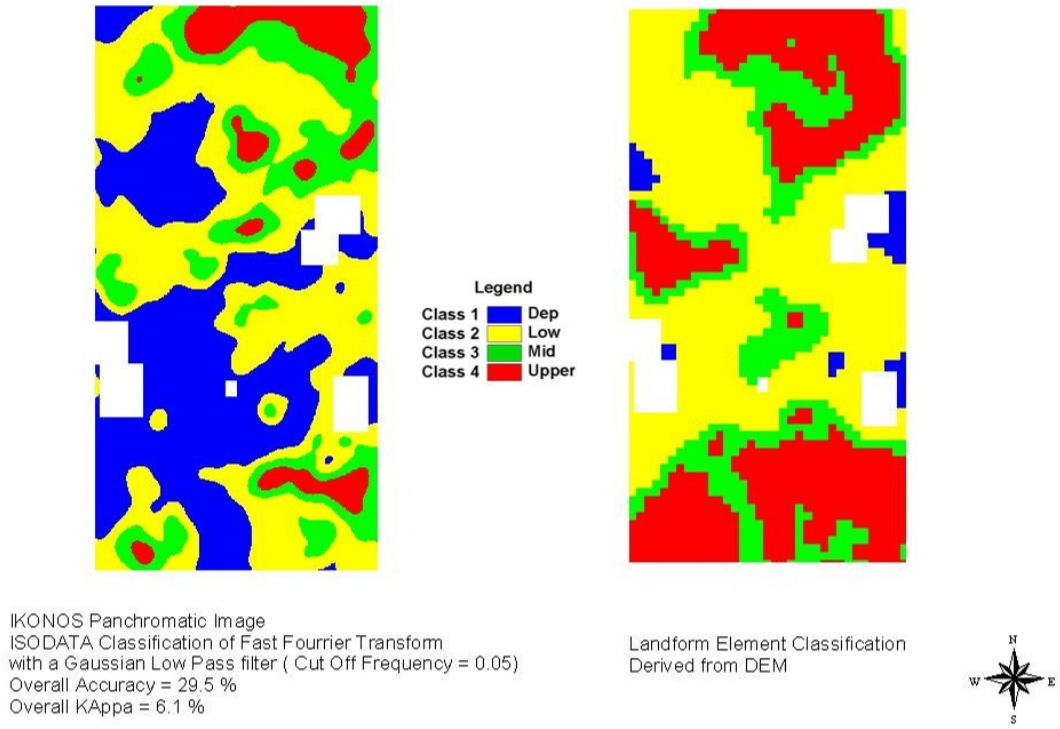

Figure 4.57 Thematic map comparison of Field 5.

The Field 5 map comparison results showed that treatments had no effects on producer's, user's and overall accuracy. Average overall accuracy was 27.7% and average overall Kappa was 4.55% which was very low. The average producer's accuracy for the Isodata classification method was the highest for the depression areas (65.1%), followed by Low (38.4%), Upper (18.1%) and Mid (16%) category (Appendix A, table

4.5a). A similar trend was found with the fuzzy k-means classification results (Appendix A, table 4.5b). The average user's accuracy for the Isodata classification method was the highest for class 4 (82.1%), followed by class 2 (39.9%), class 3 (21.4%) an class 1 (5.2%). A similar trend in results was found for the fuzzy k-means classification.

Further analyses were conducted on the treatment that yielded the best classification result (Isodata classification algorithm and a Fast Fourier transform with a Gaussian frequency cut-off of 0.05). Producer's accuracy (Figure 4.58) results showed that pixel distribution within Depression areas consisted of 74% class 1 pixels and 25.6% class 2. The Low category was composed of 51.3% of class 1 pixels, 38.7% of class 2 and 8.5% of class 3. The Mid category was composed of 48% class 2 pixels, followed by 29.4% class 1 pixels, 18.9% class 3 pixels and 3.7% class 4 pixels. The Upper category was composed of a mixture of all four class pixels with class 2,3 and 4 being the most prominent.

User's accuracy pixel distribution (Figure 4.59) showed a reverse trend in the distribution of landform element category pixels within each class. Class 1 was composed mostly of low category pixels (67.4%). Class 2 was composed of a mixture of all four landform element category pixels with Low pixels dominating the distribution (42.9%) followed by Upper (32.3%) and Mid (23.2%) category pixels. Class 3 and class 4 were composed predominantly of Upper category pixels, 58.1% and 82.7% respectively. This trend in data was observed for the burnt areas of Field 3 and 4 as well.

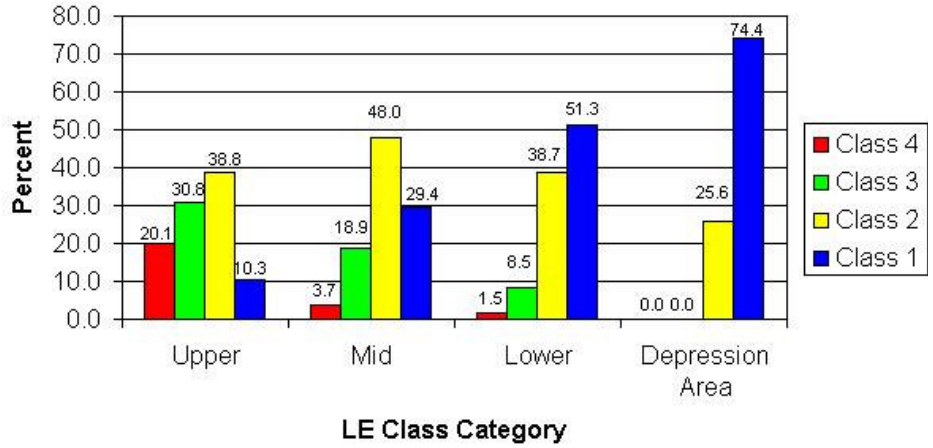

Figure 4.58 Distribution of IKONOS classified pixels within each LE class in Field 5.

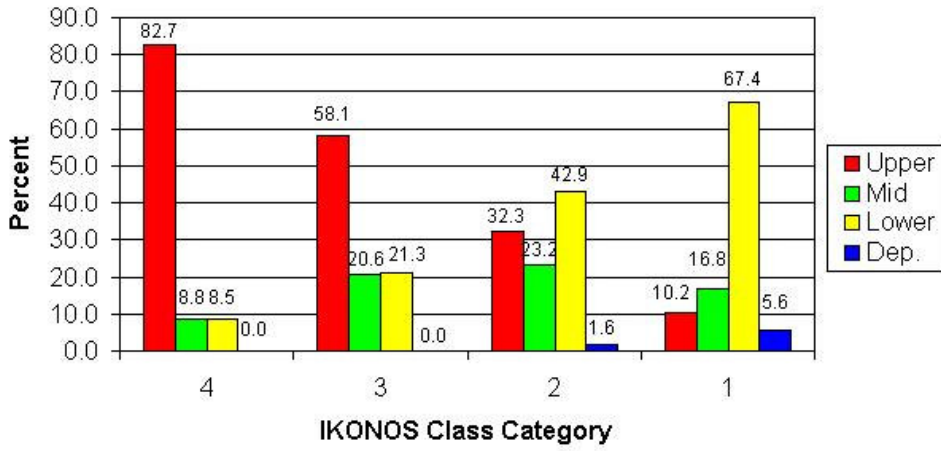

Figure 4.59 Distribution of LE pixels in each IKONOS class in Field 5.

As Field 5 was a bare soil field, surface cover was homogeneous and therefore the brightness value variations were caused by intrinsic soil properties at the time of acquisition of the image. In a hummocky landscape, differences in soil moisture regime and soil texture were more likely the causes of brightness value variations and thus class boundary location. If the IKONOS imagery would have been taken at a different time of the year, where different soil moisture conditions existed, class boundaries would have

changed drastically. Therefore, delineation of landform element from a bare soil image is not realistic.

5 GENERAL DISCUSSION

In this experiment it was demonstrated that, for agricultural fields of south-eastern Saskatchewan, classes created from an unsupervised classification of a panchromatic IKONOS image did not match landform element classes delineated from elevation data collected over the same area. Whether ground cover diversity was complex or simple, the degree of agreement between LE map and classified IKONOS map remained very low and thus the method is unreliable for precision farming purposes. As ground cover data was not quantified for all five fields studied, it was difficult to know exactly to what the four classes delineated from the imagery corresponded.

5.1 Landform Element Classification Process

Historically, classifying the type of landscape present in an area required years of field experience from soil scientists and the landscape classification work remained time consuming. Classification accuracy remained inconsistent as individual soil scientists had their own interpretation of landform element classification. With advancements in GPS and surveying equipment, elevation datasets became available over larger areas which allowed soil scientists to develop automated landform element models to characterize the existing landscape.

The automated landform delineation model used in this experiment was LandMapR[tm] (MacMillan et al., 2000). At the time of the DEM analyses, the LandMapR[tm] software was fully functional but was still in development. The software operated on a database program called FoxPro v5.0 that was sometimes unstable depending on the size of the dataset and the hardware capabilities. Several versions of the software and fuzzy set rules were released. In this analysis software version 6.0 was used and DEM data manipulation prior to analysis was intensive. In 2005, the LandMapR[tm] software was rewritten in the C++ language to run in a Microsoft Windows environment and required less data manipulation from the user prior to classification. Therefore, the software version used could have misclassified certain areas. It was assumed that the LE maps were accurate as they visually appeared correct when viewed in a 3D environment.

Another issue with the LandMapR[tm] software was the data manipulation suggested by MacMillan et al. (2000) prior to the classification process. As the LandMapR[tm] software was developed for commercial purposes, creation of crisp thematic maps was one of the primary goals of the model. Therefore modification of elevation datasets prior to analysis was critical.

The software was designed to work with first a DEM with at least 15 meters elevation range and second a smoothed surface to enhance the macro topography. Rescaling the elevation data to 25 meters allowed the software to better delineate LE where perhaps LE did not exist to the naked eye of an experienced soil surveyor. Therefore, in Field 4 for example, there might have existed only two or three landform elements but the software delineated four.

In this experiment, the model was used for research purposes thus data manipulation was kept to a minimum. The raw elevation data was first interpolated into a continuous surface using a kriging interpolation method, rescaled to 25 meters and then analysed using the model. The output LE maps were filtered using a 3 by 3 mean filter to create crisp LE classes that were used as reference maps for the image accuracy assessment. Arguably, it is possible that this data manipulation might have created fictional LE maps for each study site and as ground verification for each LE map was impossible, the image classification accuracy could have been affected. It was decided at the time of elevation data processing to select one interpolation method (kriging), to rescale the elevation dataset to 25 meters and to use the default settings suggested by MacMillan et al. (2000). Therefore, any elevation data manipulation would have created different LE maps and thus changed the image classification accuracy.

Not only did the elevation data processing affect the image classification accuracy but also the scale difference between datasets. Elevation data was interpolated to a 10 meter grid to reflect the collection interval done at the time of survey. Once landform elements were delineated from the DEM, the LE maps were resampled to 1 meter pixel size in order to match the IKONOS imagery pixel size and calculate accuracy statistics. The resampling method converted each 10-meter pixel into 100, 1-meter pixels of the same attribute value thus conserving the blocky appearance of the LE boundaries. The resampling of the LE map might have contributed to the low classification accuracy of the imagery as LE boundaries were very coarse as compared to the classified images.

5.2 Image Classification Process

As ground surface data was unavailable at the time of the imagery acquisition, it was nearly impossible to know to what each class corresponded. Only speculation on factors affecting the reflectance captured by the IKONOS sensor could be made to explain what happened.

The IKONOS satellite sensor captured the reflectance of the sunlight from the surface of the earth thus two major factors influenced the color tone of the image: the remote sensor physical properties and the ground surface cover properties.

5.2.1 Remote Sensor Physical Properties

As the IKONOS sensor is programmable to take images of specific areas on the earth, sensor angle to the earth's surface is adjustable. Therefore an image taken at nadir would look slightly different than an image taken at two degrees from nadir. Furthermore, the angle of the sun at the time of image acquisition would affect the color tone differences captured by the sensor. As the angle of the sensor could not be fixed and the sun angle to the earth was unknown (until the image is acquired), the end user has no control on the physical properties of the sensor and its corresponding impact on color tone of the image.

The imagery was supplied as coarsely geo-referenced, thus the raw image was geo-rectified which changed the value of each pixel in the image. In this experiment, the image had to be geo-rectified a second time in order for the DEM to overlay properly onto the imagery. The double geo-rectification process might have also altered the color

tone in the image as new brightness value had to be calculated for each pixel of the image.

5.2.2 Surface Cover Physical Properties

Unsupervised classification of an image is based on pixel brightness values. Each pixel value represents a reflectance value affected by the ground surface cover. In this experiment it was demonstrated that soil cover was the main factor affecting reflectance values. Ground cover such as snow patches had the highest brightness values of all as they were white in color and permanent water bodies or water logged areas had the lowest brightness value as they appeared black. Stubble type, amount, moisture content, age and degree of decomposition all affected the appearance of the surface cover of the field thus increasing the variability of color tone present even in small areas within each field. Furthermore, harvest management artefacts such as driving paths, direction of swathing and harvesting, appeared lighter or darker depending on the type of stubble. In a bare soil situation, spatial variability of the color tone was affected by soil texture, color, moisture and organic matter content.

6 SUMMARY AND CONCLUSIONS

6.1 Summary of Findings

The purpose of this experiment was to delineate landform elements, as defined by Macmillan et al. (2000), from a panchromatic high resolution IKONOS image for agricultural fields of south eastern Saskatchewan. Two panchromatic IKONOS images were acquired, one in the spring of 2000 and one in the spring of 2001, over a 100 km^2 area located south of the town of Indian Head, SK in the black soil zone. The landscape present in the area varied from gently undulating to hummocky. Elevation measurements were recorded using a survey grade GPS receiver at a 10 by 10 m grid spacing and landform elements were delineated using LandMapR^{tm} software developed by MacMillan et al. (2000). Each field was classified into four landform elements (Upper, Mid, Lower and Depression area) and a GIS map was created for each field.

The IKONOS panchromatic image was cropped around each field to create separate files. Each image file was filtered and then classified into four classes using an unsupervised classification method. There were 20 different filters and two unsupervised classification methods tested on each image file resulting in 40 classified images per field. The classified maps were compared to their respective Landform Element map and comparative accuracy statistics were calculated to evaluate which combination of image filtering algorithm and classification method resulted in the best landform element map.

A total of five fields were selected for this experiment based on contrasting landscape characteristics. At the time of image acquisition, Field 1 was covered with two types of stubble (barley and canola). Landscape features present were classified as hummocky where the dominant slope gradient was 2 to 5%, with a relative relief between 5 to 10 meters and general slope length of 175 m to 450 m. The dominant landform was Mid followed by Lower, Upper and Depression areas. Image analysis results showed that image filtering treatments had no effects on image classification accuracy which varied between 7 to 9.2%. Results showed that multiple ground cover affected the image classification process thus resulting in poor map agreement between the Landform Element map and IKONOS classification map.

Surface cover of Field 2 consisted of canola stubble and lightly cultivated stubble area. Landscape features present were similar to Field 1. Dominant landform elements present were Mid, Upper and Low with 8.8% of the field area classified as depression areas. Again, image filtering treatments had no effect on final classification accuracy. However, Field 2 had the best classification accuracy of all fields in this study (16%).

Field 3 had the most ground cover variability visible in the imagery. Landscape present in Field 3 was classified as hummocky with an even distribution of Mid, Upper and Low landform elements and only 1.3% of the area classified as Depression areas. Image filtering treatments had no effects on final classification accuracy which ranged between 1.2 to 6%.

Field 4 was also a field with several types of surface covers present. However, the landscape features present were classified as gently undulating with long slope length ranging from 600m to 1000 m. The dominant landform element was the Mid class

followed by Upper and Low with only 1.2% of the field area classified as Depression area. The image filtering techniques had no effects on final classification accuracy and produced the worst kappa statistics of all fields (-5.4% on average). This was attributed the number of different surface covers present in the imagery thus image classification classes created corresponded to ground cover type more than soil properties.

Field 5 was the only field in summer fallow and reflectance of bare soil was better captured by the IKONOS satellite sensor. Landscape features present were classified as hummocky with short slope length (150 m to 450 m), dominant slope gradient of 2% to 5% with relative relief of 10 to 20 m. Image filtering methods had no effects on final classification accuracy as mean kappa statistics was 4.5%. The low classification accuracy was attributed to the high level of soil moisture at time of image acquisition which increased the areal extent of the depression area beyond what the LandMapR^{tm} classification created.

6.2 Conclusions

Accurate delineation of landform elements from IKONOS panchromatic images for agricultural fields of south eastern Saskatchewan was not successful. Image classification accuracies achieved were very low and therefore the techniques developed in this experiment should not be used for research or commercial purposes. The most efficient and accurate way of delineating landform elements for agricultural fields remains the processing of elevation data collected in the field with the LandMapR^{tm} software developed by MacMillan et al. (2000).

Image filtering techniques employed to remove systematic noise from the raw image had no effect on classification accuracy of landform elements as classes delineated from the imagery represented the existing landcover type rather than the inherent soil properties. There was also no difference in classification accuracy between the two unsupervised classification methods used.

Harvest management practices, ground cover type and moisture content were the major factors controlling the reflectance of the sunlight capture by the satellite sensor. Thus, the use of filtering processes on the raw image did not change the classification accuracies achieved.

In certain cases, the use of panchromatic images might be useful to delineate depression areas in agricultural fields with very little ground cover variability. However the boundary of the depression areas might not be the same as the boundary of depression areas identified from the elevation data.

6.3 Recommendations for Further Studies

The key to using brightness values of remote sensing imagery for delineating LE would reside in a supervised classification of multi-temporal and multi-spectral image datasets. A multi-temporal approach is critical to environmental studies as reflectance of the surface cover changes drastically over time and a multi-spectral approach would allow the user to identify reflectance signatures of specific soil characteristics that are not detectable within the visible range of the electro-magnetic spectrum.

For bare soil fields, a combination of multi-temporal, multispectral bands with in ground truth soil data and a DEM of the area would enable the creation of a landform

element/soil redistribution model to be used in a supervised classification process. The output GIS map would not only serve as a tool to benchmark soil sampling but also be used in precision agriculture as a base map for precision input application.

For stubble covered fields, a combination of multi-temporal, multi-spectral datasets with in-situ quantitative ground truth data on the surface cover and a DEM might be used to create a crop residue model by landform elements that would be used in a supervised classification process. However, as harvesting equipment, technique and methodology vary between each producer, the creation of a crop residue by landform element model would remain very site specific and therefore could not be used at a larger scale.

In summary, a supervised classification of multi-spectral imagery in conjunction with in-situ quantitative ground truth data would constitute a more accurate way of classifying an IKONOS image into landform elements. Whether the goal to achieve is to quantify the amount of stubble on the ground, quantify the organic matter content and/or level of decomposition of the crop residue for each landform element, the important factor is the collection of ground truth data that is in direct relation with the reflectance captured by the satellite sensor. Furthermore, not only multi-spectral images but also multi-temporal images are important for the analysis as ground cover and soil texture properties change over time.

7 CONTRIBUTION TO KNOWLEDGE

This experiment has proven that using one high resolution IKONOS panchromatic image for the purpose of delineating landform elements from agricultural fields is not feasible in an accurate matter. Although no breakthrough findings occurred in this research, it is important to emphasize the fact that remote sensing data is not a panacea for elevation data when landform delineation is concerned. Perhaps a combination of both data sets may be the key to delineate landform facets that would be useful for precision agriculture.

8 REFERENCES

Aerial-Photo Interpretation in Classifying and Mapping Soils, Soil Conservation Service, October 1966. USDA, Agriculture handbook 294.

Afanas'eva, T.V., Pastushenko, N.F., 1983. Feasibility of identifying species differences in tilled soils from multizone aerial photographs. Vestnik Moskovskogo Universiteta. Pochvovedenie, Vol. 38, No 2, pp. 26-30.

Agbu, P.A., Fehrenbacher, J., Jansen I.J. 1990. Soil property relationships with Spot satellite digital data in east central Illinois. Soil Science Society American Journal, 54: 807-812.

Bernhardsen, T., 1999. Geographic information systems - an Introduction - Second Edition -John Wiley & Sons, Inc.

Biard, F. and Baret, F., 1997. Crop residue estimation using multiband reflectance. Remote Sensing of Environment. 59: 530-536

Bishop, T.F.A, McBratney A.B., 2002. Creating field extent digital elevation models for precision agriculture. Precision Agriculture 3:37-46.

Burrough, P, A., and R. McDonnell, 1998. Principles of geographical information systems. Oxford University Press, New York.

Chen F., Kissel D.E., West L.T., Adkins W., 2000. Field-scale mapping of soil organic carbon using remotely sensed Iimagery. Soil Science Society American Journal. 64:746-753

Daughtry, C.S.T, 2001. Discriminating crop residues from soil by shortwave infrared reflectance. Agronomy Journal, 93:125-131.

Daughtry, C.S.T., Hunt Jr., E.R., McMurtrey III, J.E., 2004. Assessing crop residue cover using shortwave infrared reflectance. Remote Sensing of Environment. 90: 126-134.

Fox G.A., Sabbagh G.J., 2002. Estimation of soil organic matter from red and near-infrared remotely sensed data using a soil line euclidean distance technique. Soil Science Society American Journal 66: 1922-1929

Hall, G.F., Olson, C.G., 1991. Predicting variability of soils from landscape models, Soil Sience Society of America. Spatial Variabilities of Soils and Landforms. SSSA Special Publication no. 28.

Jensen, J. R.,1996. Introductory digital image processing: a remote sensing perspective, 2nd Edition, Prentice Hall, Upper Saddle River, New Jersey, 316 pp.

Jensen, J. R., 2000. Remote sensing of the environment: an earth resource perspective. 1st Edition, Prentice Hall, Upper Saddle River, New Jersey, 544 pp.

Kyoo-Seock, L., Lee, G.B., Tyler, E.J. 1988. Thematic mapper and digital elevation modeling of soil charateristics in hilly terrain. Soil Science Society American Journal. 52:1104-1107

Lobb, D.A., Kachanoski, R.G., 1999. Modelling tillage erosion in the topographically complex landscapes of southwestern Ontario, Canada. Soil and Tillage Research 51: 261-277.

Lobell, D.B., Asner, G.P., 2002. Moisture Effects on Soil Reflectance. Soil Science Society of America Journal. 66:722-727

Macmillan R.A., Pettapiece W.W., Nolan S.C., Goddard T.W., 2000. A generic procedure for automatically segmenting landforms into landform elements using DEMs, heuristic rules and fuzzy logic. Fuzzy Sets and Systems, 113: 81-109

Manning, G., Fuller, L.G., Eilers, R.G., Florinsky, I., 2001a. Soil moisture and nutrient variation within an undulating manitoba landscape. Canadian Journal of Soil Science, 81:449 - 458.

Manning, G., Fuller, L.G., Eilers, R.G., Florinsky, I., 2001b. Topographic influence on the variability of soil properties within an undulating manitoba landscape. Canadian Journal of Soil Science, 81:439 - 447.

Major, D.J., Janzen, H.H., Olson B.M., McGinn, S.M. 1992. Reflectance characteristics of southern alberta soils. Canadian Journal of Soil Science. 72:611-615.

McCaan B., 1995. Large-scale land mapping and evaluation of solonetzic-dominated landscapes using image analysis and global positioning systems (GPS), Msc. Thesis, Soil Science Department, University of Saskatchewan.

McCaan, B.L., Pennock, D.J., Van Kessel, C., and Walley, F.L. 1996. The Development of management units for site specific farming. P. 295-302. In P.C.Robert et al. (ed.) Proceedings of the Third International Conference on Precision Agriculture. ASA, CSSA, and SSSA, Madison, WI..

Moore, G.A., Tyndale-Biscoe, J.P.,1999. Estimation of the importance of spatially variable nitrogen application and soil moisture holding capacity to wheat production, Precision Agriculture, 1:27-38.

Muller, E., Decamps, H., 2000. Modeling soil moisture reflectance. Remote Sensing of Environment, 76: 173-180.

Nagler, P.L., Daughtry, C.S.T., Goward, S.N., 2000. Plant litter and soil reflectance, Remote Sensing of Environment. 71: 207-215.

PCI Geomatica help menu, 2002

Peng, W., Wheeler, D.B., Bell, J.C., Krusemark M.G., 2003. Delineating patterns of soil drainage class on bare soils using remote sensing analyses. Geoderma. 115: 261-279.

Pennock, D.J., Anderson, D.W., de Jong, E., 1994. Landscape-scale changes in indicators of soil quality due to cultivation in Saskatchewan, Canada. Geoderma 64, 1-19.

Pennock, D.J., Corre, M.D., 2001. Development and application of landform segmentation procedures. Soil and Tillage Research, 58:151-162.

Pennock D.J., Zebarth, B.J., De Jong, E., 1987. Landform classification and soil distribution in hummocky terrain, Saskatchewan, Canada. Geoderma, 40:297-315.

Robertson, G.P. 2000. GS+: Geostatistics for the environmental sciences, Gamma Design Software, Plainwell, Michigan USA.

Saskatchewan Soil Survey, 1986. The Soils of Indian Head Rural Miunicipality No 156 Saskatchewan, Saskatchewan Institute of Pedology, Publication number S202.

Schmidt, F., Persson, A., 2003. Comparison of DEM data capture and topographic wetness indices. Precision Agriculture 4: 179-192.

Schreier H, Wiart R., Smith S., 1988. Quantifying organic matter degradation in agricultural fields using PC-based image analysis. Journal of Soil and Water Conservation, Sep-Oct: 421-424

Schumacher, T.E., Lindstrom, M.J., Schumacher, J.A., Lemme, G.D., 1999. Modeling spatial variation in productivity due to tillage and water erosion. Soil and Tillage Research. 51: 331-339.

Sullivan, D.G., Shaw, J.N., Mask, P.L., Rickman, D., Guerta, E.A., Luvall, J. Wersinger, J.M., 2004. Evaluation of multispectral data for rapid assessment of wheat straw residue cover. Soil Science Society of America Journal. 68: 2007-2013.

Troeh F.R., Hobbs J.A., Donahue R.L., 1980. Soil and water conservation for productivity and environmental protection, Prentice Hall, Toronto.

Tou, Julius T. and Rafael C. Gonzalez. 1974. Pattern recognition principles. Addison-Wesley Publishing Co.

Verity, G.E, Anderson, D.W., 1990. Soil erosion effects on soil quality and yield. Canadian Journal of Soil Science. 70: 471-484.

Walley, F., Pennock, D., Solohub, M., Hnatowich, G., 2001. Spring Wheat (Triticum Aestivum) Yield and Grain Protein Responses to N fertilizer in Topographically Defined Landscape Positions. Canadian Journal of Soil Science, 81: 505-514.

Weidong, L., Baret, F., Xingfa, G., Qingxi, T., Lanfen, Z., Bing, Z. 2002. Relating soil surface moisture to reflectance. Remote Sensing of Environment. 81:238-246

Whelan, B.M. and McBratney, A.B., 2000. The "null hypothesis" of precision agriculture management. Precision Agriculture, 2: 265-279.

APPENDIX A

Table 4.1a - Field 1 Isodata classification accuracies and statistics

	Producer's accuracy (%)				User's Accuracy (%)				Overall accuracy	Overall kappa
Class	**Dep**	**Low**	**Mid**	**Upper**	**1**	**2**	**3**	**4**	**%**	**%**
Average Filter Size:										
5 x 5	65.7	25.0	56.7	20.8	60.2	67.0	41.9	17.2	38.5	7.9
7 x 7	65.6	24.4	56.2	21.6	60.7	69.5	41.5	17.4	38.3	7.7
9 x 9	65.7	23.5	55.6	22.3	61.3	72.7	40.9	17.5	37.9	7.2
11 x 11	65.6	23.5	55.8	22.2	61.9	73.5	40.7	17.6	37.9	7.1
21 X 21	64.7	22.5	54.8	23.0	64.8	76.5	39.5	18.0	37.4	6.1
Gaussian Filter Size:										
5 x 5	65.5	25.1	56.3	20.9	60.0	66.1	41.9	17.2	38.4	7.8
7 x 7	65.7	24.5	57.1	20.8	60.2	68.3	41.8	17.2	38.5	7.8
9 x 9	65.6	24.4	56.1	21.6	60.6	69.1	41.5	17.4	38.2	7.6
11 x 11	65.6	24.4	56.3	21.6	60.8	69.7	41.5	17.4	38.3	7.7
21 X 21	65.7	23.5	55.8	22.2	61.7	73.4	40.8	17.6	37.9	7.2
Median Filter Size:										
3 x 3	65.6	26.8	56.6	19.9	59.3	61.3	42.7	16.9	38.7	8.4
5 x 5	65.7	24.9	56.3	21.0	60.0	66.8	41.9	17.1	38.3	7.8
7 x 7	65.8	24.3	56.0	21.6	60.4	69.6	41.5	17.2	38.1	7.5
Mode Filter Size:										
3 x 3	66.0	29.4	58.2	17.5	58.6	55.2	43.8	16.8	39.7	9.5
5 x 5	66.1	30.4	58.4	16.7	58.5	54.3	44.2	16.4	39.9	9.8
7 x 7	65.6	25.8	56.6	19.9	59.0	62.7	42.4	16.7	38.4	7.9
Fourrier Transformation Butterworth Low Pass Filter Cut-Off Frequency:										
0.1	64.8	23.5	55.8	21.7	61.5	72.1	40.9	17.3	37.8	7.0
0.05	65.3	23.5	57.9	20.9	62.4	72.3	40.9	17.7	38.5	7.4
Gaussian Low Pass Filter Cut-Off Frequency:										
0.1	65.7	23.6	55.5	22.4	61.7	73.4	40.7	17.6	37.9	7.1
0.05	65.1	23.4	55.4	22.7	64.4	76.4	39.9	18.0	37.8	6.8
Average	**65.5**	**24.8**	**56.4**	**21.1**	**60.9**	**68.5**	**41.5**	**17.3**	**38.3**	**7.7**

Table 4.1b - Field 1 Fuzzy K-means classification accuracies and statistics

	Producer's accuracy (%)				User's Accuracy (%)				Overall accuracy	Overall kappa
Class	**Dep**	**Low**	**Mid**	**Upper**	**1**	**2**	**3**	**4**	**%**	**%**
Average Filter Size:										
5 x 5	65.7	25.0	56.7	20.8	60.2	67.0	41.9	17.2	38.5	7.9
7 x 7	65.6	24.0	56.4	21.6	60.7	70.5	41.3	17.4	38.2	7.5
9 x 9	65.7	23.9	56.7	21.4	61.3	71.6	41.2	17.4	38.3	7.5
11 x 11	65.5	23.6	55.8	22.2	62.1	73.5	40.7	17.6	37.9	7.1
21 X 21	64.4	22.6	56.2	22.0	65.6	76.5	38.2	17.8	37.8	6.5
Gaussian Filter Size:										
5 x 5	65.7	25.6	57.3	20.1	59.8	65.0	42.2	17.0	38.7	8.2
7 x 7	65.7	24.5	57.1	20.8	60.2	68.3	41.8	17.2	38.5	7.8
9 x 9	65.7	24.4	57.4	20.7	60.4	69.1	41.7	17.2	38.5	7.9
11 x 11	65.6	24.0	56.5	21.6	60.8	70.7	41.3	17.4	38.2	7.5
21 X 21	65.5	23.6	55.8	22.2	61.9	73.4	40.8	17.6	38.0	7.2
Median Filter Size:										
3 x 3	65.4	26.3	57.0	19.9	59.5	62.6	42.6	16.9	38.7	8.3
5 x 5	65.7	24.9	57.5	20.1	60.0	66.8	42.0	16.9	38.6	8.0
7 x 7	65.8	24.3	56.0	21.6	60.4	69.6	41.5	17.2	38.1	7.5
Mode Filter Size:										
3 x 3	66.0	30.0	57.6	17.5	58.6	54.2	44.0	16.8	39.7	9.5
5 x 5	66.1	29.6	57.8	17.5	58.5	55.4	43.9	16.6	39.6	9.4
7 x 7	65.6	26.3	56.3	19.9	58.7	61.7	42.6	16.7	38.5	8.1
Fourrier Transformation Butterworth Low Pass Filter Cut-Off Frequency:										
0.1	64.5	23.3	55.6	22.1	61.7	72.7	40.8	17.4	37.7	6.9
0.05	64.4	21.2	50.8	70.8	64.1	75.8	56.5	33.3	46.7	24.0
Gaussian Low Pass Filter Cut-Off Frequency:										
0.1	65.6	23.5	55.6	22.4	61.9	73.7	40.7	17.6	37.9	7.1
0.05	65.0	23.5	57.2	21.5	64.6	76.2	40.3	17.8	38.3	7.2
Average	**65.5**	**24.7**	**56.4**	**23.3**	**61.0**	**68.7**	**42.3**	**18.0**	**38.8**	**8.6**

Table 4.2a - Field 2 Isodata classification accuracies and statistics

	Producer's accuracy (%)				User's Accuracy (%)				Overall accuracy	Overall kappa
Class	**Dep**	**Low**	**Mid**	**Upper**	**1**	**2**	**3**	**4**	**%**	**%**
Average Filter Size:										
5 x 5	44.1	27.0	53.0	38.0	43.5	66.5	31.8	26.4	37.9	16.0
7 x 7	44.3	27.3	55.3	35.3	43.7	66.5	32.0	26.6	38.2	16.2
9 x 9	45.0	27.6	57.1	32.8	43.5	66.3	32.0	26.9	38.5	16.3
11 x 11	40.0	22.6	22.1	73.9	49.7	66.6	25.4	25.2	33.5	13.2
21 X 21	48.9	28.0	57.1	31.6	43.0	65.4	32.3	27.4	38.9	16.8
Gaussian Filter Size:										
5 x 5	44.1	27.0	52.6	38.3	43.3	66.3	31.9	26.4	37.9	16.0
7 x 7	44.0	27.1	53.2	37.9	43.6	66.5	31.8	26.5	38.0	16.1
9 x 9	44.3	27.3	53.3	37.5	43.4	66.5	31.8	26.5	38.0	16.1
11 x 11	44.3	27.3	53.6	37.1	43.7	66.6	31.8	26.6	38.1	16.1
21 X 21	45.4	27.6	56.0	34.2	43.5	66.5	31.9	27.0	38.4	16.4
Median Filter Size:										
3 x 3	44.3	27.5	54.1	36.6	43.3	66.0	32.2	26.4	38.2	16.2
5 x 5	44.1	27.4	54.1	37.2	43.5	66.6	32.2	26.5	38.3	16.4
7 x 7	43.6	27.3	53.9	37.7	44.1	67.2	32.1	26.4	38.2	16.3
Mode Filter Size:										
3 x 3	44.6	28.1	54.3	35.0	42.7	64.4	32.4	26.4	38.3	16.1
5 x 5	43.9	27.4	53.7	36.4	43.3	65.4	32.1	26.1	38.0	15.9
7 x 7	43.8	27.3	53.9	36.3	43.1	66.1	32.2	25.8	37.9	15.9
Fourrier Transformation Butterworth Low Pass Filter Cut-Off Frequency:										
0.1	45.2	27.5	55.6	34.7	43.6	66.5	31.9	27.0	38.4	16.4
0.05	49.6	28.2	63.7	27.1	42.8	65.2	33.3	29.7	40.0	17.9
Gaussian Low Pass Filter Cut-Off Frequency:										
0.1	46.4	27.4	59.1	29.8	41.7	65.2	32.4	27.0	38.5	16.3
0.05	46.3	28.0	60.7	26.6	44.5	64.6	32.2	26.0	38.6	16.1
Average	**44.8**	**27.3**	**53.8**	**36.7**	**43.7**	**66.0**	**31.8**	**26.6**	**38.1**	**16.1**

Table 4.2b - Field 2 Fuzzy K-means classification accuracies and statistics

	Producer's accuracy (%)				User's Accuracy (%)				Overall accuracy	Overall kappa
Class	**Dep**	**Low**	**Mid**	**Upper**	**1**	**2**	**3**	**4**	**%**	**%**
Average Filter Size:										
5 x 5	42.9	27.4	54.9	36.5	44.7	66.6	31.9	26.6	38.2	16.2
7 x 7	43.6	27.4	55.6	35.3	44.3	66.6	31.9	26.6	38.3	16.2
9 x 9	43.8	26.9	48.8	41.6	44.4	66.9	30.9	26.0	37.3	15.5
11 x 11	46.3	27.0	39.4	55.8	42.9	66.5	40.0	22.9	37.6	17.6
21 X 21	48.9	27.3	49.3	37.9	43.0	65.7	30.8	26.4	37.6	15.7
Gaussian Filter Size:										
5 x 5	43.3	27.1	56.1	35.3	44.0	66.5	32.0	26.7	38.2	16.2
7 x 7	42.9	27.5	55.2	36.2	44.7	66.7	31.9	26.6	38.2	16.2
9 x 9	43.2	27.3	55.6	35.7	44.6	66.8	31.9	26.6	38.2	16.2
11 x 11	43.1	27.4	55.9	35.3	44.8	66.8	31.9	26.6	38.3	16.2
21 X 21	43.8	27.1	46.9	43.2	44.8	66.9	30.6	26.0	37.2	15.4
Median Filter Size:										
3 x 3	43.4	27.6	55.8	35.1	43.9	66.0	32.2	26.5	38.3	16.2
5 x 5	42.9	27.3	56.2	35.8	44.5	66.8	32.2	26.7	38.4	16.4
7 x 7	42.8	27.4	55.9	36.0	44.7	67.2	32.1	26.5	38.4	16.4
Mode Filter Size:										
3 x 3	43.8	27.7	53.7	36.3	43.3	64.9	32.2	26.2	38.1	15.9
5 x 5	43.0	27.5	55.5	35.0	43.8	65.6	32.2	26.1	38.1	16.0
7 x 7	42.5	27.2	56.0	35.2	43.9	66.6	32.2	26.1	38.1	16.0
Fourrier Transformation Butterworth Low Pass Filter Cut-Off Frequency:										
0.1	43.9	26.8	45.0	51.0	44.7	66.9	39.6	22.4	37.9	17.6
0.05	48.3	27.6	45.7	41.3	43.7	65.9	30.1	26.3	37.2	15.4
Gaussian Low Pass Filter Cut-Off Frequency:										
0.1	45.5	26.8	36.5	57.6	42.3	65.9	39.5	22.8	37.0	16.9
0.05	48.3	27.4	56.0	29.5	43.0	64.4	31.7	25.1	37.8	15.5
Average	**44.3**	**27.3**	**51.7**	**39.3**	**44.0**	**66.3**	**32.9**	**25.8**	**37.9**	**16.2**

Table 4.3a - Field 3 Isodata classification accuracies and statistics

	Producer's accuracy (%)				User's Accuracy (%)				Overall accuracy	Overall kappa
Class	**Dep**	**Low**	**Mid**	**Upper**	**1**	**2**	**3**	**4**	**%**	**%**
Average Filter Size:										
5 x 5	0.0	25.9	37.4	31.1	0.0	22.2	32.7	60.9	32.2	4.8
7 x 7	0.0	25.2	38.2	33.2	0.0	22.5	32.9	60.6	33.2	5.3
9 x 9	0.0	23.8	40.5	34.4	0.0	22.6	33.1	60.5	34.3	5.7
11 x 11	0.0	23.7	40.3	35.5	0.0	22.6	33.0	60.4	34.7	5.8
21 X 21	0.0	22.9	41.1	36.8	0.0	23.1	32.7	60.7	35.4	6.0
Gaussian Filter Size:										
5 x 5	0.0	26.2	36.2	30.0	0.0	21.9	32.3	60.7	31.3	4.3
7 x 7	0.0	25.9	36.9	31.8	0.0	22.2	32.7	60.8	32.3	4.9
9 x 9	0.0	25.1	38.2	33.2	0.0	22.4	32.9	60.6	33.2	5.3
11 x 11	0.0	24.5	38.4	33.9	0.0	22.4	33.0	60.6	33.5	5.5
21 X 21	0.0	23.2	40.2	34.9	0.0	22.5	33.0	60.5	34.3	5.6
Median Filter Size:										
3 x 3	0.0	28.7	32.9	25.2	0.0	20.7	31.0	60.7	28.5	2.5
5 x 5	0.0	25.8	36.3	30.6	0.0	21.8	32.4	60.9	31.5	4.5
7 x 7	0.0	24.6	39.3	32.0	0.0	22.3	32.8	60.7	32.9	5.0
Mode Filter Size:										
3 x 3	0.0	30.4	30.5	22.2	0.0	19.7	30.1	60.5	26.7	1.2
5 x 5	0.0	26.1	38.1	27.0	0.0	21.4	31.8	60.0	30.6	3.2
7 x 7	0.0	27.3	34.8	25.8	0.0	20.5	31.1	60.4	21.4	2.5
Fourrier Transformation Butterworth Low Pass Filter Cut-Off Frequency:										
0.1	0.0	23.5	39.8	35.7	0.0	22.7	33.1	60.2	34.6	5.8
0.05	0.0	24.9	36.7	34.2	0.0	22.7	31.9	60.9	33.1	5.1
Gaussian Low Pass Filter Cut-Off Frequency:										
0.1	0.0	23.2	40.3	35.5	0.0	22.5	33.1	60.4	34.6	5.8
0.05	0.0	22.4	39.8	35.9	0.0	22.1	32.5	61.0	34.5	5.5
Average	**0.0**	**25.2**	**37.8**	**31.9**	**0.0**	**22.0**	**32.4**	**60.6**	**32.1**	**4.7**

Table 4.3b - Field 3 Fuzzy K-means classification accuracies and statistics

	Producer's accuracy (%)				User's Accuracy (%)				Overall accuracy	Overall kappa
Class	**Dep**	**Low**	**Mid**	**Upper**	**1**	**2**	**3**	**4**	**%**	**%**
Average Filter Size:										
5 x 5	0.0	25.3	37.7	31.8	0.0	22.3	32.8	60.7	32.4	5.0
7 x 7	0.0	24.8	38.2	33.2	0.0	22.5	32.9	60.6	33.1	5.3
9 x 9	0.0	23.4	39.4	35.1	0.0	22.5	33.1	60.4	34.1	5.7
11 x 11	0.0	23.2	39.6	35.5	0.0	22.5	33.0	60.4	34.4	5.7
21 X 21	0.0	22.6	39.8	35.8	0.0	22.2	32.4	61.1	34.4	5.5
Gaussian Filter Size:										
5 x 5	0.0	25.5	37.3	30.7	0.0	22.2	32.5	60.5	31.9	4.6
7 x 7	0.0	25.2	37.7	31.8	0.0	22.3	32.7	60.8	32.4	5.0
9 x 9	0.0	24.3	38.2	33.2	0.0	22.4	32.9	60.6	33.0	5.3
11 x 11	0.0	24.1	38.4	33.9	0.0	22.4	33.0	60.6	33.4	5.5
21 X 21	0.0	22.8	40.2	34.9	0.0	22.4	33.0	60.5	34.2	5.6
Median Filter Size:										
3 x 3	0.0	26.6	35.1	27.1	0.0	21.1	31.5	60.4	29.7	3.1
5 x 5	0.0	25.1	37.9	30.6	0.0	22.0	32.6	60.9	32.0	4.6
7 x 7	0.0	24.2	38.3	33.4	0.0	22.3	32.9	60.5	33.1	5.2
Mode Filter Size:										
3 x 3	0.0	27.9	33.7	25.0	0.0	20.5	30.9	59.9	28.5	2.2
5 x 5	0.0	25.2	37.9	28.2	0.0	21.5	31.9	59.9	30.9	3.4
7 x 7	0.0	25.9	35.9	27.6	0.0	20.9	31.5	60.1	30.1	3.0
Fourrier Transformation Butterworth Low Pass Filter Cut-Off Frequency:										
0.1	0.0	23.6	39.2	35.4	0.0	22.7	33.0	60.3	34.3	5.7
0.05	0.0	23.8	38.1	35.5	0.0	22.8	32.1	60.6	34.0	5.3
Gaussian Low Pass Filter Cut-Off Frequency:										
0.1	0.0	23.3	39.7	35.1	0.0	22.5	33.0	60.5	34.3	5.7
0.05	0.0	22.7	39.2	35.5	0.0	21.9	32.5	61.2	34.1	5.4
Average	**0.0**	**24.5**	**38.1**	**32.5**	**0.0**	**22.1**	**32.5**	**60.5**	**32.7**	**4.8**

Table 4.4a - Field 4 Isodata classification accuracies and statistics

	Producer's accuracy (%)				User's Accuracy (%)				Overall accuracy	Overall kappa
Class	**Dep**	**Low**	**Mid**	**Upper**	**1**	**2**	**3**	**4**	**%**	**%**
Average Filter Size:										
5 x 5	0.0	16.9	25.7	8.6	0.0	28.3	35.8	20.4	18.0	-5.3
7 x 7	0.0	17.9	25.2	8.8	0.0	28.4	35.8	20.1	18.0	-5.3
9 x 9	0.0	18.3	25.4	8.5	0.0	28.4	36.0	19.8	18.1	-5.2
11 x 11	0.0	18.9	25.5	8.1	0.0	28.5	35.9	19.3	18.2	-5.2
21 X 21	0.0	20.1	25.4	8.0	0.0	27.0	36.0	18.7	18.3	-5.5
Gaussian Filter Size:										
5 x 5	0.0	15.9	25.8	8.4	0.0	22.9	35.7	20.2	17.8	-5.3
7 x 7	0.0	16.7	25.7	8.6	0.0	28.6	35.8	20.3	18.0	-5.3
9 x 9	0.0	17.6	25.5	8.6	0.0	28.4	35.8	20.1	18.0	-5.3
11 x 11	0.0	17.9	25.3	8.7	0.0	28.4	35.8	20.1	18.1	-5.3
21 X 21	0.0	18.8	25.5	8.3	0.0	28.1	36.0	19.5	18.2	-5.3
Median Filter Size:										
3 x 3	0.0	14.8	26.9	8.2	0.0	28.6	36.1	20.4	18.0	-5.4
5 x 5	0.0	15.5	26.6	8.2	0.0	28.8	36.0	20.1	18.0	-5.4
7 x 7	0.0	16.4	25.9	8.5	0.0	29.2	35.9	20.2	18.0	-5.3
Mode Filter Size:										
3 x 3	0.0	16.2	19.1	6.7	0.0	24.0	32.1	19.7	14.2	-6.0
5 x 5	0.0	13.9	27.1	7.6	0.0	30.0	35.7	20.1	17.7	-5.4
7 x 7	0.0	14.3	27.4	7.6	0.0	29.3	36.0	19.9	17.9	-5.5
Fourrier Transformation Butterworth Low Pass Filter Cut-Off Frequency:										
0.1	0.0	18.6	25.7	8.5	0.0	27.7	36.2	19.7	18.3	-5.3
0.05	0.0	20.0	25.5	8.6	0.0	27.3	36.3	19.5	18.5	-5.3
Gaussian Low Pass Filter Cut-Off Frequency:										
0.1	0.0	18.7	25.6	8.3	0.0	28.1	36.0	19.4	18.2	-5.3
0.05	0.0	20.2	25.5	8.0	0.0	27.0	35.9	18.8	18.4	-5.5
Average	**0.0**	**17.4**	**25.5**	**8.2**	**0.0**	**27.8**	**35.7**	**19.8**	**17.9**	**-5.4**

Table 4.4b - Field 4 Fuzzy K-means classification accuracies and statistics

	Producer's accuracy (%)				User's Accuracy (%)				Overall accuracy	Overall kappa
Class	**Dep**	**Low**	**Mid**	**Upper**	**1**	**2**	**3**	**4**	**%**	**%**
Average Filter Size:										
5 x 5	0.0	16.7	25.7	8.2	0.0	29.0	35.6	20.1	17.9	-5.3
7 x 7	0.0	17.6	25.3	8.6	0.0	28.7	35.8	20.0	18.0	-5.3
9 x 9	0.0	18.6	25.4	8.5	0.0	28.1	36.0	19.8	18.2	-5.3
11 x 11	0.0	19.0	25.6	8.3	0.0	28.1	36.1	19.5	18.3	-5.2
21 X 21	0.0	20.1	25.5	7.9	0.0	27.0	35.9	18.8	18.4	-5.5
Gaussian Filter Size:										
5 x 5	0.0	16.4	26.2	8.4	0.0	28.3	35.9	20.2	18.0	-5.4
7 x 7	0.0	17.1	25.7	8.6	0.0	28.3	35.8	20.3	18.0	-5.3
9 x 9	0.0	17.5	25.5	8.4	0.0	28.8	35.7	19.9	18.0	-5.3
11 x 11	0.0	17.9	25.4	8.5	0.0	28.4	35.8	20.0	18.1	-5.3
21 X 21	0.0	18.6	25.7	8.3	0.0	28.0	36.0	19.5	18.3	-5.3
Median Filter Size:										
3 x 3	0.0	14.9	27.2	8.0	0.0	28.2	36.1	20.3	18.1	-5.4
5 x 5	0.0	15.7	26.7	8.2	0.0	28.5	36.0	20.1	18.1	-5.4
7 x 7	0.0	16.5	26.2	8.4	0.0	28.7	35.9	20.1	18.1	-5.3
Mode Filter Size:										
3 x 3	0.0	15.7	20.8	6.8	0.0	26.0	32.6	19.7	14.9	-5.9
5 x 5	0.0	14.2	27.0	7.2	0.0	30.5	35.4	19.7	17.5	-5.5
7 x 7	0.0	14.9	27.8	7.6	0.0	27.6	36.1	19.9	18.2	-5.6
Fourrier Transformation Butterworth Low Pass Filter Cut-Off Frequency:										
0.1	0.0	18.7	25.7	8.6	0.0	27.5	36.2	19.8	18.4	-5.3
0.05	0.0	20.4	25.7	8.3	0.0	26.9	36.2	19.3	18.6	-5.4
Gaussian Low Pass Filter Cut-Off Frequency:										
0.1	0.0	18.8	25.6	8.4	0.0	27.9	36.0	19.5	18.3	-5.3
0.05	0.0	20.4	25.6	7.9	0.0	26.9	35.9	18.8	18.4	-5.5
Average	**0.0**	**17.5**	**25.7**	**8.1**	**0.0**	**28.1**	**35.8**	**19.7**	**18.0**	**-5.4**

Table 4.5a - Field 5 Isodata classification accuracies and statistics

	Producer's accuracy (%)				User's Accuracy (%)				Overall accuracy	Overall kappa
Class	**Dep**	**Low**	**Mid**	**Upper**	**1**	**2**	**3**	**4**	**%**	**%**
Average Filter Size:										
5 x 5	63.2	38.2	15.1	17.5	5.2	39.0	21.5	82.1	26.9	4.0
7 x 7	63.9	38.1	15.6	17.7	5.2	39.2	21.6	82.4	27.1	4.2
9 x 9	66.0	37.4	15.1	17.7	5.3	38.8	21.5	82.7	26.7	4.0
11 x 11	67.0	37.3	15.4	18.0	5.4	39.0	21.5	82.8	26.9	4.3
21 X 21	66.8	39.0	16.8	19.5	5.8	40.6	21.2	82.9	28.4	5.6
Gaussian Filter Size:										
5 x 5	63.4	38.1	15.1	17.5	5.2	39.0	21.5	82.0	26.9	4.0
7 x 7	63.3	38.2	15.2	17.5	5.2	39.0	21.5	82.2	26.9	4.0
9 x 9	63.6	37.8	15.8	18.1	5.2	39.3	21.8	82.0	27.1	4.4
11 x 11	63.9	37.9	15.8	18.1	5.2	39.3	21.7	82.1	27.2	4.4
21 X 21	64.6	37.7	16.4	18.8	5.3	39.7	21.8	82.0	27.5	4.9
Median Filter Size:										
3 x 3	62.9	38.6	14.9	17.3	5.2	39.1	21.3	82.0	27.0	3.9
5 x 5	63.8	38.4	15.2	17.7	5.2	39.1	21.5	81.9	27.1	4.1
7 x 7	65.5	37.6	14.8	17.6	5.3	38.6	21.5	82.2	26.7	3.9
Mode Filter Size:										
3 x 3	60.4	39.7	15.7	17.5	5.1	40.2	21.4	81.7	27.6	4.5
5 x 5	58.6	41.0	15.5	17.9	5.1	40.4	21.4	81.3	28.2	4.7
7 x 7	63.5	38.6	14.8	17.4	5.2	39.3	21.1	81.9	27.0	4.0
Fourrier Transformation Butterworth Low Pass Filter Cut-Off Frequency:										
0.1	67.5	38.5	18.6	18.7	4.9	41.8	21.9	82.0	28.7	5.1
0.05	69.5	39.3	18.0	19.4	5.3	42.2	20.6	82.1	29.2	5.4
Gaussian Low Pass Filter Cut-Off Frequency:										
0.1	69.3	38.3	18.1	18.7	5.1	41.6	21.3	82.1	28.6	4.9
0.05	74.4	38.7	18.9	20.1	5.6	42.9	20.7	82.7	29.5	6.1
Average	**65.1**	**38.4**	**16.0**	**18.1**	**5.2**	**39.9**	**21.4**	**82.1**	**27.6**	**4.5**

Table 4.5b - Field 5 Fuzzy K-means classification accuracies and statistics

	Producer's accuracy (%)				User's Accuracy (%)				Overall accuracy	Overall kappa
Class	**Dep**	**Low**	**Mid**	**Upper**	**1**	**2**	**3**	**4**	**%**	**%**
Average Filter Size:										
5 x 5	61.7	39.1	15.6	17.5	5.2	39.5	21.6	82.1	27.4	4.2
7 x 7	63.9	38.1	15.6	17.7	5.2	39.2	21.6	82.4	27.1	4.2
9 x 9	62.6	39.2	15.9	18.0	5.3	39.7	21.7	82.4	27.7	4.6
11 x 11	62.9	39.2	16.2	18.2	5.3	39.9	21.7	82.6	27.8	4.8
21 X 21	66.8	39.0	16.9	19.1	5.8	40.6	21.1	83.5	28.3	5.4
Gaussian Filter Size:										
5 x 5	61.7	39.0	15.6	17.3	5.1	39.5	21.5	82.1	27.3	4.1
7 x 7	61.8	39.1	15.6	17.5	5.2	39.4	21.6	82.2	27.4	4.2
9 x 9	63.6	38.0	15.6	17.7	5.2	39.1	21.7	82.3	27.0	4.2
11 x 11	62.2	39.1	15.9	17.9	5.2	39.6	21.7	82.2	27.6	4.5
21 X 21	62.8	39.1	16.2	18.2	5.3	39.9	21.6	82.4	27.8	4.7
Median Filter Size:										
3 x 3	61.4	39.6	15.2	17.5	5.2	39.6	21.4	81.8	27.5	4.2
5 x 5	63.8	38.4	15.2	17.7	5.2	39.1	21.5	81.9	27.1	4.1
7 x 7	63.9	38.3	15.7	17.6	5.3	39.3	21.6	82.2	27.2	4.2
Mode Filter Size:										
3 x 3	58.5	40.9	15.7	17.5	5.1	40.5	21.4	81.7	28.1	4.6
5 x 5	56.4	42.1	15.9	17.8	5.0	40.9	21.4	81.3	28.6	4.9
7 x 7	61.4	39.7	15.3	17.6	5.2	39.9	21.3	81.6	27.6	4.4
Fourrier Transformation Butterworth Low Pass Filter Cut-Off Frequency:										
0.1	67.1	39.0	18.3	18.3	4.9	41.8	21.7	82.2	28.7	4.9
0.05	68.8	40.0	17.8	19.0	5.3	42.4	20.5	82.4	29.4	5.3
Gaussian Low Pass Filter Cut-Off Frequency:										
0.1	67.3	39.1	18.6	18.8	5.0	42.2	21.4	82.0	29.0	5.2
0.05	72.9	39.5	18.8	19.7	5.6	43.1	20.5	83.1	29.7	6.1
Average	**63.6**	**39.3**	**16.3**	**18.0**	**5.2**	**40.3**	**21.4**	**82.2**	**27.9**	**4.6**